AD

USAAVLABS TECHNICAL REPORT 67-9B

IN-FLIGHT MEASUREMENT OF ROTOR BLADE AIRLOADS, BENDING MOMENTS, AND MOTIONS, TOGETHER WITH ROTOR SHAFT LOADS AND FUSELAGE VIBRATION, ON A TANDEM ROTOR HELICOPTER

VOLUME II

CALIBRATIONS AND INSTRUMENTED COMPONENT TESTING

By

William J. Grant

Richard R. Pruyn

May 1967

U. S. ARMY AVIATION MATERIEL LABORATORIES

FORT EUSTIS, VIRGINIA

VERTOL DIVISION

THE BOEING COMPANY

MORTON, PENNSYLVANIA

Distribution of this document is unlimited

134

DISCLAIMER NOTICE

THIS DOCUMENT IS BEST QUALITY PRACTICABLE. THE COPY FURNISHED TO DTIC CONTAINED A SIGNIFICANT NUMBER OF PAGES WHICH DO NOT REPRODUCE LEGIBLY.

Disclaimers

When Government drawings, specifications, or other data are used for any purpose other than in connection with a definitely related Government procurement operation, the United States Government thereby incurs no responsibility nor any obligation whatsoever; and the fact that the Government may have formulated, furnished, or in any way supplied the said drawings, specifications, or other data is not to be regarded by implication or otherwise as in any manner licensing the holder or any other person or corporation, or conveying any rights or permission, to manufacture, use, or sell any patented invention that may in any way be related thereto.

Trade names cited in this report do not constitute an official endorsement or approval of the use of such commercial hardware or software.

Disposition Instructions

Destroy this report when no longer needed. Do not return it to originator.

ACCESSION for
CFSTI WHITE SECTION
DDC BUFF SECTION
UNANNOUNCED
JUSTIFICATION
BY
DISTRIBUTION/AVAILABILITY CODES
DIST. AVAIL. and/or SPECIAL

DEPARTMENT OF THE ARMY
U. S. ARMY AVIATION MATERIEL LABORATORIES
FORT EUSTIS, VIRGINIA 23604

This report has been reviewed by the U. S. Army Aviation Materiel Laboratories and is considered to be technically sound. The work was performed under Contract DA-44-177-AMC-124(T) for the purpose of measuring the dynamic air pressures on the blades of a tandem rotor helicopter and the resulting blade and shaft stresses and fuselage vibrations during flight. It is published for the dissemination and application of information and the stimulation of ideas.

Task 1F125901A14604
Contract DA 44-177-AMC-124(T)
USAAVLABS Technical Report 67-9B
May 1967

IN-FLIGHT MEASUREMENT OF ROTOR BLADE AIRLOADS, BENDING MOMENTS, AND MOTIONS, TOGETHER WITH ROTOR SHAFT LOADS AND FUSELAGE VIBRATION, ON A TANDEM ROTOR HELICOPTER

VOLUME II

CALIBRATIONS AND INSTRUMENTED COMPONENT TESTING

D8-0382-2

by

William J. Grant
and
Richard R. Pruyn

Prepared by

VERTOL DIVISION
THE BOEING COMPANY
Morton, Pennsylvania

for

U.S. ARMY AVIATION MATERIEL LABORATORIES
FORT EUSTIS, VIRGINIA

Distribution of this document is unlimited.

SUMMARY

Calibration and instrumented component testing were accomplished to provide reliable, accurate instrumentation for the measurement of rotor airloads, blade bending moments, rotor shaft loads, fuselage response, and control system loads on a large tandem rotor helicopter. All transducers and instrumented components were initially calibrated in routine single-load tests. Rotor shaft load and blade bending calibrations also included combined-loads tests to determine interaction coefficients, utilizing automated data acquisition and rigorous data analysis. Blade tension instrumentation was also calibrated by whirl testing.

The use of combined-loads calibrations is believed to be an extension of the state of the art, especially for elastic structures such as rotor blades. Therefore, the differences between the results obtained by the routine calibration procedures and the combined-loads procedures are presented and discussed. For example, rotor shaft lift, shear, and bending (but not torque) have significant interactions which must be accounted for in data reduction; the same is true of rotor blade chordwise bending and flapwise bending (but not tension or torsion). A summary of the quality of these calibrations is presented, showing maximum hysteresis and deviation errors and including calibration load application and instrumentation accuracies. Generally, the error in these calibrations is less than 3 percent.

Component testing consisted of whirl tests and dynamic response tests of the rotor blades, and functional testing of the airloads pressure transducers. Whirl testing was performed to ensure the structural integrity of the rotor blade instrumentation, to provide a calibration of the radial tension gages, and to adjust the blade balance weights for blade tracking. Dynamic response tests of the rotor blades were conducted to provide a reference for isolating blade bending effects in the final airloads data. Airloads pressure transducer functional tests were performed to check the repeatability of the calibrations and to determine the interactions of acceleration and temperature. The fuselage vibration accelerometers were also tested for dynamic response.

FOREWORD

This report presents the rationale, the procedures, and the results of component tests and calibrations performed in support of the measurement of dynamic airloads on a tandem rotor helicopter as executed under Contract DA 44-177-AMC-124(T). Explanations as to why the instrumentation was provided, how it was flight-tested, and the results obtained are provided in the other volumes of this report. These volumes are as follows:

Volume I, Instrumentation and In-Flight Recording System

Volume III, Data Processing and Analysis System

Volume IV, Summary and Evaluation of Results

The findings of this project are also discussed in references 2 and 4; and tabular data summaries, references 1 and 5, are available. An extension to this program to obtain data under extreme operating conditions for subsequent analysis will produce an additional tabular data summary and a fifth volume of this report, as follows:

Volume V, Investigation of Blade Stall Conditions

This project was conducted under the technical cognizance of William T. Alexander, Jr., of the Aeromechanics Division of USAAVLABS. The authors of this report are William J. Grant and Richard R. Pruyn (Boeing-Vertol Project Engineer), of the Dynamic Airloads Project Group of the Rotor Dynamic Stability Unit, Structures Technology Staff. The analyses discussed in this report were prepared by Walter S. Koroljow, and were reduced to practice and expanded by Alfred B. Meyer. Other Boeing-Vertol personnel who contributed significantly to this phase of the contract were E. Haren, M. Leone, D. McKenzie, J. Zimmartore, and V. Nielsen. This portion of the program was conducted during the period of May 1965 through June 1966.

CONTENTS

	Page
SUMMARY	iii
FOREWORD	v
LIST OF ILLUSTRATIONS	ix
LIST OF TABLES	xii
LIST OF SYMBOLS	xiv
INTRODUCTION	1
DESCRIPTION OF TEST ITEMS	3
ROTOR BLADES	3
ROTOR SHAFTS	15
CONTROL SYSTEM COMPONENTS	17
EXPERIMENTAL PROCEDURE	21
CALIBRATION OF ROTOR SHAFTS	21
ROTOR BLADE TENSION AND MOMENT GAGE CALIBRATIONS	25
CONTROL COMPONENT CALIBRATIONS	33
CALIBRATION OF AIRFRAME RESPONSE ACCELEROMETERS	33
INTEGRITY AND FUNCTIONAL WHIRL TESTING OF BLADES	36
AIRLOAD PRESSURE TRANSDUCER FUNCTIONAL TESTS	36
DYNAMIC RESPONSE TESTING OF BLADE	40
CALIBRATION DATA ANALYSIS	45
INPUT DATA MANIPULATIONS	45

CONTENTS

	Page
RESOLUTION OF COEFFICIENTS	47
EVALUATION OF RESULTS	49
EXPERIMENTAL RESULTS	55
PRIMARY CALIBRATION COEFFICIENTS	55
INTERACTION MATRICES FOR ROTOR SHAFTS	60
ROTOR BLADE INTERACTION MATRICES	65
TEMPERATURE AND ACCELERATION INTERACTIONS ON PRESSURE TRANSDUCERS	71
DYNAMIC RESPONSE OF ACCELEROMETERS	77
ROTOR BLADE DYNAMIC RESPONSE	77
ROTOR BLADE TRACKING DATA	77
EVALUATION	84
QUALITY OF CALIBRATION	84
BIBLIOGRAPHY	92
APPENDIXES	
I. Analysis of an Elastic Structure Under Predominantly Axial Load for Combined-Loads Calibration of Instrumentation for Measuring Bending and Torsion	93
II. Multiparameter Least-Squares-Curve Fitting Analysis	115
DISTRIBUTION	119

ILLUSTRATIONS

Figure		Page
1	Installation of Rotor Blade Instrumentation . . .	4
2	Typical Pressure Transducer Installation at 55-Percent Span of Forward Rotor Blade	5
3	Modification of CH-47A Rotor Blade Design to Provide Dynamic Airload Instrumentation. . . .	6
4	Fluoroscopic Photographs of Typical Clamp Installations in Aft Rotor Blade.	7
5	Rotor Blade Balance Weight Locations.	9
6	Spanwise Mass Distribution of Instrumented Blade and Noninstrumented Blades.	11
7	Rotor Shaft Strain-Gage Installation.	16
8	General Arrangement of Instrumented Rotor Shafts	18
9	Installation of Forward Rotor Shaft and Control Instrumentation	19
10	Installation of Aft Rotor Shaft and Control Instrumentation	20
11	Calibration of Lift, Shear, and Moment Gages on Forward Rotor Shaft.	23
12	Test Fixture for Calibration of Rotor Blades under Combined Loads	29
13	Rotor Blade Whirl Tower	32
14	Calibration of Swashplate Control Actuator Mounting Load Gages.	34
15	Dynamic Calibration Equipment for Aircraft Accelerometers.	35

ILLUSTRATIONS

Figure		Page
16	Static Calibration Equipment for Aircraft Accelerometers	37
17	Airload Pressure Transducer Test Equipment. . .	39
18	Flapwise Response (Shake) Test Setup with Airloads-Instrumented Aft Rotor Blade	42
19	Test Setup for Chordwise and Torsional Dynamic Response (Shake) Testing	43
20	Shaker Electronics, Instrumentation Signal-Conditioning, and Recording Equipment Used for Blade Dynamic Response Tests	44
21	Illustration of Geometry and Notation of Rotor Shaft Calibration Problem	46
22	Relation Between Correlation Coefficient and Average Error of Curve Fitting	52
23	Illustration of Definitions Used to Calculate Hysteresis and Deviation	54
24	Comparison of Static and Whirl Test Calibrations of Blade Tension Gages	59
25	Rotor Shaft Calibration Data Showing Interactions in Forward Shaft Shear Readings. .	61
26	Interactions of 0-180 Shear Gage Readings Due to an Orthogonal Shear on the Forward Shaft . .	64
27	Interactions in Readings of Flap Bending Gage at Station 231 of the Forward Blade	72
28	Interactions in Readings of Chord Bending Gage at Station 231 of the Forward Blade	73
29	Typical Test Data Obtained from Normal Acceleration Test of a Pressure Transducer. . .	76

ILLUSTRATIONS

Figure		Page
30	Frequency Response of Airframe Accelerometers	78
31	Phase Lag of Airframe Accelerometer Output Signals	79
32	Calculated Rotor Blade Dynamic Characteristics and Comparative Nonrotating Test Data	80
33	Nodal Points Obtained in Nonrotating Blade Response Tests	81
34	Forward Rotor Tracking Data	82
35	Aft Rotor Tracking Data	83
36	Summary of Data on the Quality of Single-Load Calibrations	86
37	Single-Load Calibration of the Chordwise Bending Gage at Station 230, Illustrating a Case of High Hysteresis	87
38	Repeatability of Airloads Pressure Transducer Calibrations	88
39	Schematic Diagram of Blade Calibration with Combined Loads	94
40	Illustration of Geometry and Notation of Blade Calibration Problem	95
41	Rotor Blade Coordinates	97
42	Details of Blade Load Application Geometry	99
43	Blade Loads and Geometry of Application	101

TABLES

Table		Page
I	Summary of Rotor Blade Balance and Tracking Weights	10
II	Mass Properties of Instrumented Rotor Blades.	12
III	Stiffness Properties of Instrumented Rotor Blades	13
IV	Mass Properties of Noninstrumented Rotor Blades	14
V	Stiffness Properties of Noninstrumented Rotor Blades	15
VI	Summary of Rotor Shaft Calibration Test Conditions	22
VII	Rotor Blade Combined-Loads Calibrations.	26
VIII	Rotor Blade Single-Load Calibrations	28
IX	Pressure Standards Used for Transducer Calibrations	38
X	Summary of Dynamic Response Test Configurations	41
XI	Equivalent Load Values - Rotor Shaft Strain Gages	56
XII	Interaction and Single-Load Calibration Values for Forward and Aft Blades.	58
XIII	Primary Calibration Coefficients - Control Components	60
XIV	Rotor Shaft Interaction Coefficients	62
XV	Rotor Blade Interaction Coefficients	66

TABLES

Table		Page
XVI	Temperature Correction Coefficients - Rotor Blade Differential-Pressure Transducers. . .	74
XVII	Correlation Coefficients of Rotor Shaft Combined-Loads Calibration	89
XVIII	Correlation Coefficients of Rotor Blade Combined-Loads Calibration	90

SYMBOLS

a_{kn}	k^{th} value of n-type primary calibration coefficient
CF	centrifugal force, pounds
E	fractional error
g	acceleration of gravity, 32.2 feet per second per second
g_{np}	n^{th} type gage reading with p^{th} type calibration load applied
k	integer denoting type of load
KΩ	thousands of ohms, resistance
n	integer denoting type of gage or gage reading
p	integer denoting specific test point in calibration
r	blade spanwise distance from shaft centerline, inches
r_k	correlation coefficient
R	blade tip span, 354.6 inches
Rcal	resistance calibration
s	total number of tests
S_z	standard deviation from the arithmetic mean of the load
S_{zg}	standard error of estimate, Z_{est} or g_{np}
$\overline{Z}$	arithmetic mean value of Z_{kp}
Z_{est}	p^{th} value of Z_{kp} predicted from the calibration equation
Z_{kp}	p^{th} value of kth type load
$\sigma(\beta)$	rotor blade static mass moment with respect to center of rotation, lb-sec^2

SYMBOLS

$\sigma(\beta_R)$	estimated static mass moment of blade root fittings with respect to center of rotation, lb-sec^2
Ω	rotor blade rotational speed, radians per second

INTRODUCTION

The supporting tests performed for the Dynamic Airloads Program included various component tests and an extensive instrumentation calibration program. Component tests were conducted to establish the structural integrity of the rotor blade instrumentation installation, the dynamic characteristics of the instrumented blade, and the frequency-response characteristics of the fuselage accelerometers. The effects of temperature on the output of the pressure transducers were also determined, since past experience has shown that the linearity and zero reference of these transducers were affected by changes in temperature.

The calibrations performed were of the following basic types:

1. Routine single loadings
2. Combined loads on a simple, low-strain sensitivity structure (rotor shafts)
3. Combined loads on an elastic structure (rotor blades)

The routine single-loading tests are delineated, summarized, and evaluated in this report, but are not of themselves of particular technical interest. The combined-loads calibrations are believed to be an advance of the state of the art, at least for helicopter instrumentation. Very little had been done in the past to establish and isolate the effects of load interactions on strain-gaged rotor system components. These rotor system components characteristically resist large loads in one direction which are of secondary interest (such as blade tension and shaft lift); at the same time, these components resist the relatively small loads which are to be measured (blade flap bending, rotor shaft shear, etc.). It was known from past experience that the load interaction coefficients could be sizable and that proper compensation for these coefficients was difficult. Calibrations were therefore performed based on the following concepts:

1. Provide well-defined requirements and establish common notation, reference axes, and positive value direction.
2. Use automated data acquisition for the highly instrumented rotor blades so that the mistakes inherent in recording such a large volume of data would be consistent and therefore correctable.
3. Apply all calibration forces from fixed points and use

the computer to correct for deflections and to resolve the loads into a convenient structure reference.

In addition to the interaction analyses, all primary coefficient data were evaluated by performing a least-squares fit of a linear or quadratic function, depending on which function produced the least error. This approach was also used in evaluating the single-valued input and output data for the less complex strain-gaged components, such as the control links, as well as the basic calibration data for the pressure transducers.

DESCRIPTION OF TEST ITEMS

ROTOR BLADES

One forward and one aft rotor blade were manufactured from standard CH-47A blade components, with modifications as required to provide the instrumentation illustrated in Figure 1. The components used were selected for minimum weight so that the instrumented blades could be balanced with the standard blades. The external modifications to the blades are typified by the transducer installation at the 55-percent span shown in Figure 2. An adhesive sleeve was provided which enclosed all external wiring and provided recesses for the pressure transducers. This sleeve was approximately 7 inches wide and was 0.080 inch thick at its center, tapering to a featheredge at both sides except aft of the midchord. Behind the midchord of the blade, the fairing sleeve was removed from the inboard side of the pressure transducers, so that a chamfered edge approximately 0.75 inch wide and 0.080 inch high was located approximately 1 inch from the transducers. This prominent spanwise ramp was required to provide an adequate chordwise balance of the blade; it should not have caused any greater obstruction to radial boundary-layer flow than the same height with a featheredge. Thus the addition of the fairing sleeves is believed to have caused little change in the basic 0012 airfoil section of the CH-47A blades. The changes made in the basic design of the rotor blade, with the extension of the blade chord from 21 to 23 inches by the addition of a stainless-steel nose cap of NACA 0011.6 section and a flat trailing edge extension, are probably more significant. No modifications were made to the CH-47A root end hardware or to the rolled D-section steel blade spar. However, the fiber-glass-covered trailing-edge fairing boxes were internally modified to accommodate and support the instrumentation wiring bundle. As shown in Figure 3, various internal and external clamps were provided to restrain the wire bundle against centrifugal force. To prevent wire failures due to creeping, two centrifugal-force relief bends were provided in the wire bundle. The wire bundle passed through and was supported by the aluminum ribs of the blade fairing boxes; the existing lightening holes in the ribs were modified for this purpose. Internal details of the wire installation are shown in the Figure 4 fluoroscopic photographs; these components were installed in the fairing boxes before the boxes were bonded to the spar. The standard CH-47A blade twist was maintained within production tolerances when the blade boxes were bonded. This blade twist is linear and causes a 9-degree

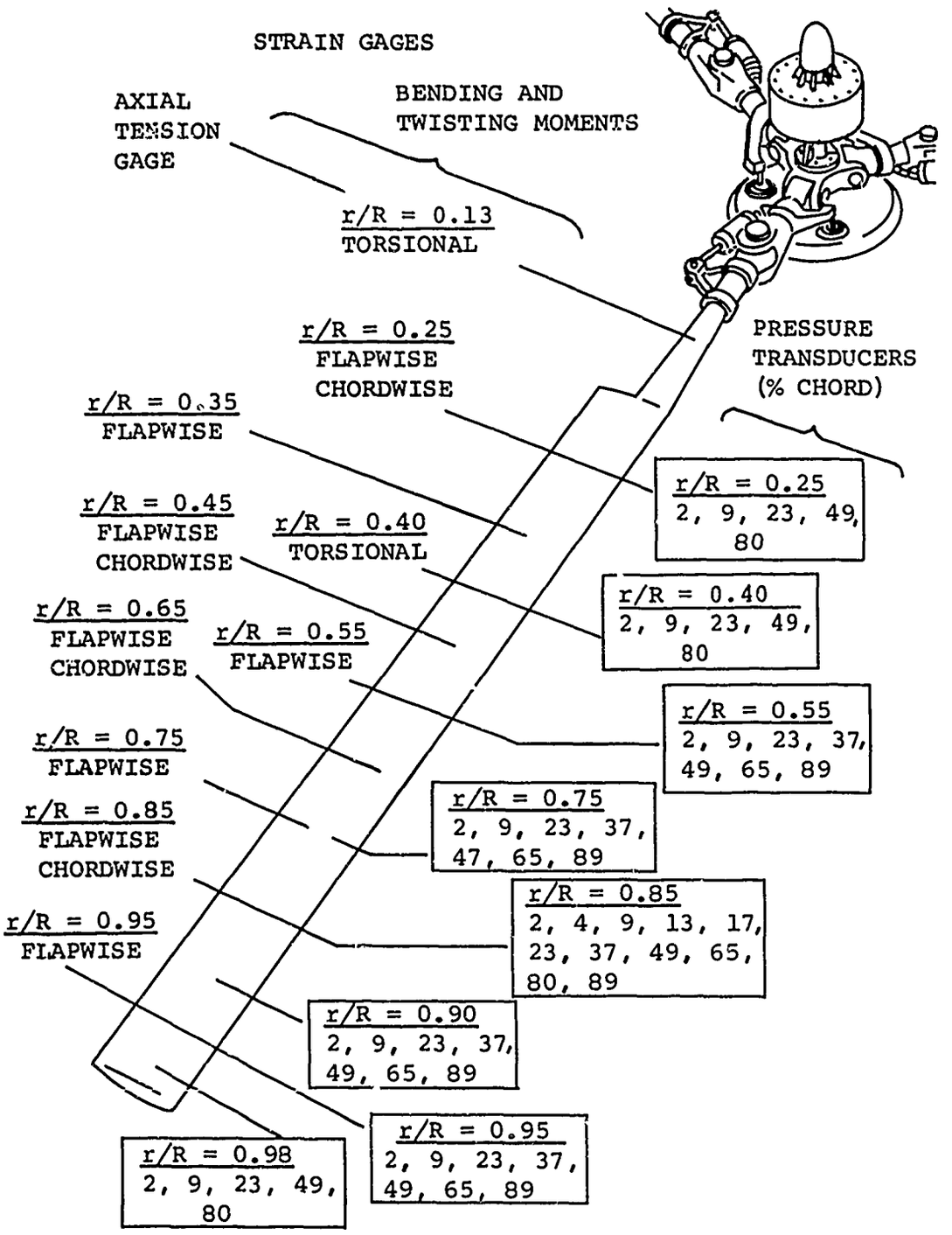

Figure 1. Installation of Rotor Blade Instrumentation.

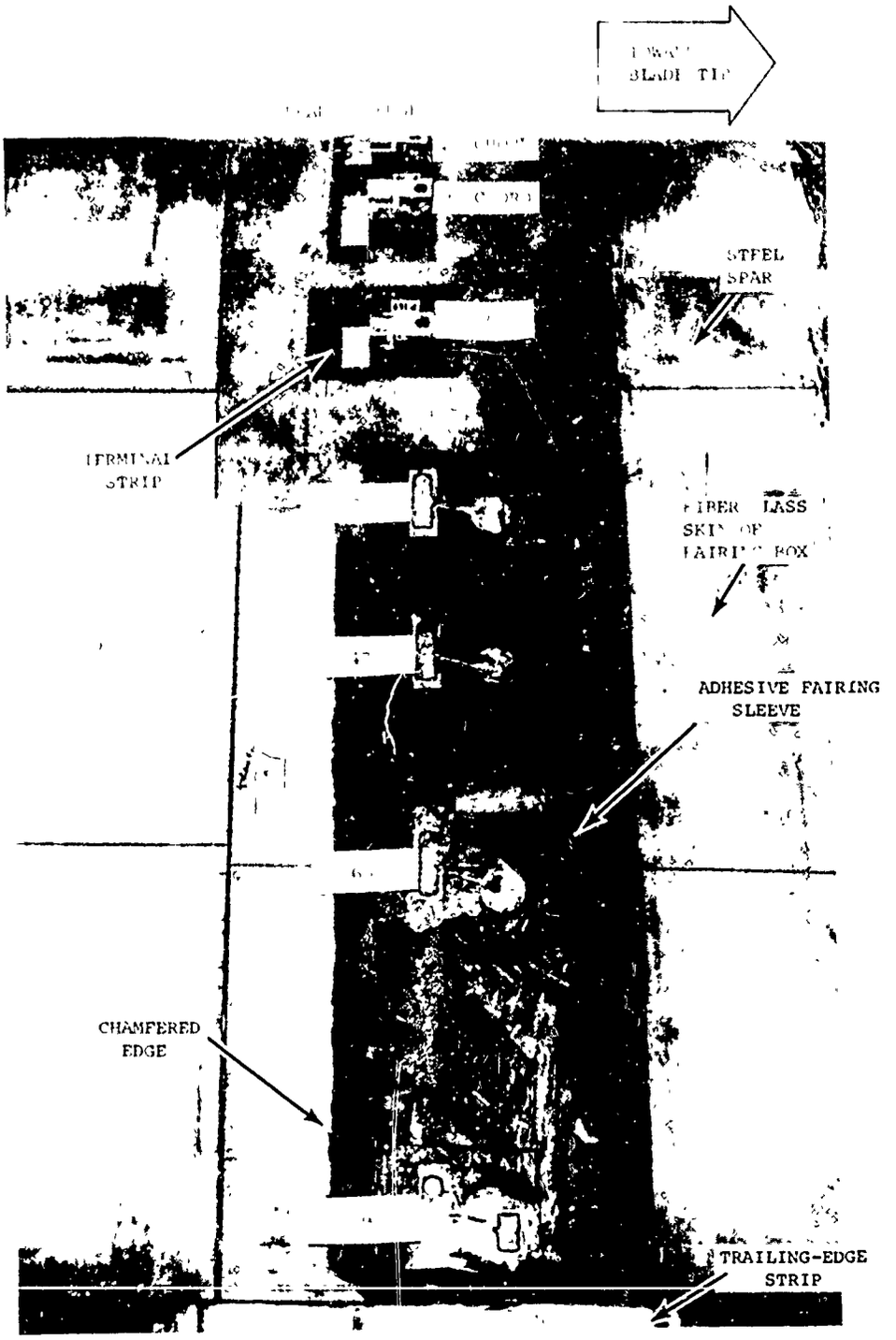

Figure 2. Typical Pressure Transducer Installation at 55-Percent Span of Forward Rotor Blade.

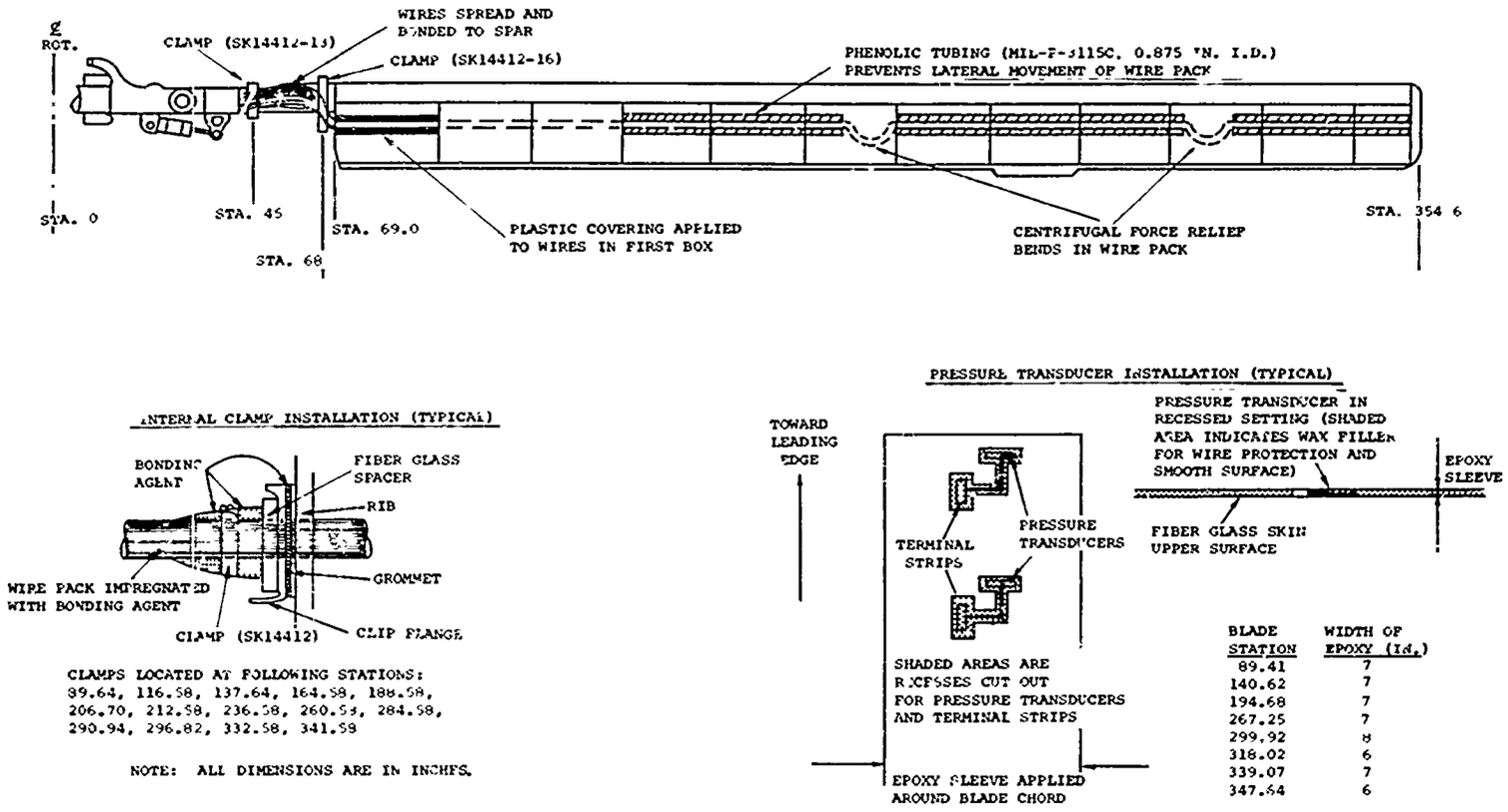

Figure 3. Modification of CH-47A Rotor Blade Design to Provide Dynamic Airload Instrumentation.

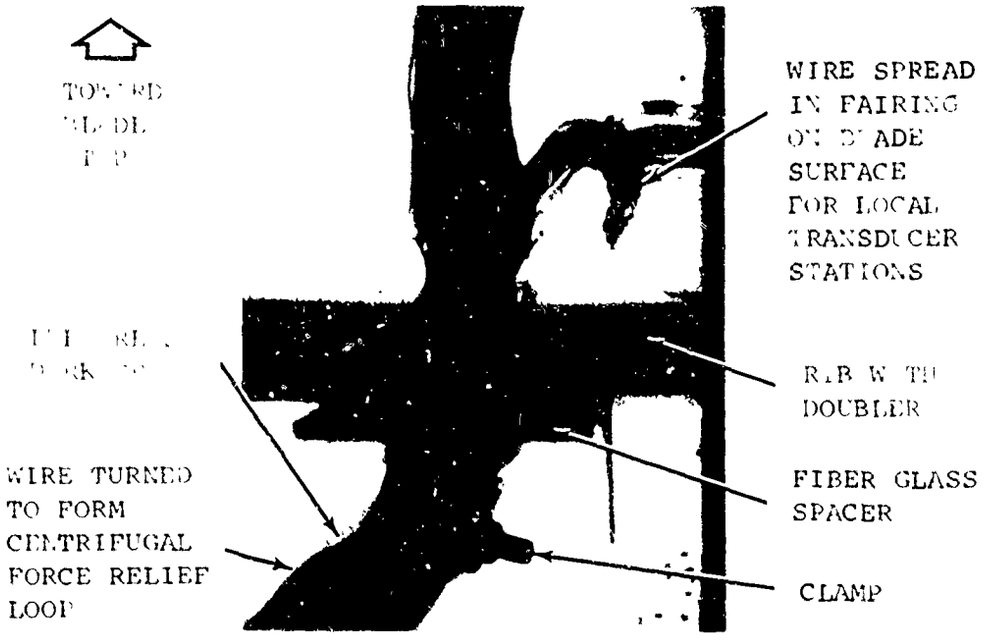

A. CLAMP AT STATION 256.82 (BOX 10)

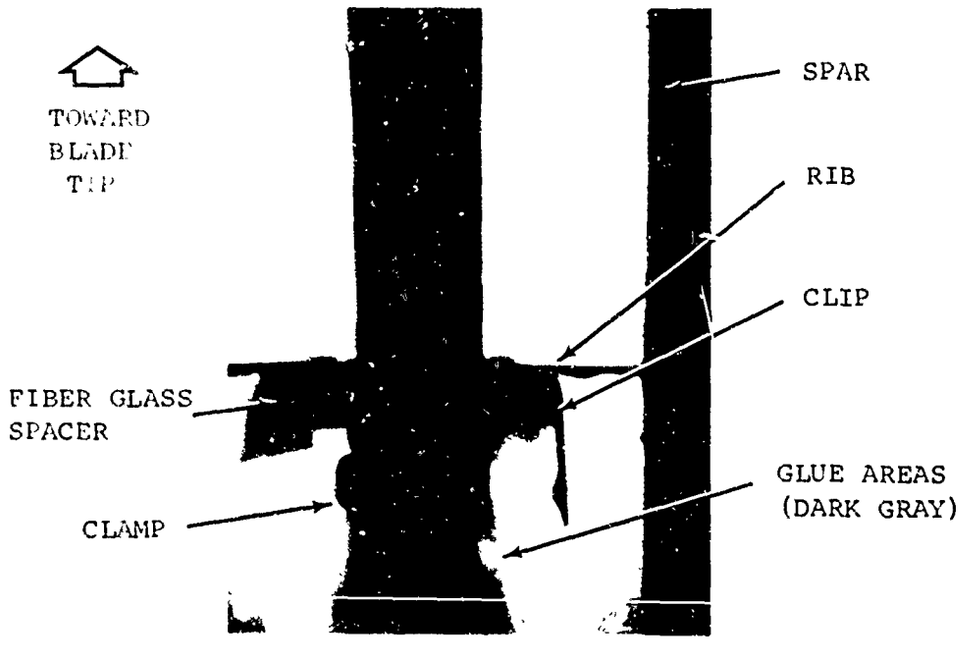

B. CLAMP AT STATION 260.58 (BOX 8)

Figure 4. Fluoroscopic Photographs of Typical Clamp Installations in Aft Rotor Blade.

washout of blade pitch between the center of rotation and the 354.6-inch radius of the blade tip.

Rotor blade instrumentation consisted of strain gages and pressure transducers. Strain-gage bridges were located as illustrated in Figure 1 to determine flapwise and chordwise bending moment distributions, as well as radial tension and torsional loads. These bridges were made using Budd type C6-141-350 gages. Absolute- and differential-pressure transducers were used to measure the rotor airloads over a chordwise and spanwise array of blade locations. Electrically paired absolute-pressure transducers were installed on the top and bottom of the spar section of the blade; the differential-pressure units were mounted on the fiber glass box sections. This arrangement was used so that it was not necessary to drill holes in the spars to provide differential-pressure ports. A plastic tube supported within the blade was used to port each differential transducer to the bottom blade surface. The transducers were attached to the blades by bonding the mounting tabs to the blade surface in the recesses provided in the fairing sleeves. An elastic adhesive, which allowed negligible strain transmittal from the blade, was used to mount the transducers. This installation provided flush mounting of the pressure transducers with little change in the airfoil dimensions.

The CH-47A blade design incorporates flapwise static-moment balance weights and chordwise balance weights which are used for blade tracking. As shown in Figure 5, chordwise balance can be achieved by adjusting the weight in the leading-edge cylinder, or by adding weights to either the leading-edge (L.E.) or trailing-edge (T.E.) studs. To expedite tracking of these heavily instrumented blades, the forward noninstrumented blades contained a quantity of lead tape in the tip covers. The aft noninstrumented blades also had additional chordwise balance weights bonded to the external surface of the tip trailing-edge boxes near the trailing-edge strip. These modifications were necessary to provide an adequate track within the limited capability of the production blade balance-weight design. The balance-weight configuration of the blades as flight-tested is summarized in Table I. These weights provided a flapwise static moment of 51,150 inch-pounds for the forward blades and 52,468 inch-pounds for the aft blades, within a quoted tolerance of ±1 inch-pound. The results of the blade whirl tower tracking will be discussed later.

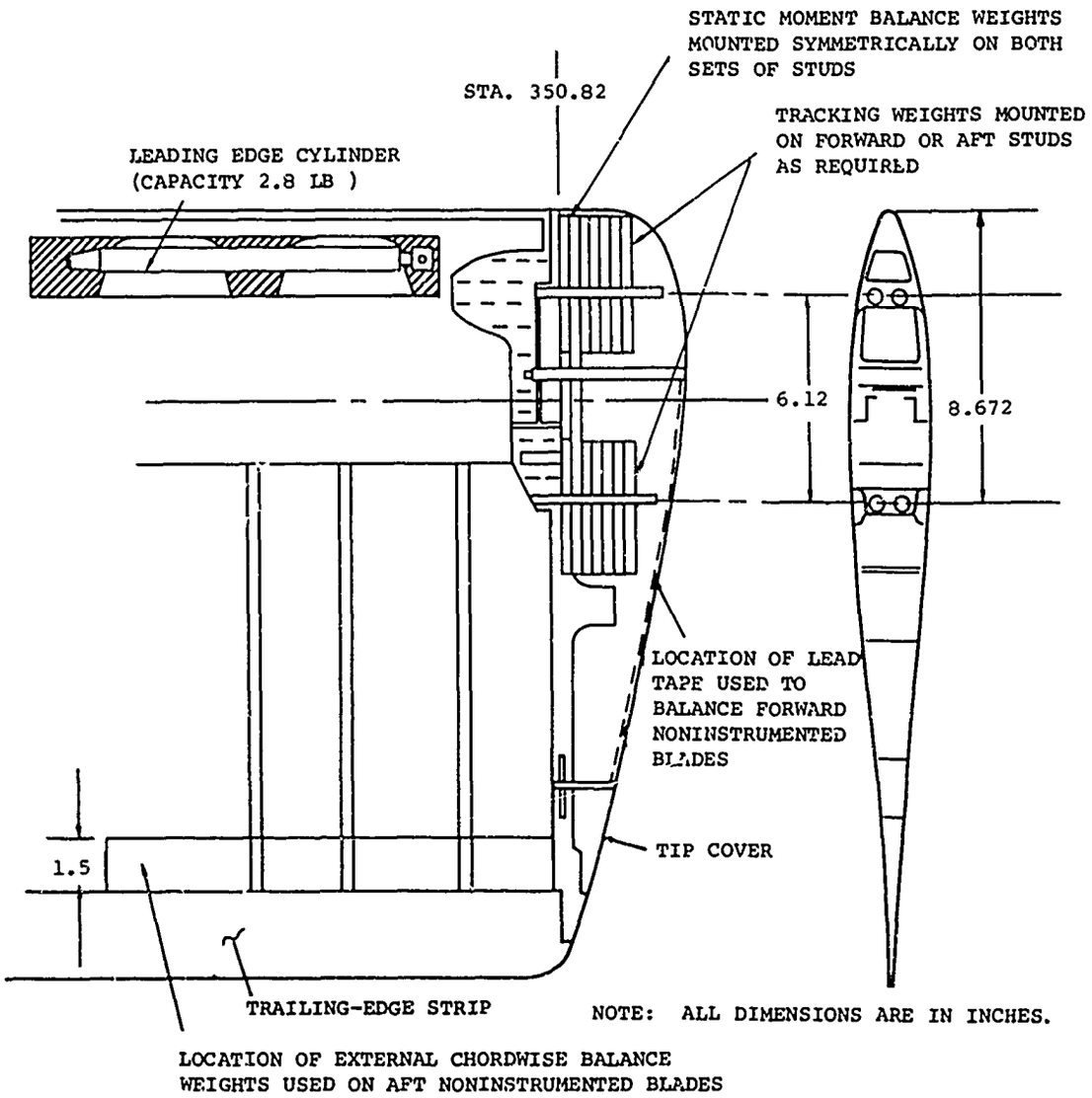

Figure 5. Rotor Blade Balance Weight Locations.

TABLE I

SUMMARY OF ROTOR BLADE BALANCE AND TRACKING WEIGHTS

Blade Serial No.	L.E. Cylinder Weight (lb)	Stud Weight (lb) L.E.	Stud Weight (lb) T.E.	Additional Weight Required for Tracking (lb)
		Forward Blades		
SK14412-1 (Instrumented)	2.8	5.38	0	0
A-1-416	2.8	8.145	8.145	1.0*
A-1-423	2.8	7.905	7.905	1.75*
		Aft Blades		
SK14412-2 (Instrumented)	2.8	2.85	0	0
A-2-254	0	7.425	7.425	2.3**
A-2-267	0	7.17	7.17	2.3**

* Weight added in form of lead tape to inside of tip cover.
**Weight added in form of stainless-steel strips bonded to the trailing edge of blade boxes 11 and 12.

The calculated physical properties of the airloads-instrumented blades, based on the measured thicknesses and weights of their constituent components, are given in Tables II and III; comparative noninstrumented blade properties are given in Tables IV and V. The instrumented blades were made with lightweight spars which provided a lower-than-standard weight and stiffness distribution as shown in Figure 6. The lower distributed weight was more than offset by the concentrated weights of the transducer installations and the clamps, clips, and wire loops of the instrumentation bundle. As a result, the noninstrumented blades contained the larger tip balance weights. It is believed that the variation between these blades is close to the maximum variation that is possible without causing excessive blade stresses or prohibitive vibrations.

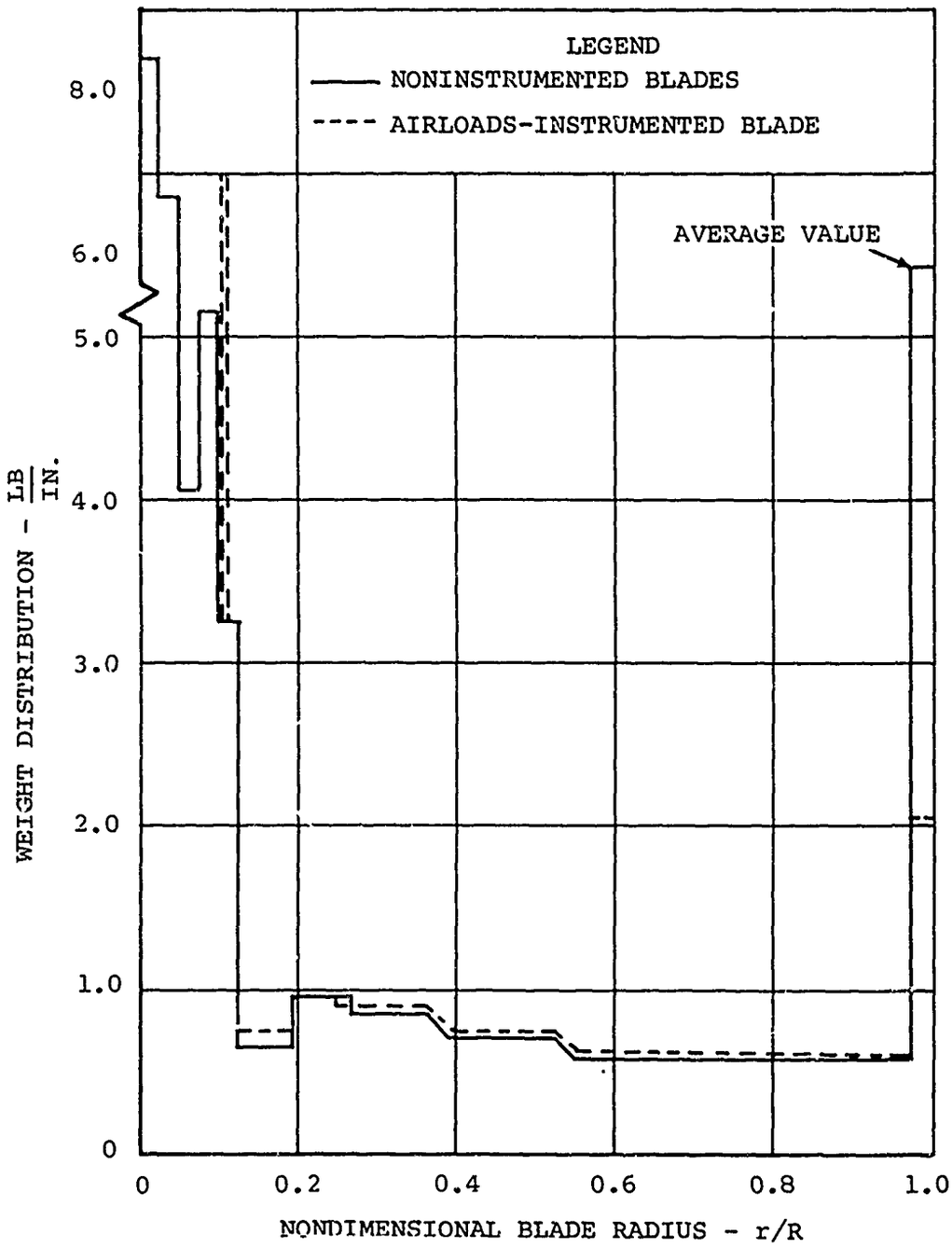

Figure 6. Spanwise Mass Distribution of Instrumented Blade and Noninstrumented Blades.

TABLE II

MASS PROPERTIES OF INSTRUMENTED ROTOR BLADES

Blade Span Location (inches)	Mass Distribution (lb per inch)	Location of Centroid from Leading Edge (inches aft)	Pitch Inertia Per Unit Span (lb-sec^2 x 10^2)
0-8.85	8.466	4.49	4.38
8.85-17.70	6.72	4.49	4.38
17.70-20.10	4.047	4.49	4.38
20.10-26.60	4.047	4.49	3.27
26.60-29.50	5.356	4.49	3.27
29.50-35.40	5.356	4.49	1.865
35.40-40.0	3.27	4.49	1.865
40.0 -40.05	7.03	4.49	1.865
40.05-45.0	3.27	4.49	1.865
45.0 -57.70	0.755	4.49	1.01
57.70-69.0	0.755	4.53	1.01
69.0 -86.6	0.9667	6.50	10.704
86.6 -89.6	1.175	6.50	13.431
89.6 -92.6	1.1129	6.50	13.431
92.6 -96.0	0.9046	6.50	10.704
96.0 -128.0	0.9046	5.32	5.961
128.0-137.0	0.9046	5.32	5.961
137.0-138.1	0.7573	5.46	5.508
138.1-141.1	0.9673	5.46	8.234
141.1-144.1	0.9613	5.46	8.234
144.1-186.0	0.7513	5.46	5.508
186.0-192.0	0.7513	5.46	5.508
192.0-195.0	0.8885	5.46	7.998
195.0-198.0	0.8317	5.69	7.998
198.0-239.0	0.6217	5.69	5.272
239.0-264.0	0.6283	5.80	5.272
264.0-267.0	0.8268	5.44	8.303
267.0-270.0	0.8228	5.44	8.303
270.0-274.0	0.6128	5.44	5.577
274.0-292.0	0.6128	5.44	4.791
292.0-297.0	0.605	5.38	4.791
297.0-303.0	0.815	5.38	7.517
303.0-315.0	0.605	5.38	4.791
315.0-321.0	0.815	5.38	7.517
321.0-334.0	0.605	5.38	4.791
334.0-336.0	0.605	5.38	6.048
336.0-342.0	0.815	5.38	6.048

TABLE II - Continued

Blade Span Location (inches)	Mass Distribution (lb per inch)	Location of Centroid from Leading Edge (inches aft)	Pitch Inertia Per Unit Span ($lb\text{-}sec^2 x10^2$)
342.0-344.5	0.815	5.38	6.048
344-5-345.0	0.815	5.38	8.774
345.0-347.0	2.268	5.38	8.774
347.0-350.5	2.268	5.38	7.517
350.5-354.3	2.058	5.38	8.412

Pitch inertia values include all root hardware that rotates on pitch bearings; moment reference is pitch axis.

TABLE III

STIFFNESS PROPERTIES OF INSTRUMENTED ROTOR BLADES

Blade Span Location (inches)	Flapwise Stiffness in Unit Span ($lb\text{-}in.^2 x10^{-6}$)	Chordwise Stiffness in Unit Span ($lb\text{-}in.^2 x10^{-6}$)	Torsional Stiffness in Unit Span ($lb\text{-}in.^2/radian \times 10^{-6}$)
0- 29.5	1159.0	365.0	69.7
29.5- 43.3	365.0	365.0	69.7
45.3- 59.5	218.0	218.0	69.7
59.5- 69.0	135.5	322.0	69.7
69.0- 96.0	58.2	416.0	59.0
96.0-137.0	58.2	1077.0	59.0
137.0-195.0	47.3	968.0	45.6
195.0-239.0	36.5	869.0	33.5
239.0-354.3	36.5	654.0	33.5

TABLE IV

MASS PROPERTIES OF NONINSTRUMENTED ROTOR BLADES

Blade Span Location (inches)	Mass Distribution (lb per inch)	Location of Centroid from Leading Edge (inches aft)	Pitch Inertia Per Unit Span (lb-sec^{2}x10^2)
0 - 8.85	8.466	4.49	5.92
8.85-17.70	6.721	4.49	5.92
17.70-26.60	4.047	4.49	5.92
26.60-29.50	5.356	4.49	5.92
29.50-35.40	5.356	4.49	1.865
35.40-45.0	3.27	4.49	1.865
45.0 -59.5	0.645	4.49	1.218
59.5 -69.0	0.645	4.315	1.218
69.0 -96.0	0.951	6.35	10.565
96.0 -128.0	0.863	5.288	5.746
128.0 -137.0	0.789	5.379	5.519
137.0 -156.0	0.7152	5.491	5.293
156.0 -186.0	0.7116	5.491	5.293
186.0 -195.0	0.6498	5.620	5.175
195.0 -241.5	0.5881	5.749	5.057
241.5 -250.0	0.5996	5.683	5.057
250.0 -265.5	0.5996	5.683	5.362
265.5 -274.0	0.5819	5.578	5.362
274.0 -286.0	0.5819	5.578	4.577
286.0 -292.0	0.5819	5.596	4.577
292.0 -312.72	0.5965	5.596	4.577
312.72-334.4	0.6267*	6.326*	9.006*
334.4 -345.2	1.1022*	4.263*	9.006*
345.2 -347.0	1.1022*	4.263*	14.18*
347.0 -350.82	0.6267*	6.326*	14.18*
350.82-354.3	5.8707*	5.599*	9.75*

* Data are average values between forward and aft blades.

TABLE V

STIFFNESS PROPERTIES OF NONINSTRUMENTED ROTOR BLADES

Blade Span Location (inches)	Flapwise Stiffness in Unit Span (lb-in.^{2}x10^{-6})	Chordwise Stiffness in Unit Span (lb-in.^{2}x10^{-6})	Torsional Stiffness in Unit Span (lb-in.x10^{-6})
0- 29.5	1159.0	365.0	69.7
29.5- 45.3	365.0	365.0	69.7
45.3- 59.5	176.5	270.0	69.7
59.5- 69.0	97.85	378.5	65.45
69.0- 81.5	60.2	640.0	61.16
81.5- 96.0	60.2	971.5	61.16
96.0-128.0	60.2	1098.0	61.16
128.0-131.5	49.75	1038.5	61.16
131.5-137.0	49.75	1038.5	54.5
137.0-186.0	49.30	979.0	47.85
186.0-189.5	43.80	930.5	47.85
189.5-195.0	43.80	930.5	41.69
195.0-265.5	38.30	882.0	35.53
265.5-354.3	38.30	685.0	35.53

ROTOR SHAFTS

The forward and aft rotor shafts were instrumented with strain gages for measuring torque and lift (tension), plus shear and moment in two perpendicular planes. Additional alternating-lift gages and several spare gages were installed. Epoxy-backed foil gages (Budd C6-141-350) were used, except for the alternating-lift gages which were P-type semiconductor gages (Baldwin-Lima-Hamilton SPB2-07-35-C6). These strain gages were installed as shown in Figure 7. Spare gages were provided to measure shear, torque, steady lift, and alternating lift. The strain gages on the aft rotor shaft were widely spaced along the vertical axis to increase the sensitivity of the shear bridges; the shorter length of the forward shaft prevented such wide placement. It should be noted that the rotor shaft azimuth angle given in Figure 7 is the angle measured in the clockwise direction when viewing either shaft from above.

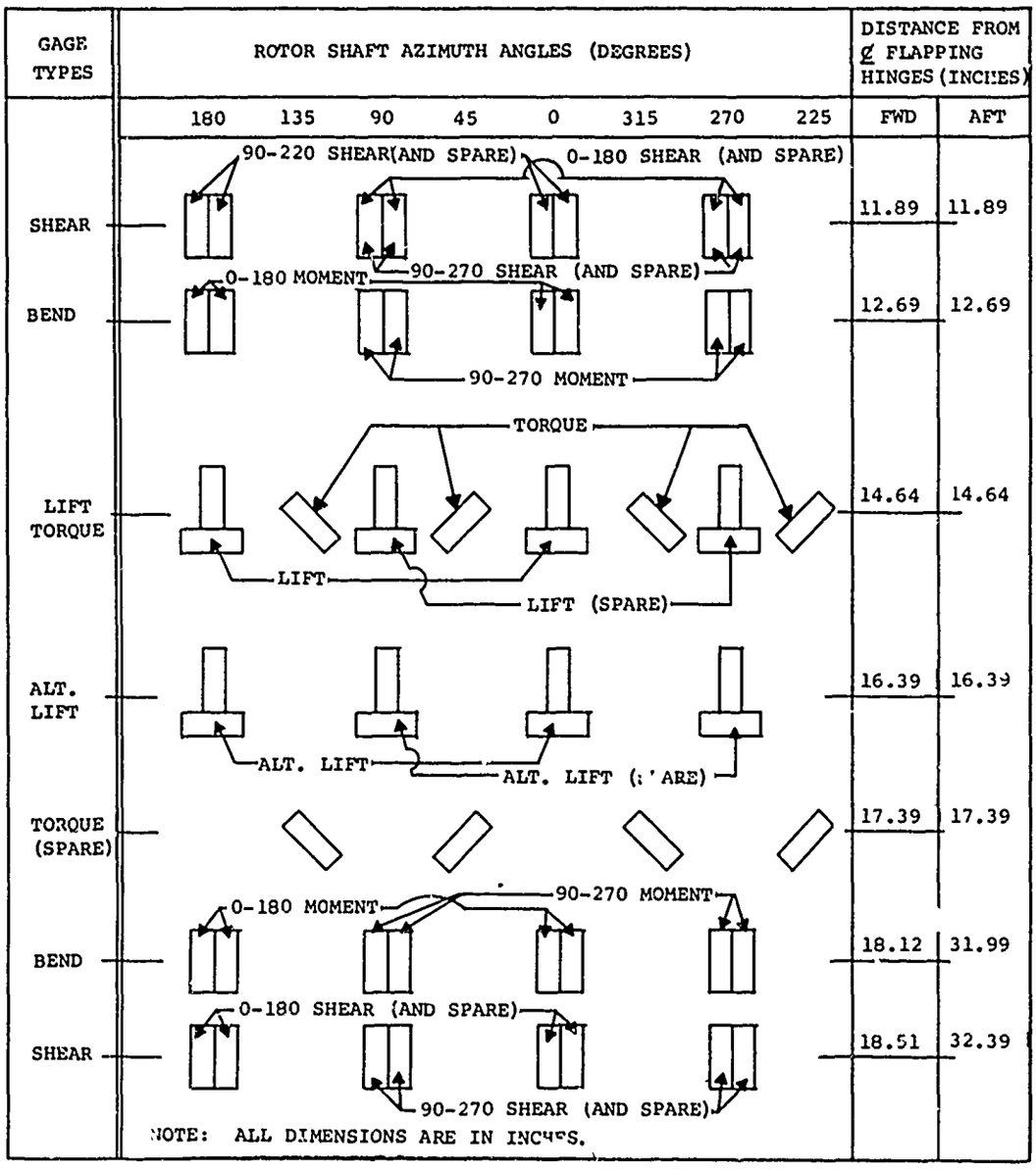

Figure 7. Rotor Shaft Strain-Gage Installation.

The instrumented rotor shafts were production CH-47A components on which the strain gages were mounted in the region shown in Figure 8. The CH-47A forward rotor shaft is a 1-piece stub shaft integral with the second-stage planet carrier of the forward transmission; it is splined to receive the forward rotor hub. The aft rotor shaft is a 3-piece unit consisting of a lower splined steel adapter which connects to the aft transmission, an intermediate aluminum section, and an upper steel adapter which is splined to the aft rotor hub. These three components are swaged together to form the aft shaft. One tooth is omitted from the splined upper end of each shaft to provide a datum for shaft angle measurements.

CONTROL SYSTEM COMPONENTS

Instrumentation for determining control system loads at each rotor consisted of a strain-gaged pitch link in the rotating control system and three strain-gage bridges which determined the nonrotating control system reactions. The two strain-gaged pitch links were connected to the instrumented blades. Nonrotating control loads were measured by strain-gage bridges on the actuator mounting lugs of the nonrotating swashplate and a strain-gaged fixed link in the longitudinal cyclic trim system. These components are shown in Figures 9 and 10 for the forward and aft rotors respectively.

The control system of the test aircraft was an experimental unit that had been used to develop an improved production control system. This unit is known as the SK system and is geometrically similar to the production control system that is used in aircraft which incorporate Engineering Change Proposal 140/190. This modification incorporates a control system with increased strength and rigidity.

Control of the aircraft in flight is provided through differential collective pitch of the two rotors and lateral cyclic control of each rotor. Simultaneous motions of the swiveling and pivoting actuators cause collective pitch changes; differential motions of these actuators produce lateral cyclic pitch changes. The parallelogram linkage of the longitudinal cyclic control system rotates on a yoke and is unchanged by collective or lateral cyclic pitch changes. Longitudinal cyclic pitch is used only for trim adjustment and is controlled through an electromechanical actuator.

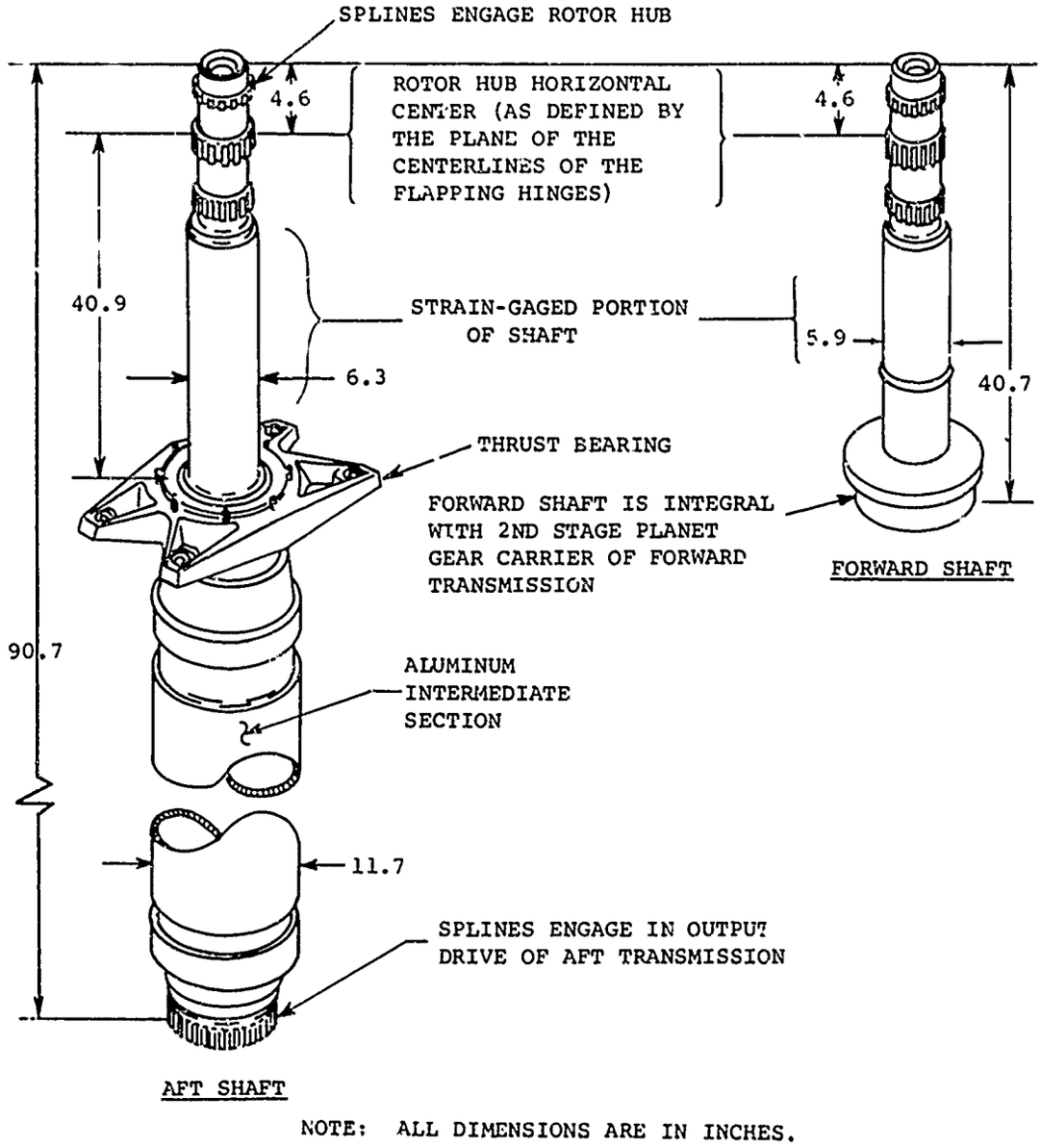

NOTE: ALL DIMENSIONS ARE IN INCHES.

Figure 8. General Arrangement of Instrumented Rotor Shafts.

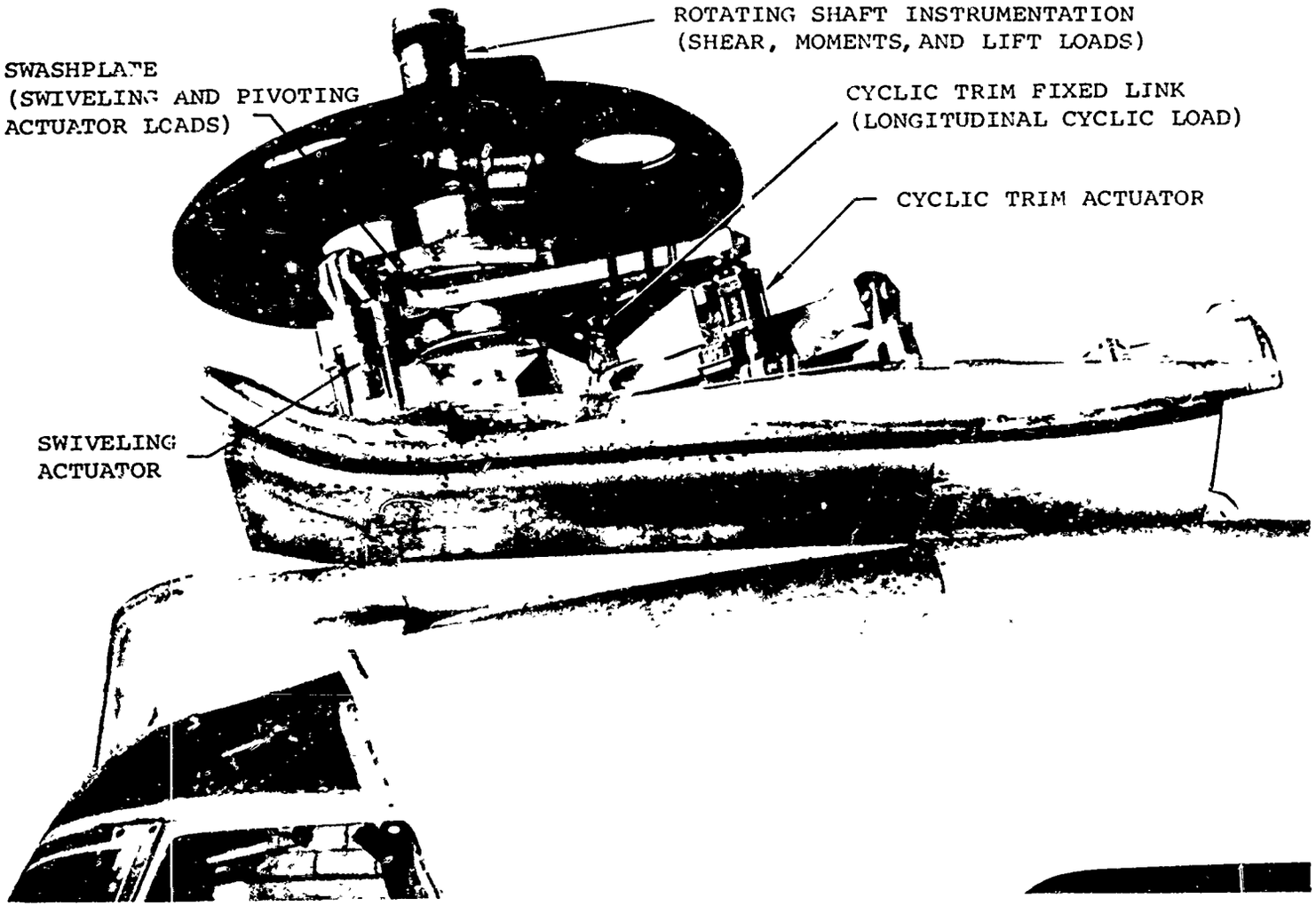

Figure 9. Installation of Forward Rotor Shaft and Control Instrumentation.

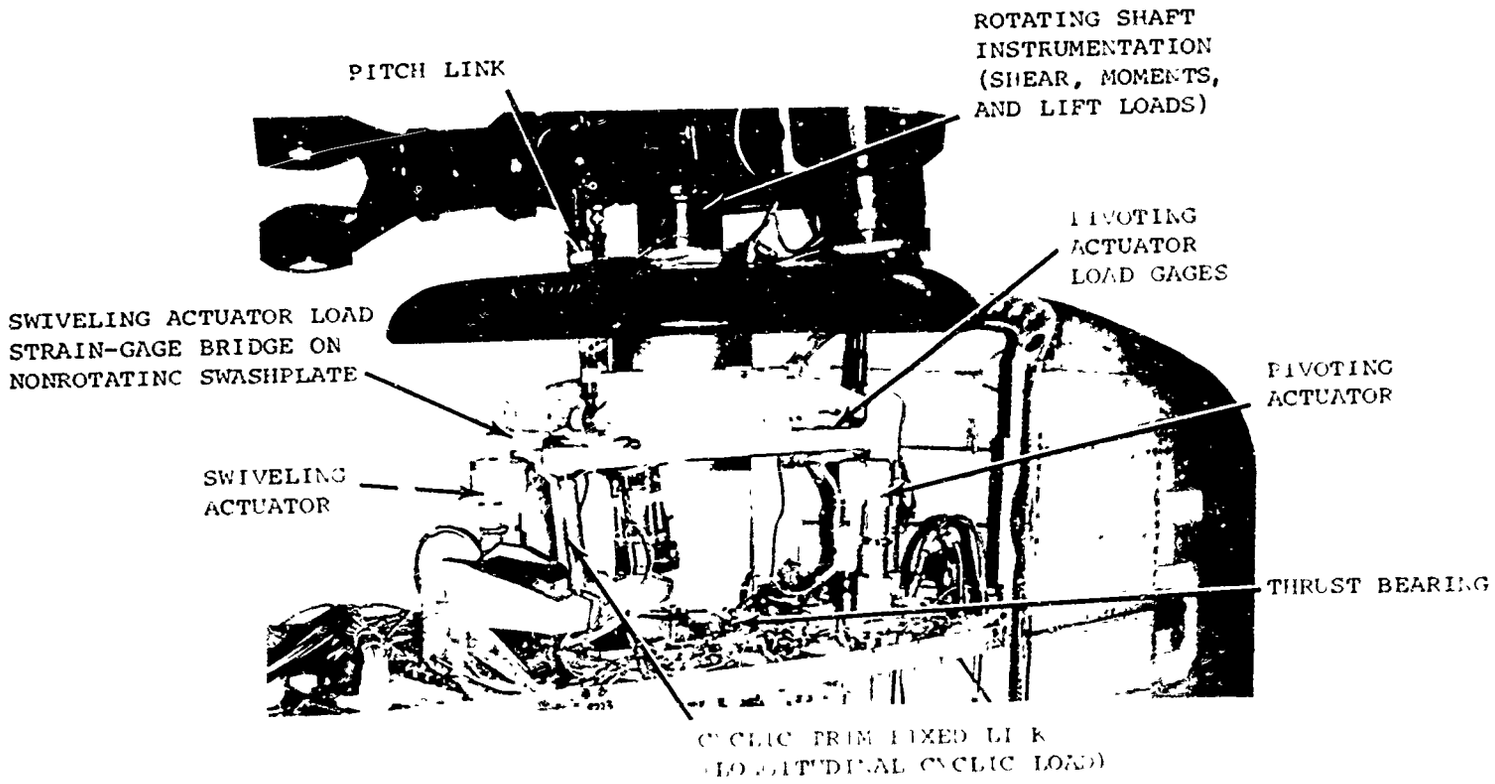

Figure 10. Installation of Aft Rotor Shaft and Control Instrumentation.

EXPERIMENTAL PROCEDURE

CALIBRATION OF ROTOR SHAFTS

The rotor shafts were calibrated, using several load combinations applied at various shaft reference angles, to determine interaction coefficients and the effect of varying azimuth position. In all cases the shaft was rotated in the fixture while the loads remained fixed. Shaft reference angles at which the loads were applied, together with the maximum values of the loads, are given in the summary of test conditions in Table VI. An inclinometer was used to measure all shaft angles. Primary calibration loads were applied in 13 equal increments to facilitate the determination of the most accurate calibration relation. Six increments of decreasing load were used to provide for definition of hysteresis. Measurements of the shaft deflection due to the calibration loads were used in the data analysis to further refine the calculation of the applied loads. Bending moments and torque were applied to the shaft by exerting equal and opposite forces a known distance from the centerline of the shaft, thus precluding the possibility of shear loads during these calibrations. Axial load (lift) calibrations were performed as quickly as possible to minimize the drift of the semiconductor strain gages that were used to record the alternating-lift data. Shear and bending interactions were investigated by applying shear loads at two points on the length of the shaft. With this exception, all calibration loads were applied at the top of the shaft. Figure 11 shows details of the test arrangements, including the shear load clamp and the torque and bending moment arms used to transmit loads to the shaft. All calibration loads were applied with hydraulic cylinders except for the bending moment loads, for which turnbuckles were used. In all cases, load cells (Baldwin-Lima-Hamilton Type U-1) connected to appropriate indicating equipment were used to measure and record the magnitude of the applied loads.

TABLE VI

SUMMARY OF ROTOR SHAFT CALIBRATION TEST CONDITIONS

Loading Descriptor (load identification)	Shaft Angle (degrees)	Primary Calibration Load	Maximum Value of Primary Load	Constant Interaction Loads
		Single Loads		
01	0	Lift	12,000 lb	None
08	45	Bending moment	$+10^5$ in.-lb	None
09	45	Bending moment	-10^5 in.-lb	None
		Combined Loads		
02	45	Shear at 3.5 in.*	5000 lb	Lift=6000 lb
03	45	Shear at 3.5 in.*	5000 lb	Lift=12,000 lb
04	225	Shear at 3.5 in.*	5000 lb	Lift=6000 lb
05	225	Shear at 3.5 in.*	5000 lb	Lift=12,000 lb
06	45	Shear at 12.0 in.*	5000 lb	Lift=12,000 lb
07	225	Shear at 12.0 in.*	5000 lb	Lift=12,000 lb
10	0	Torque	$\pm 80^5$ in.-lb	Lift=12.000 lb
11	Varied 0 to 360	Shear at 3.5 in.*	5000 lb	None

*Distance of applied shear load from top of shaft.

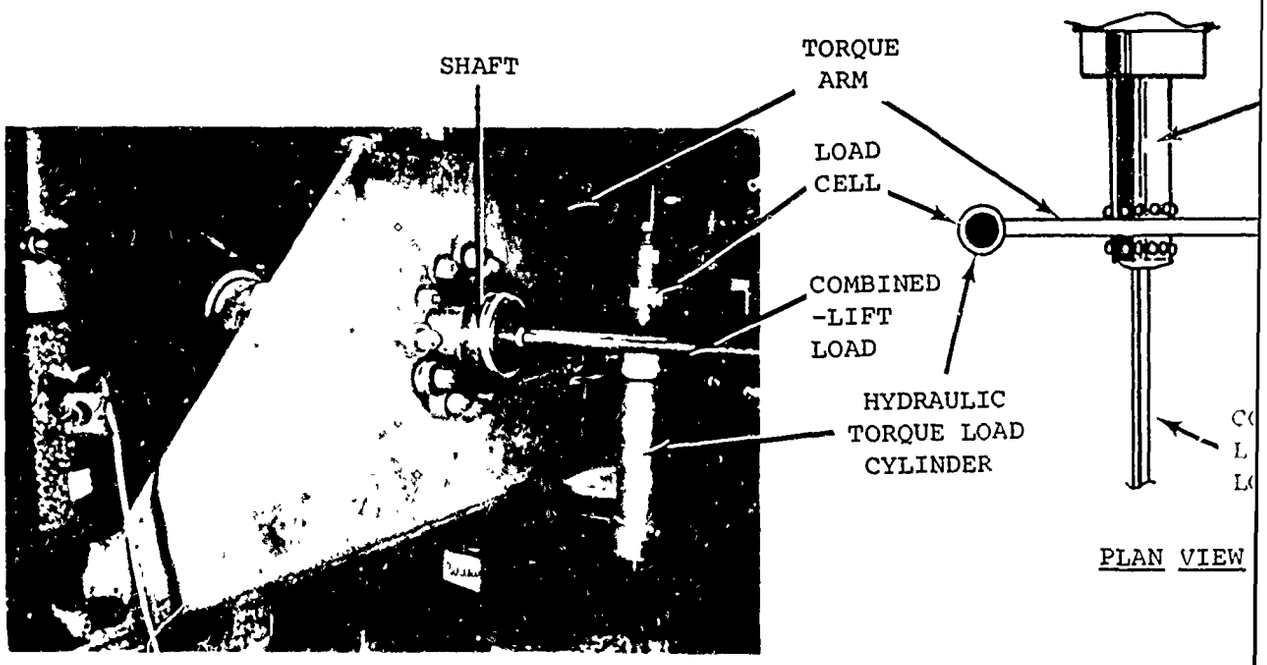

TORQUE - WITH LIFT - CALIBRATION

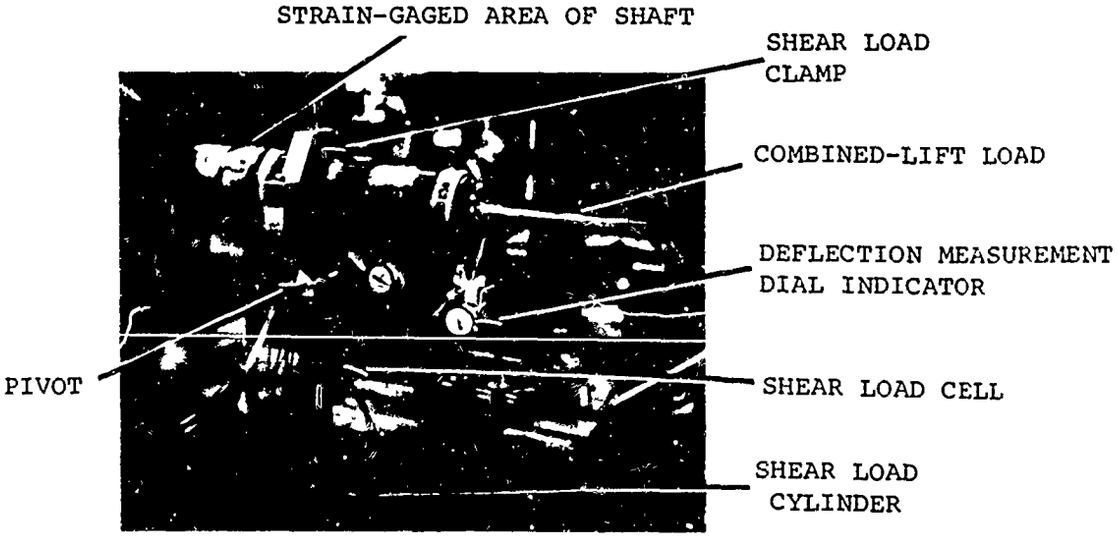

SHEAR - WITH LIFT - CALIBRATION

Figure 11. Calibration of Lift, Forward Rotor Shaft.

A

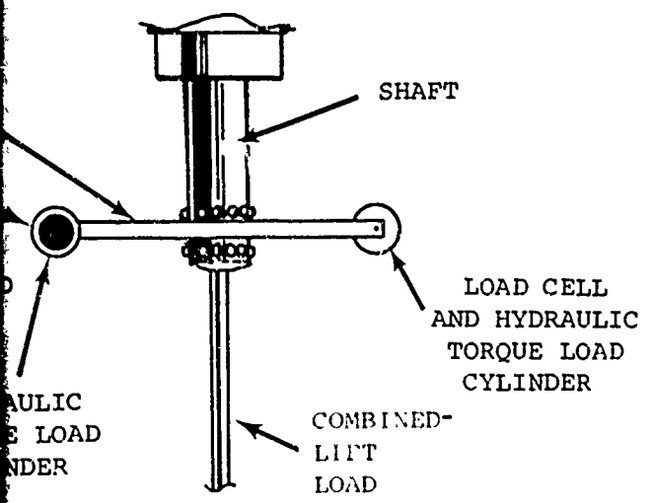

PLAN VIEW

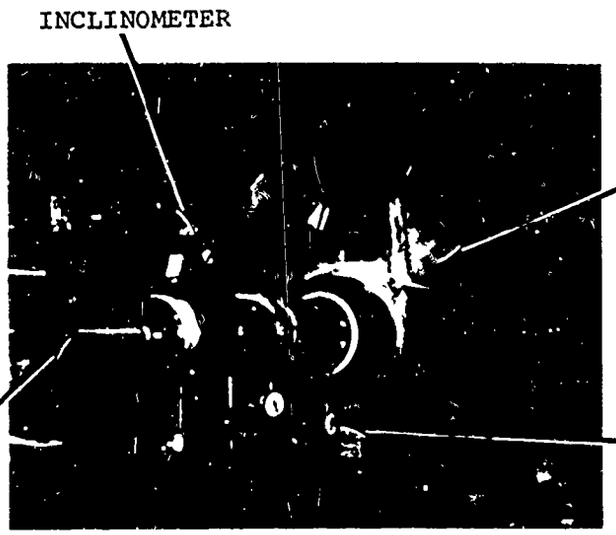

LIFT (SINGLE-LOAD) CALIBRATION

LOAD

ASUREMENT
R

LL

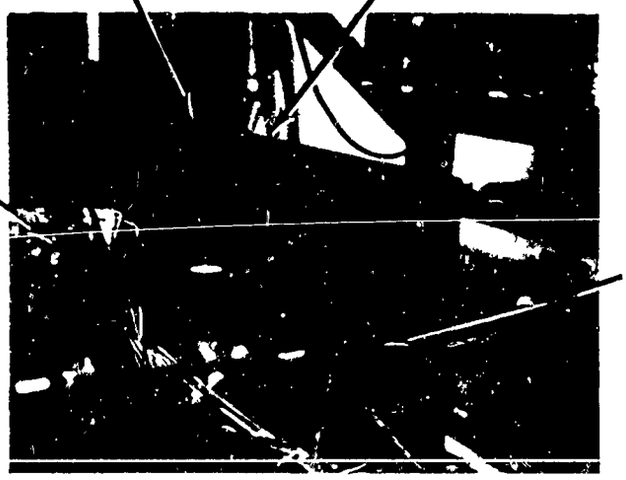

NORMAL AND INPLANE PURE
BENDING (SINGLE-LOAD) CALIBRATION

libration of Lift, Shear, and Moment Gages on
rward Rotor Shaft.

B

All strain-gage outputs from the rotor shaft calibration were read from strain indicators (Baldwin-Lima-Hamilton Type SR4 or Budd Model 350). Two 10-position switching units were used so that the output of all strain gages could be shown on two indicators. The data were handwritten for subsequent card-punching as inputs to the data analysis program. The output signals from the more sensitive semiconductor strain gages were attenuated, using a Baldwin-Lima-Hamilton SR4 strain converter, to a level equivalent to that of the foil gages to permit use of the SR4 indicator. Calibration load magnitudes were tabulated for subsequent cardpunching, using the load cell output signals which were also transmitted to the strain indicators. Shaft deflection data were recorded using dial indicators located as shown in Figure 11.

ROTOR BLADE TENSION AND MOMENT GAGE CALIBRATIONS

Due to the complicated structural cross section and the very high centrifugal loading of the rotor blades, it was suspected that large interactions would occur in the gage outputs. This was especially true for the torsion and chordwise bending gages for the reasons given, and was aggravated by the relatively low sensitivity of the chordwise bending gages. However, it would have been prohibitively expensive to simulate the 70,000- to 90,000-pound centrifugal force loading on the blade for a static calibration. The tip weight fitting is the only fitting on the blade through which such a load could be applied. It was decided to make a combined-loads calibration using the maximum allowable radial load (4000 lb) which could be applied to the tip fitting, with substantiation to higher loads provided by single-load calibrations and whirl testing. All interactions were determined in the combined-loads tests, with the single-load calibrations and the whirl testing substantiating the magnitude and linearity of the primary coefficients.

For the combined-loads calibration, it was decided to support the blade as a simple beam using the standard blade root hardware and a single point support (no moments) at the blade tip. Restraint of the outboard end of the blade was provided by a strap and ballast-weight arrangement. These support fittings and the various load-application devices are shown in Figure 12. Note that the root end hardware provides two orthogonal hinges and a blade pitch motion pivot. The rotor blade tip support consisted of steel straps attached to the blade tip

through a ball joint and a fitting attached to the blade tip balance-weight studs. Support straps were mounted to the overhead structure of the fixture, with separate straps connected to a 4000-pound ballast weight which prevented excessive chordwise blade motions. Steel clamps fitted to the blade cross section were used to transmit the applied loads to the blade spar. Ball joints or similar devices were used at each fitting to minimize friction.

The combined-loading technique included the simultaneous application of flapwise, chordwise, torsional, and radial tension loads using the load values given in Table VII. As shown in Figure 12, all blade calibration loads were applied from fixed, well-defined points, or by weights. Primary calibration load values were applied in 13 equal increments of increasing load. All values were also recorded as the loads were incrementally removed to check hysteresis. Since flight loads are always combined loads, this method of calibration, with proper data analysis, provided for a more accurate and complete measure of the flight loads. The single-calibration loads given in Table VIII were applied to calibrate the strain gages to the anticipated in-flight loads. Due to blade stress considerations, this was not possible in the combined-loads arrangement for some strain-gage locations. Single loads thus provided some definition of the upper end of the strain-gage calibration curves. Also, the data obtained from the individual-load calibrations provided a measure of the increase in accuracy that was achieved with the combined-loads calibration method. The blade was supported as a cantilever beam for the single-loads tests.

TABLE VII
ROTOR BLADE COMBINED-LOADS CALIBRATIONS

	Primary Load			Interaction Loads			
Load. Descr.	Type	Point of Applic. r/R	Maximum Load (lb or in.-lb)	Type	Point of Applic. r/R	Load (lb or in.-lb)	Purpose
*01/13	F	0.30	600	C	0.50	700	Calibrate inbd. flap bending gages
				Tor.	0.30	5000	
				Ten.	1.00	4000	

TABLE VII - Continued

Load. Descr.	Primary Load Type	Point of Applic. r/R	Maximum Load (lb or in.-lb)	Interaction Loads Type	Point of Applic. r/R	Load (lb or in.-lb)	Purpose
*02/14	F	0.30	600	C Tor. Ten.	0.50 0.30 1.00	350 2000 2000	Calibrate inbd. flap bending gages
*03/15	F	0.80	250	C Tor. Ten.	0.50 0.30 1.00	700 5000 4000	Calibrate outbd. flap bending gages
*04/16	F	0.80	250	C Tor. Ten.	0.50 0.30 1.00	350 2000 2000	Calibrate outbd. flap bending gages
*05/17	F	0.70	250	C Tor. Ten.	0.50 0.30 1.00	700 5000 4000	Determine effect of flap shear on flap bending gages
*06/18	C	0.50	700	F Tor. Ten.	0.80 0.30 1.00	250 5000 4000	Calibrate chord bending gages
*07/19	C	0.50	700	F Tor. Ten.	0.80 0.30 1.00	100 2000 2000	Calibrate chord bending gages
*08/20	C	0.40	700	F Tor. Ten.	0.80 0.30 1.00	250 5000 4000	Determine effect of chord shear on chord bending gages
09	Ten.	1.00	4000	F C Tor.	0.80 0.50 0.30	250 700 5000	Calibrate radial tension gage
10	Ten.	1.00	4000	F C Tor.	0.80 0.50 0.30	100 350 2000	Calibrate radial tension gage

TABLE VII - Continued

Load. Descr.	Primary Load Type	Point of Applic. r/R	Maximum Load (lb or in.-lb)	Interaction Loads Type	Point of Applic. r/R	Load (lb or in.-lb)	Purpose
*11/21	Tor.	0.30	5000	F	0.80	250	Calibrate torque gages
		0.80	5000	C	0.50	700	
				Ten.	1.00	4000	
*12/22	Tor.	0.30	5000	F	0.80	100	Calibrate torque gages
				C	0.50	350	
				Ten.	1.00	2000	

*Noted calibrations were repeated with the primary load applied in the negative direction. The higher loading descriptor value denotes the negative load test conditions.

F = Flap C = Chord Ten. = Tension Tor. = Torsion

TABLE VIII
ROTOR BLADE SINGLE-LOAD CALIBRATIONS

Loading Descriptor	Load Factor	Point of Application	Maximum Load
*23/27	Flap	r/R=1.00	100 lb
*24/28	Chord	r/R=0.80	100 lb
*25/29	Torsion	r/R=0.30 and r/R=0.80	5000 in.-lb and 5000 in.-lb
26	Tension	r/R=1.00	4000 lb

*Noted loads were also applied in the negative direction. The higher value of the loading descriptor denotes the negative load test conditions.

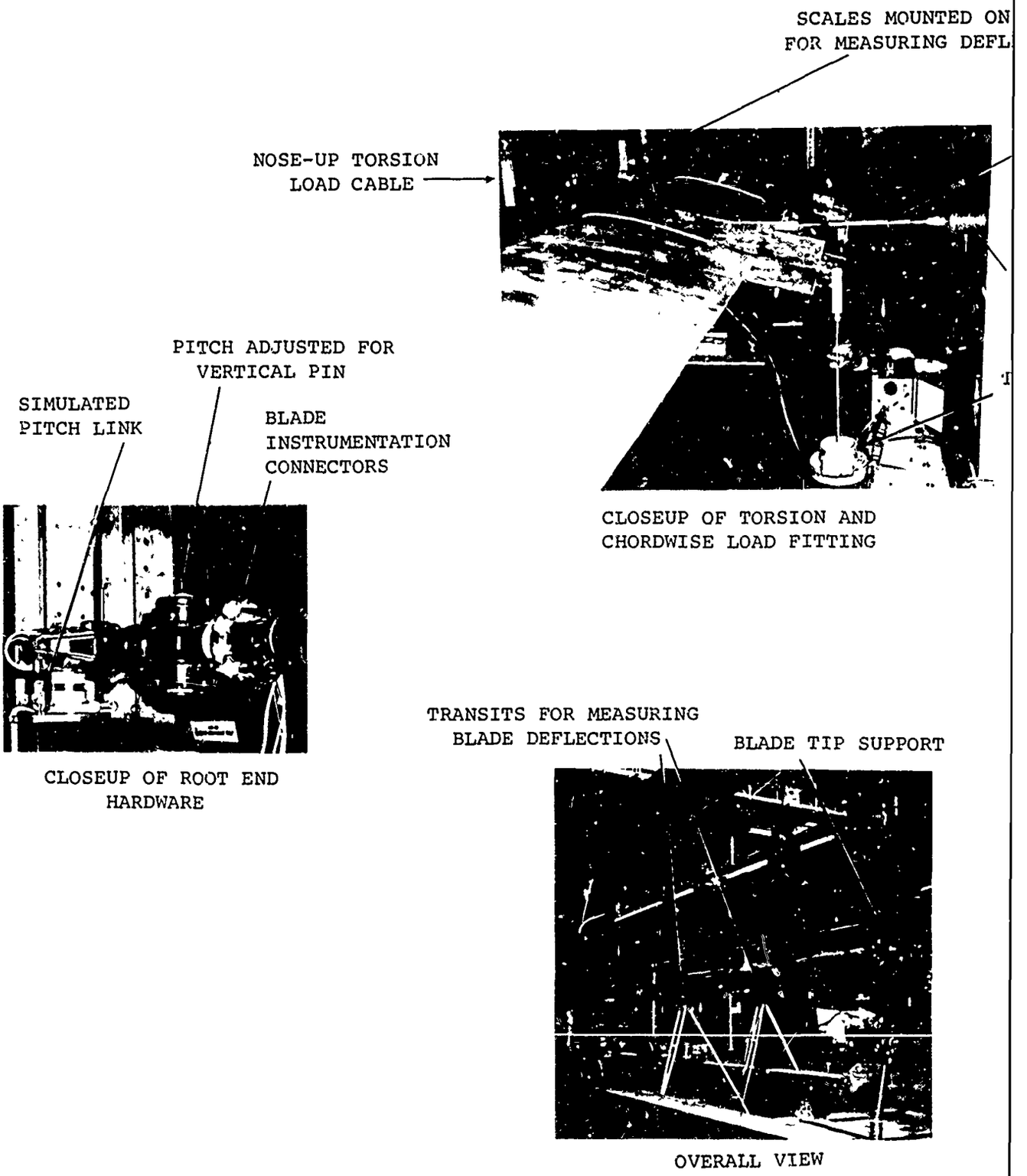

Figure 12. Test Fixture for Calibration of Rotor Blades und

A

SCALES MOUNTED ON BLADE
FOR MEASURING DEFLECTIONS

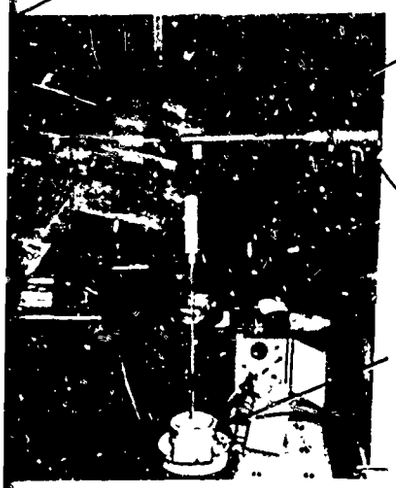

CHORDWISE LOAD
TURNBUCKLE

LOAD CELL

TORSION LOAD
WEIGHTS

OF TORSION AND
SE LOAD FITTING

TIP FITTING - ALLOWS TORSION
MOTION OF BLADE AND CHORDWISE
MOTION OF BLADE AND STRAPS

UPPER
SUPPORT
STRAPS

AXIAL TENSION
LOAD CYLINDER

BLADE

LOAD CELL

LOWER
SUPPORT
STRAPS

BALLAST WEIGHT
(RESISTS DEFLECTION
OF BLADE AXIS UNDER
CHORDWISE LOAD)

CLOSEUP OF TIP FITTING
AND BALLAST WEIGHT

BLADE TIP SUPPORT

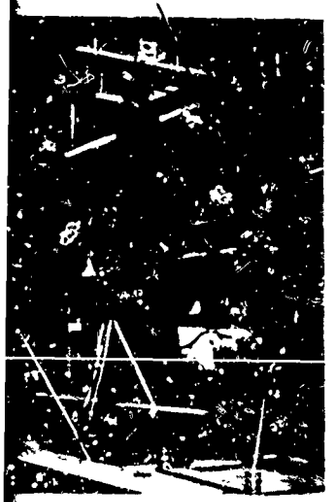

VERALL VIEW

ration of Rotor Blades under Combined Loads.

B

The calibration data analysis included a check of the correctness of the load-application techniques and elastic-deflection analysis through the use of measured blade deflections. For this purpose, steel scales with graduations of 0.01 inch were attached to the loading clamps. Surveying transits with magnification of 18X were used to record the deflection of the blade at the point of application of the primary calibration load.

The data acquisition system employed in the static blade calibration was capable of automatically conditioning and recording the 15 channels of strain-gage data. The data were amplified, filtered, and scanned by a high-speed, direct-readout, digital voltmeter. The voltmeter had a binary output which was fed into a converter, which converted the data to decimal equivalents and stored it until the program control commanded the summary punch (IBM 526) to record the data on punched cards.

Whirl testing of the rotor blades on the tower shown in Figure 13 was required to test the structural integrity of the blades functionally, and to ensure that the blade balance would produce acceptably low aircraft vibration. This testing was also used to perform a high-σ load calibration of the blade axial tension gages through the centrifugal force loads. While this calibration was compromised by the fact that all interaction on these gages was assumed to be negligible, this procedure was necessary, since the provision of adequate attachments to simulate the required 90,000-pound load in the blade would have been prohibitively expensive. The blade was static-balanced prior to whirl testing so that the blade static moment, $\sigma(\beta)$, was accurately known. The centrifugal force (CF) in the blade at the gage station could then be accurately determined as:

$$CF = \Omega^2\left[\sigma(\beta) - \sigma(\beta_R)\right] \tag{1}$$

where

Ω = rotational speed
$\sigma(\beta_R)$ = estimated static mass moment of blade root fittings.

The blade tension gage output was indicated on a strain indicator (Budd Model P-350) using the whirl tower slipring assembly to transmit the signals from the rotating blade to the stationary equipment. Recordings were taken for 204, 215, 230, and 260 rpm values with the blades in flat pitch (2 degrees at

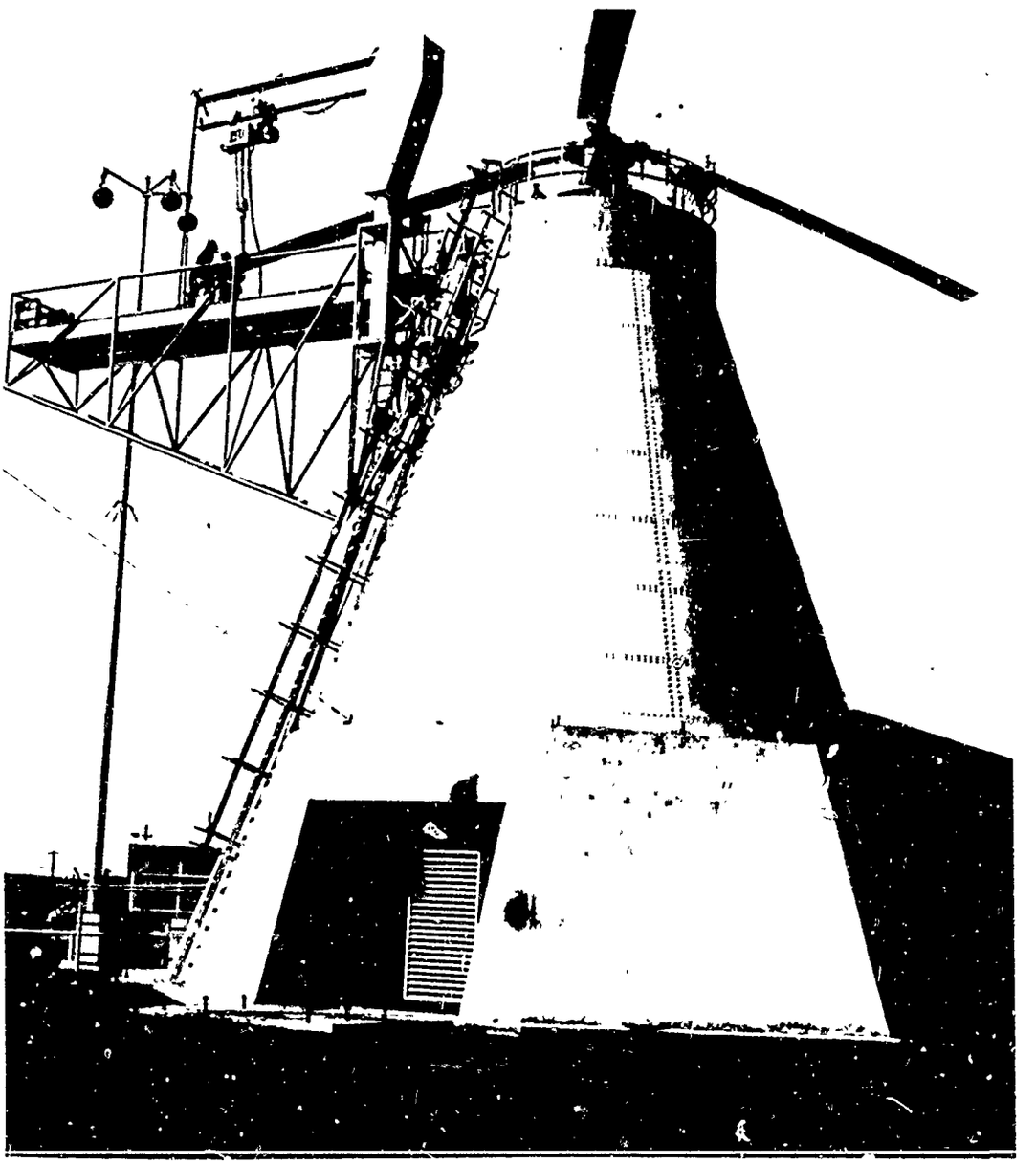

Figure 13. Rotor Blade Whirl Tower.

blade station 265). This test was also repeated with the blades installed on the test helicopter, making use of the in-flight recording system to measure the output of the tension gages.

CONTROL COMPONENT CALIBRATIONS

The instrumented control components were subjected to tension and compression calibration loads to a maximum of 2000 pounds. The method of load application for the swashplate gages is illustrated in Figure 14. Load magnitudes were monitored using load cells connected to appropriate indicating equipment. Strain-gage output signals were tabulated for subsequent use in the calibration data analysis.

CALIBRATION OF AIRFRAME RESPONSE ACCELEROMETERS

The airframe response accelerometers (Systron-Donner Model 4310A) were tested dynamically for frequency response and phase shift. Static tests were also made to determine hysteresis, case alinement, and nonlinearity. A highly accurate accelerometer (Kistler Servo Accelerometer Model 350M) was used as a reference for these tests. This reference accelerometer had the following characteristics:

Frequency response = flat, 0 to 600 cps
Phase shift = ±2° up to 50 cps
Maximum nonlinearity from best straight line = 0.0208 feet per second^2
Maximum hysteresis plus nonrepeatability = 0.0193 feet per second^2

Dynamic tests of the accelerometers were performed with the equipment shown in Figure 15. Test data were obtained at 7, 10, 15, 20, 30, 40, 50, 70, 100, 150, 250, and 400 cycles per second. Instrumentation included a frequency analyzer (Spectral Dynamics Model SD 101) and a phase meter (Action Laboratories Type 320-AB). The phase data obtained were based on the output of the reference accelerometer (Kistler) which was known to have less than a 2-degree phase shift over the range of 0 to 50 cycles per second.

The static tests were performed with a tilt table to vary the angle of the accelerometers. The applied acceleration was then equal to the cosine of the angle of the sensitive axis to the vertical multiplied by the acceleration of gravity.

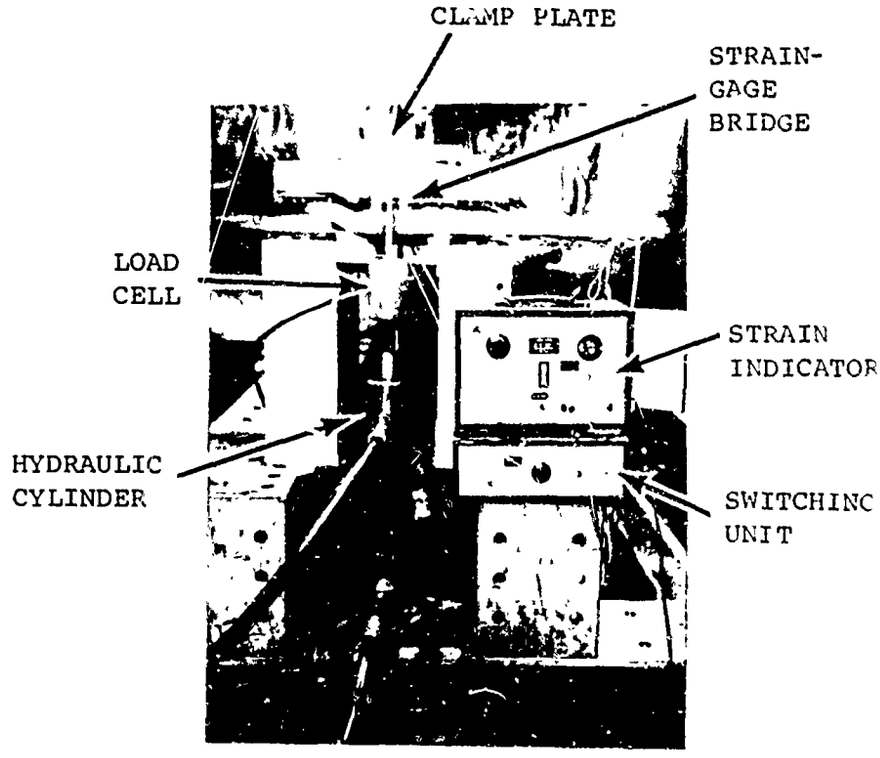

Figure 14. Calibration of Swashplate Control Actuator Mounting Load Gages.

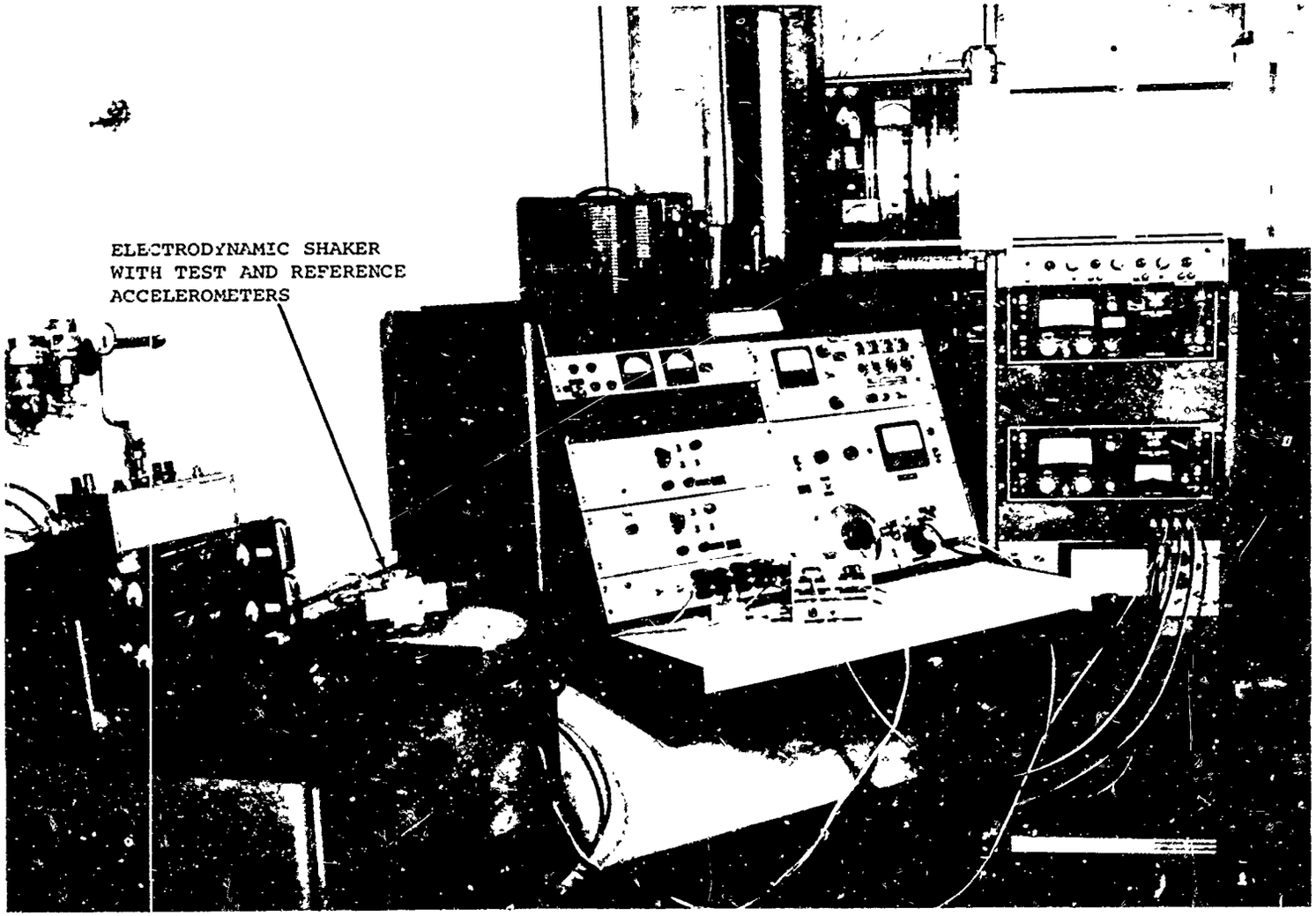

Figure 15. Dynamic Calibration Equipment for Aircraft Accelerometers.

A plate was designed to enable 14 accelerometers to be tested against the standard in one operation, using the equipment shown in Figure 16. The accelerometer output signals were routed to a 48-channel scanner and a digital voltmeter. The voltmeter output was automatically punched on IBM cards and printed on tape. The reference accelerometer output was measured by means of a self-balancing potentiometer and was manually recorded on an IBM card. The data cards were then sent to the central computer for data analysis.

INTEGRITY AND FUNCTIONAL WHIRL TESTING OF BLADES

Each set of one instrumented blade and two noninstrumented blades was mounted on the whirl tower and tested at different rotational speeds and pitch settings. Optical height measurements were made to determine the relative tracking positions of the three blades. Blade tension gage output and whirl tower control system loads were measured.

To ensure structural integrity, fluoroscopic photographs were made before and after whirl testing. The blades were rotated at the maximum allowable flight speed of 260 rpm. The initial test of the forward instrumented blade at this speed resulted in a wire slippage after 15 minutes. Modifications were made to the aft instrumented blade to prevent a similar occurrence, after which the aft blade set was tested successfully for 2 hours at 260 rpm. The modified forward blade was then tested at the same speed for 15 minutes with no further difficulty.

AIRLOAD PRESSURE TRANSDUCER FUNCTIONAL TESTS

The airload pressure transducers which were to be used for measuring rotor blade pressures were tested to determine repeatability, nonlinearity, hysteresis, temperature effects, and acceleration effects. Temperature effects on the reference zero and on sensitivity were investigated, since there would be a large variation (70 degrees F) between the hangar temperature and the temperature at the test altitude (5000 feet). Acceleration effects were investigated because of the large magnitudes of acceleration due to rotation (100 to 400 g, cross-axis) and to blade flapping and bending (10 to 30 g, normal). The actual calibration of these transducers was performed after the transducers were installed on the blades. These in situ (as installed) calibrations used the in-flight signal-conditioning modules and provided for the adjustment of the standardizing resistor against a reference pressure.

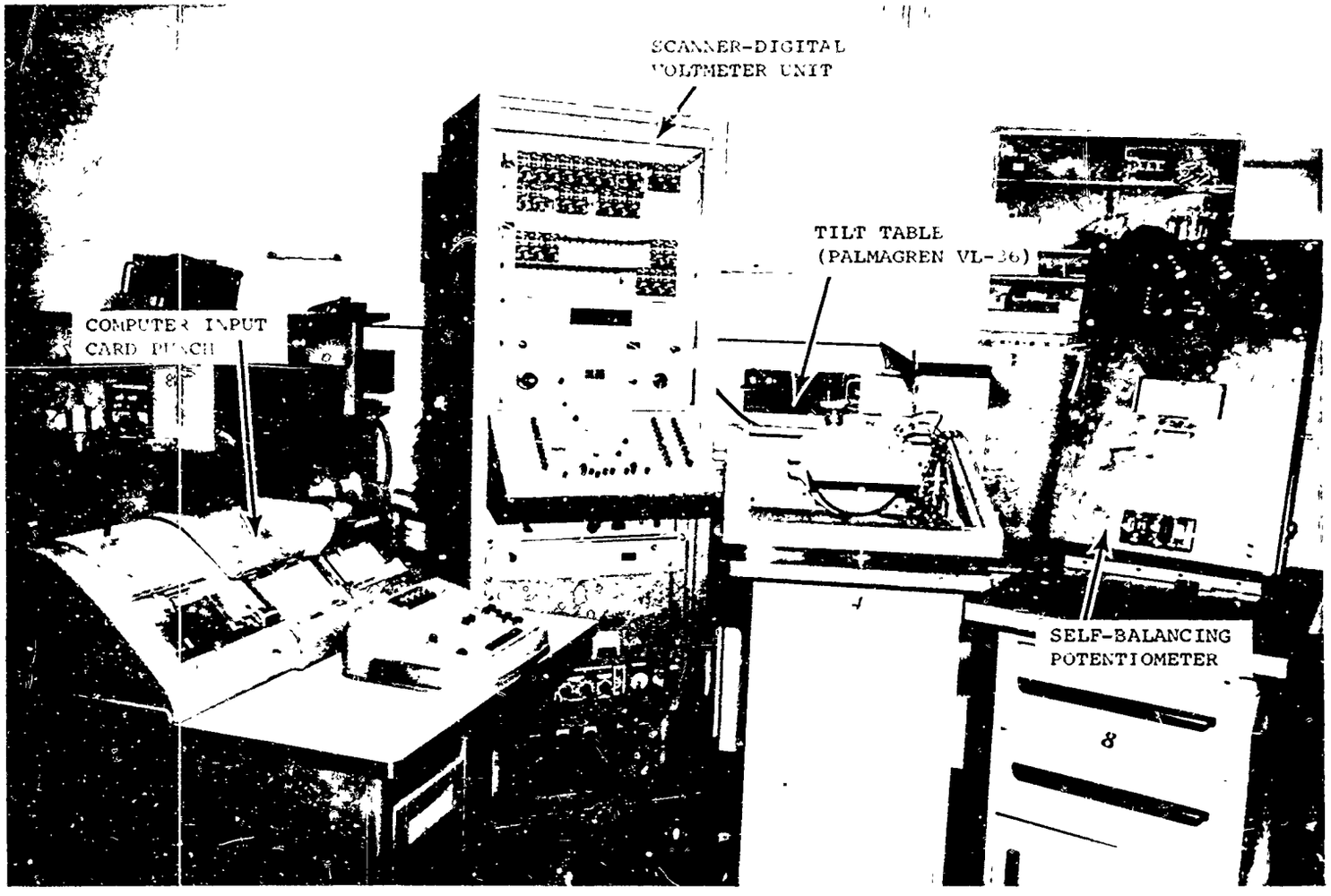

Figure 16. Static Calibration Equipment for Aircraft Accelerometers.

For the repeatability, linearity, and hysteresis calibration, the transducers were mounted in individual aluminum fixtures in a pressure chamber (see Figure 17). The port of each differential-pressure transducer was connected to a pressure manifold inside the chamber. The pressures inside the chamber and the manifold were independently controlled. Electrical connections were made with spring contacts held against the solder terminals on the transducer paddle. The applied air pressure was monitored with the pressure standards shown in Table IX. Twelve transducers were tested at one time using a bridge power supply, individual strain-gage balance modules, a 48-channel scanner, and a digital voltmeter. The accuracy of this sytem is ±0.25 percent of the reading with a resolution of one microvolt. The bridge voltage and the transducer output due to application of a shunt standardizing resistor were recorded at the beginning and end of each calibration. The transducer output was recorded for a minimum of eight incremental changes in air pressure, both increasing and decreasing, through the transducer range.

TABLE IX
PRESSURE STANDARDS USED FOR TRANSDUCER CALIBRATIONS

Transducer Range	Pressure Standard	Accuracy of Standard	Resolution of Standard
5-20 psia	Pressure cell system	±0.25% of indication (max.=±0.005 psi)	5×10^{-4} psi
±2 psid	Water manometer	±0.01 psi	10^{-3} psi
±5 and ±10 psid	Mercury manometer	±0.05 psi	10^{-2} psi

A temperature chamber (Wyle), which was heated electrically and cooled by gaseous evaporation, was used to determine temperature effects. The aluminum pressure chamber was installed in the temperature chamber using the same pressure standards and readout equipment as were used for the linearity and hysteresis calibration. A mercury-filled glass thermometer indicated the temperature of the chamber. The pressure was set to zero psid for the differential-pressure transducers and normal atmospheric for the absolute-pressure transducers during

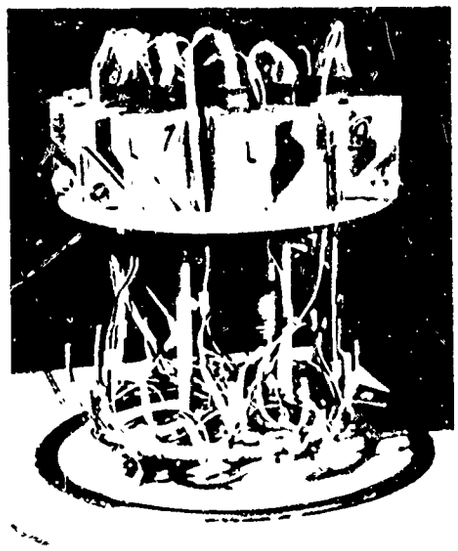

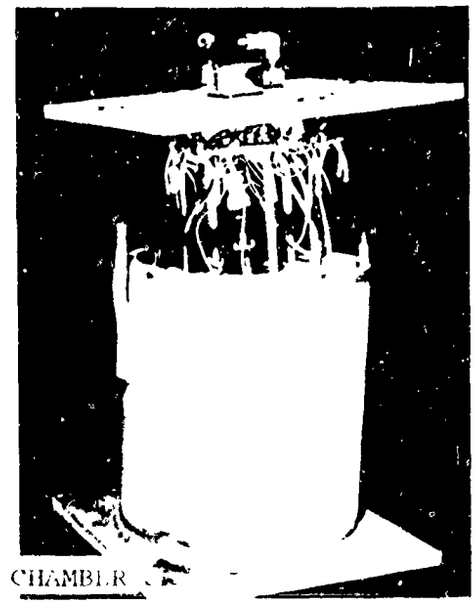

A. PRESSURE CHAMBER

TEST COMPONENTS
ASSEMBLED TO UNDERSIDE
OF PRESSURE CHAMBER LID

PRESSURE CHAMBER
ASSEMBLY

RECORDING
SYSTEM

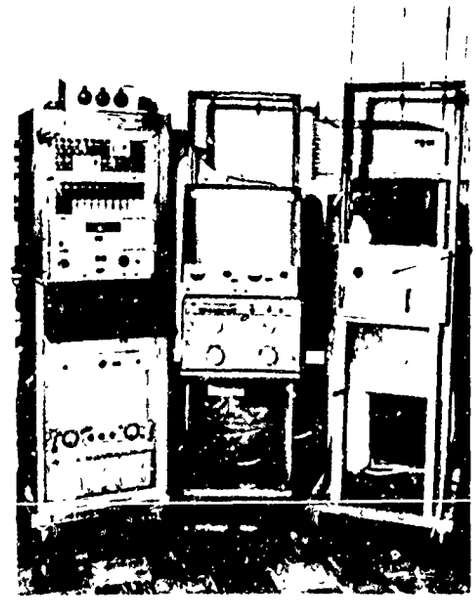

TEMPERATURE
CHAMBER

B. TEST EQUIPMENT

Figure 17. Airload Pressure Transducer Test Equipment.

the calibration of the temperature effect on zero position. Ten minutes or more after the temperature had stabilized in the chamber, the bridge voltage and the transducer output were recorded for 10-degree F step changes in temperature from 0 to 80 degrees, and back to 0 degrees in a single step. Temperature effects on sensitivity were determined by recording bridge voltage and transducer output at the extremes of the transducer range at 0 degrees F, at 125 degrees F, and again at 0 degrees F. Once again no data were recorded until 10 minutes or more after the temperature inside the chamber had stabilized.

Acceleration sensitivity of typical pressure transducers was determined by using the shaker and related equipment which were used for the accelerometer tests.

DYNAMIC RESPONSE TESTING OF BLADE

The systematic measurement of dynamic airloads on a rotor required complete resolution of the instrumented-blade dynamic properties so that analyses of the resulting data could properly include the effects of blade bending. Static (nonrotating) shake tests of the aft instrumented blade were conducted with the blade in a configuration that was slightly different from the flight configuration. The changes to the blade between the shake test and the flight test were made after the shake test to improve the blade tracking characteristics. Calculations have shown, however, that these differences did not cause a significant change in the dynamic response of the blade.

This testing was guided by an analysis of the blade dynamic response. An indication of the approximate natural frequencies and the approximate locations of the blade nodal points was provided to the test personnel. The shaker frequency sweeps were made with a smaller increment near an expected natural frequency. The knowledge of the node location was required so that the blade could be properly supported, and so that test personnel would know where to find the nodes during the testing. The analysis was also used to extrapolate the static tests to the rotating condition and to estimate the effects of variations in blade and control configuration.

Shake tests of the blade were conducted to determine flapwise, chordwise, and torsional natural frequencies. For all tests the blade was positioned in a nose-down attitude and the shaker

was rotated to give the desired direction of force. The blade was supported at the root end by standard CH-47A rotor hub hardware in a manner which allowed for movement about the horizontal and vertical pins. For the flapwise and chordwise tests, elastic cables were used to provide a nodal support outboard on the blade. The outboard support for the blade torsion tests was by cables directed to intersect the blade elastic axis. Figures 18 and 19 show the features of the test configurations for the three modes that were investigated. A summary of the support configurations tested is given in Table X.

Instrumentation consisting of a strain-gaged link, frequency counter, and displacement transducer was used to monitor and record the shaker force, as well as the frequency and amplitude of the shaker motion. A lightweight accelerometer was used to probe the blade for the location of nodal points. The electronic equipment and the recorder are shown in Figure 20.

TABLE X
SUMMARY OF DYNAMIC RESPONSE TEST CONFIGURATIONS

Type of Test	Location of Shaker Input (inches of blade radius)	Location of Support Cable (inches of blade radius)
Flapwise	65	133
Flapwise	65	175
Flapwise	65	171
Flapwise	65	189
Flapwise	65	223
Chordwise	65	179
Chordwise	65	270
Chordwise	65	275
Torsion	354 (with offset input point)	354

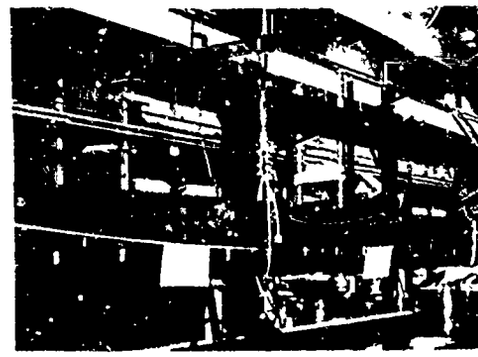

A. OUTER PORTION OF BLADE

B. VIEW OF TOP OF BLADE ROOT END

C. VIEW OF BOTTOM OF BLADE ROOT END

Figure 18. Flapwise Response (Shake) Test Setup with Airloads-Instrumented Aft Rotor Blade.

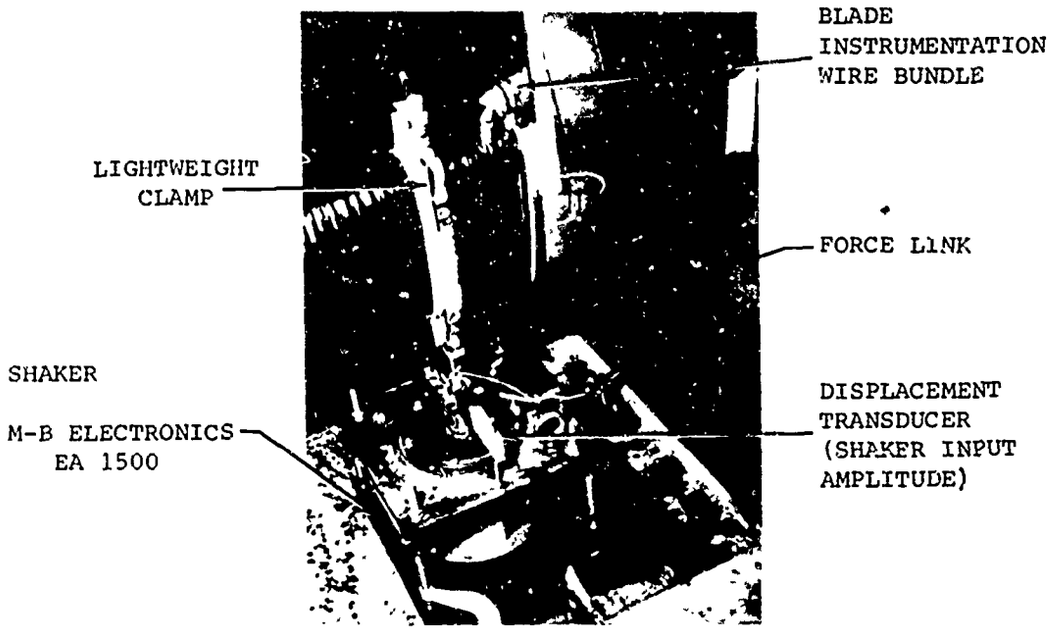

A. SHAKER ORIENTED FOR CHORDWISE FORCE INPUT

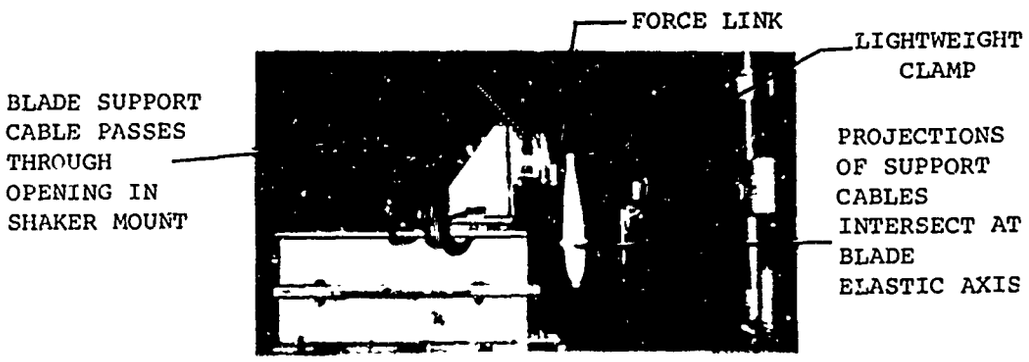

B. CABLE SUPPORT AND SHAKER INPUT ARRANGEMENT FOR TORSIONAL TESTS

Figure 19. Test Setup for Chordwise and Torsional Dynamic Response (Shake) Testing.

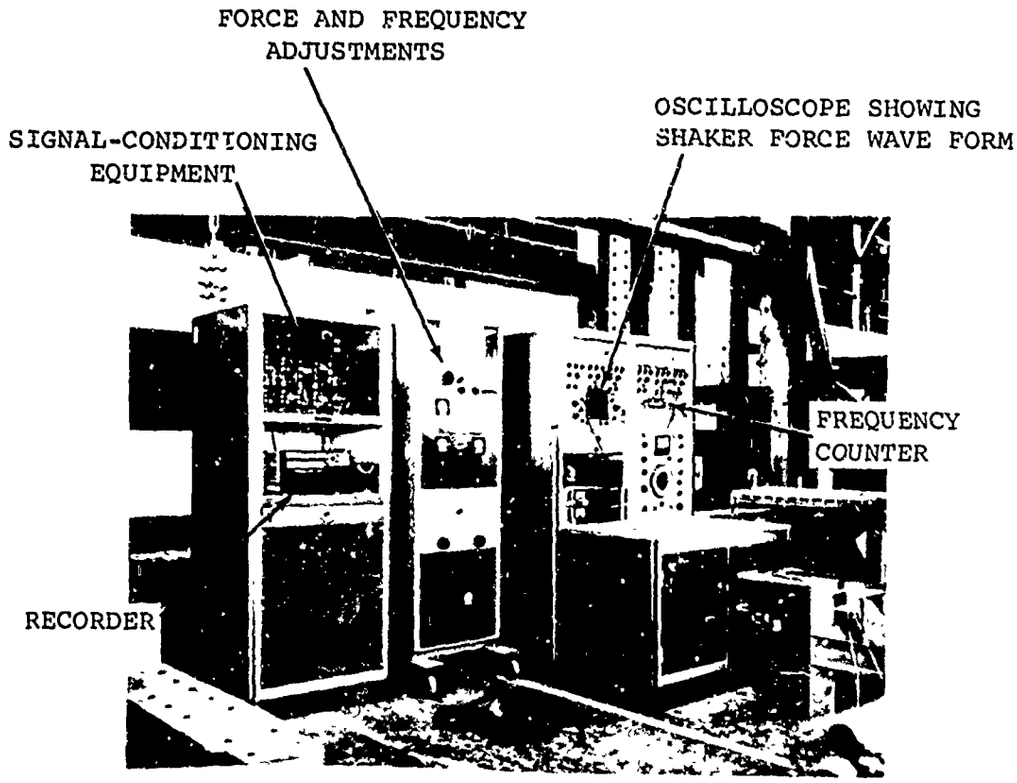

Figure 20. Shaker Electronics, Instrumentation Signal-Conditioning, and Recording Equipment Used for Blade Dynamic Response Tests.

CALIBRATION DATA ANALYSIS

It is generally easier to conduct tests than it is to resolve the results into usable form. This is particularly true of calibrations, since a most important aspect of the analysis is to determine the quality or accuracy of the results. For all the calibrations discussed in this report, least squares curve fits were obtained together with the deviation from the best fit and the hysteresis of the data. This was a routine task except for the rotor shaft and blade calculations which required specialized analyses.

INPUT DATA MANIPULATIONS

Input data manipulations were performed as required to correct gage readings to a standard zero reference and to convert the calibration loads into structure-referenced shears and moments. This type of manipulation was not required for the single-load calibrations, but was essential for the shaft and blade calculations. All calibration reading inputs were made with IBM cards, and a computer routine was provided to correct all readings to the same zero reference. The zero reference was taken as the no-applied-load condition for both the shafts and the blades. Since gravity loads are insignificant to the shafts, no further definition of the zero reference was required. This was not the case for the blades, for which the zero reference consisted of the blades being supported on the blade root hinge and at the tip support (as a simple beam) with the blade in the same attitude as installed on the helicopter. The blade pitch at the 75-percent radius was 2 degrees.

For the rotor shafts, the resolution of loads which were applied from fixed points into the shaft axes reference system required straightforward consideration of the geometry of the problem. Figure 21 illustrates the relations between the applied loads and the resulting shears and moments at strain-gage locations for a rigid structure such as a rotor shaft. It was assumed that the structure and calibration stand were sufficiently rigid, so that a simple tip deflection correction to the applied loads was adequate to account for deflections. The tip deflection in the direction parallel to the shear load was an input value. Since the flight loads on a shaft vary with azimuth, the calibration was performed to evaluate the effect of this variation. It was assumed in the analysis that the calibration loads were fixed and the shaft was rotated. Also the loads

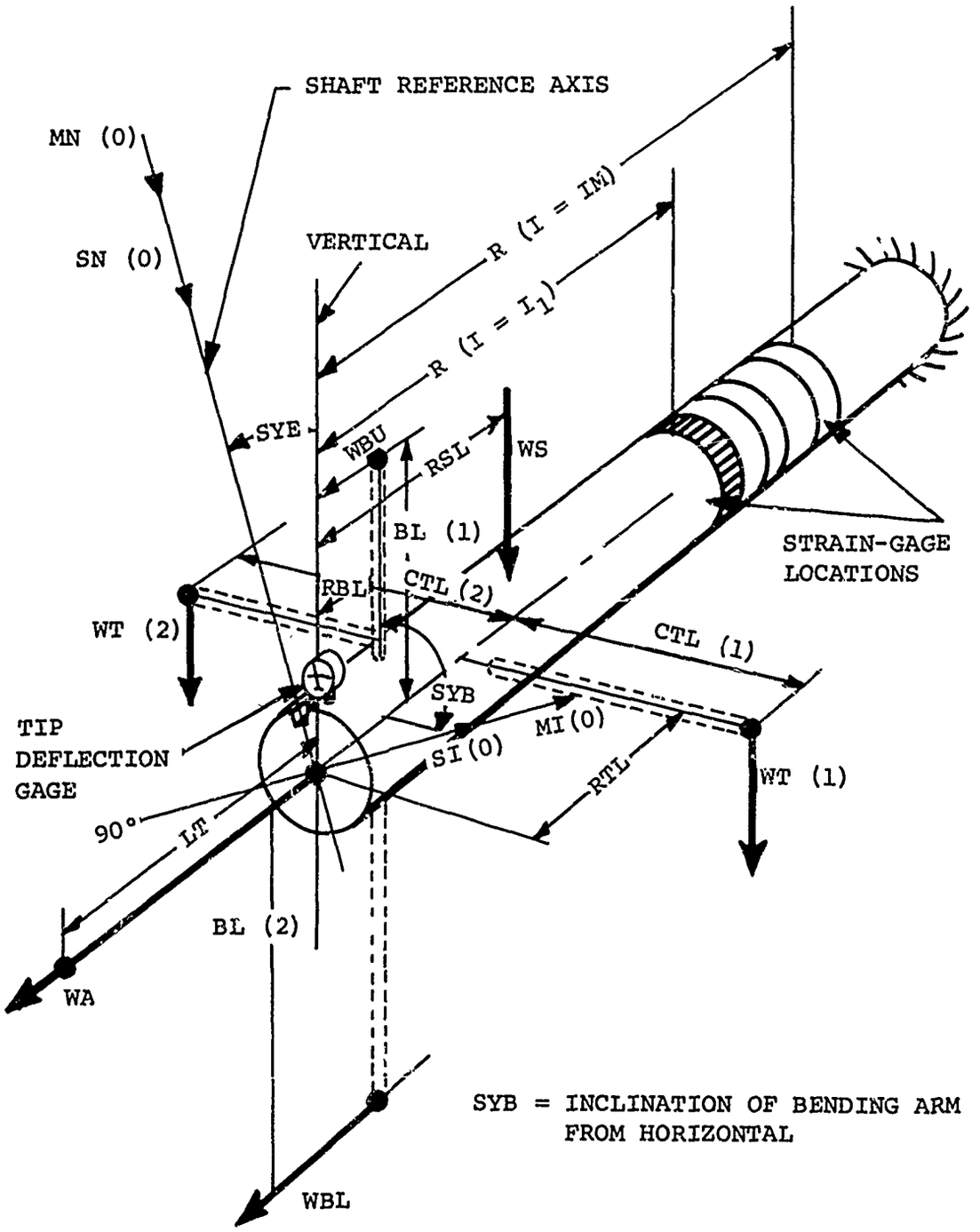

Figure 21. Illustration of Geometry and Notation of Rotor Shaft Calibration Problem.

were assumed to remain sufficiently undeflected so that the cosine of the angle of deflection could be approximated by unity. The sine components of the combined loads could be significant and were included.

The rotor blade calibration presented a more complex problem, since all deflections due to applied loads were significant. The analysis to resolve the blade loads was an iterative solution of the differential equations which defined the blade elastic deflection when loaded from certain fixed points. This analysis is presented in detail in Appendix I. It should be noted that while this approach to a calibration depends on having available the elastic properties of the rotor blade, the sensitivity of the result to inaccuracies in these properties is small. Also, since a check of the analysis against measured changes in blade deflection was provided, the possibility of errors due to the analysis was precluded.

RESOLUTION OF COEFFICIENTS

Calibration coefficients were determined by using a least-squares data fitting analysis, as derived and discussed in Appendix II. This method provides the coefficients which produce a minimum error relationship between the independent variables (the resolved applied loads) and the dependent variables (the corrected gage readings). For a linear single-load calibration, this calculation determines the best value of the primary coefficient a_{11} for all the p values of the applied load Z_{1p}, and the p values of the gage reading g_{1p} where the subscript figure 1 applies, since only one type of load and the same type of gage are involved. The calibration relationship is

$$Z_{1p} = a_{11}\, g_{1p} \quad . \tag{2}$$

As is common practice with flight-test instrumentation, the primary coefficients a_{11} to a_{66} were multiplied by the gage output due to a standardizing resistor. This Rcal output was experimentally determined at the time of calibration with the same gage excitation. This resultant value is called an equivalent load because of the dimensional relationship involved.

The calculation of the calibration coefficients follows in a similar manner for the interaction load calibrations. However, at every station of interest on the structure, the three forces and three moments are evaluated, and as many as six gages are provided to determine these loads. Therefore, Z_{kp} and g_{np}

can each take up to six values for a linear calibration. If there were no interactions in the gage readings, the calibration relationships for the loading value, n, would be:

$$
\begin{aligned}
z_{1p} &= a_{11}\, g_{1p} \\
z_{2p} &= a_{22}\, g_{2p} \\
&\;\;\vdots \\
z_{6p} &= a_{66}\, a_{6p} \quad .
\end{aligned}
\tag{3}
$$

The a_{11} to a_{66} coefficients are the primary calibration coefficients which can be converted to equivalent loads.

The next step in the development is to consider interaction in the gage outputs. For example, a torque load may cause a lift gage output; these interactions have been found experimentally to be very significant, especially for the rotor shafts. The calibration relationship for the pth value of a load of type k=1 and with gages of type n=1 to n=6 is as follows:

$$z_{1p} = a_{11}\, g_{1p} + a_{12}\, g_{2p} + a_{13}\, g_{3p} + \ldots + a_{16}\, g_{6p} \,. \tag{4}$$

This relationship can be written in matrix notation for all the k-type loads as:

$$\left[z_{kp}\right] = \left[a_{kn}\right] \left[g_{np}\right] \tag{5}$$

All the tested loading conditions, p, were applied, and the Appendix II analysis was performed to solve for the matrix of calibration coefficients a_{kn}. As noted previously, when k and n are equal, a_{kn} are the primary calibration coefficients. In order that the data from the interaction load calibration could be handled in the same manner as the simple single-load calibration data, the primary coefficients were divided out of the calibration matrix. Thus, an interaction matrix was defined as:

$$\left[z_{kp}\right] = \left[b_{kn}\right] \left[a_{ii}\, g_{np}\right] \tag{6}$$

where

$a_{ii} = a_{kn}$ from above relation with $i = n$,

$b_{kn} = a_{kn}/a_{ii}$;

therefore, when $k = n$, $b_{kn} = 1.0$.

The advantage of this relation is that a_{ii} can be converted into an equivalent load; and the apparent loads on the structure, $a_{ii}\ g_{np}$, can be calculated in the usual manner. After the column matrix of apparent loads is determined, this matrix is multiplied by the interaction matrix, b_{kn}, to determine the actual loads. This calculation must be repeated for each loading condition which is measured. If the calibration is linear - that is, good correlation is obtained without recourse to using the square of readings for some of the g_{np} values - the multiplication by the interaction matrix for flight data reduction can be performed on the harmonic coefficients of the apparent load data, rather than on each of the original data ordinates, to minimize the computing required.

As noted in Appendix II, the analysis is based on a very general relationship between the loads and the readings. The values of g_{np} can be taken as constants or any products or powers of the gage readings. Also, the parameters such as time or temperature could be applied as g_{np} values. If these parameters were significant to the problem, perhaps due to a systematic time or temperature drift of the recording system, the interaction correlation coefficient to be discussed in the next section would provide a means of evaluating the improvement in the calibration which is obtained by considering such parameters.

EVALUATION OF RESULTS

An important aspect of any calibration is the evaluation of the accuracy of the result. Automated data systems provide very little visibility of the data; therefore, they require a system of checks and evaluations to catch the errors and misinterpretations that invariably occur. For this program several thorough automated checks were made on all calibrations. The determination of the correlation coefficient provided the most sensitive indicator of overall calibration accuracy. To provide visibility to the interaction calibration data, the percent contributions to the estimated loads by the various gages were calculated for every calibration load point. Finally, the hysteresis and deviation of all single-load calibrations were calculated to indicate hysteretic effects

(from the calibrated structure or the test apparatus), repeatability, and maximum error of the calibration.

The correlation coefficient which was used is defined as the square root of the ratio of the sum of the squares of the explained variation of a parameter to the sum of the squares of the total variation, with the sums calculated for all the test points. For the calibrations, the parameters considered were the loads Z_{kp}. Thus, the correlation coefficient for the kth type load, r_k, was of the form:

$$r_k = \sqrt{\frac{\sum_p (Z_{est} - \bar{Z})^2}{\sum_p (Z_{kp} - \bar{Z})^2}} \quad , \tag{7}$$

where

Z_{est} = pth value of Z_{kp} predicted from the calibration equation,

Z_{kp} = actual load for load point, p ,

$\bar{Z}$ = arithmetic mean value of Z_{kp}

$= \frac{1}{s} \sum^{p} Z_{kp}$,

s = total number of tests p .

The significance of this coefficient is more obvious when expressed in the following form:

$$r = \sqrt{1 - \frac{(S_{zg})^2}{(S_z)^2}} \quad , \tag{8}$$

where

S_{zg} = standard error of estimate, Z_{est} on g_{np}

$$= \sqrt{\frac{\sum_p (Z_{kp} - Z_{est})^2}{S}} \quad , \tag{9}$$

S_z = standard deviation from the arithmetic mean of the load, Z_{kp},

$$= \sqrt{\frac{\sum_p (Z_{kp} - \bar{Z})^2}{S}} \quad . \tag{10}$$

Thus, the correlation coefficient is a measure of the overall error of the fitted curve expressed as a fraction of the variation of the independent variable. This again is rather difficult to relate to a calibration, since, in concept, the loads Z_{kp} are not applied in a random manner. However, for a reasonably uniform distribution of loading conditions, the standard deviation of the load will be somewhat less than one-half of the maximum load applied. Thus, if the statistically averaged error of the calibration is expressed as E times maximum load, equation (8) can be approximated as:

$$r = \sqrt{1 - \frac{\left[E(Z_{kp})_{max}\right]^2}{\left[0.5(Z_{kp})_{max}\right]^2}} \quad . \tag{11}$$

From this relation it can be seen that, for reasonably small errors, the value of the correlation must be near unity. For example, if the fractional error, E, is 5 percent of the full-scale load, the correlation coefficient is approximately equal to 0.990. This variation has been accurately calculated for sample cases with the results shown in Figure 22. As shown for values near unity, small changes in coefficient indicate large changes in error, and therefore provide a vernier measure of small improvements in a good calibration. Also, this coefficient is tolerant of very large errors and provides an indication as to the state of the data fit even when the fit is extremely poor. Since the correlation coefficient is nondimensional and is not very sensitive to the load range considered, this coefficient can be uniformly applied to measure the quality of all calibrations accurately.

In evaluating the interaction load calibrations, it was found that the calculation of the percent contribution of the various gages in determining the estimated load was of value. This calculation was as follows:

$$\text{Percent contribution} = \frac{100\ (a_{kn}\ g_{np})}{\sum_n a_{kn}\ g_{np}} \quad . \tag{12}$$

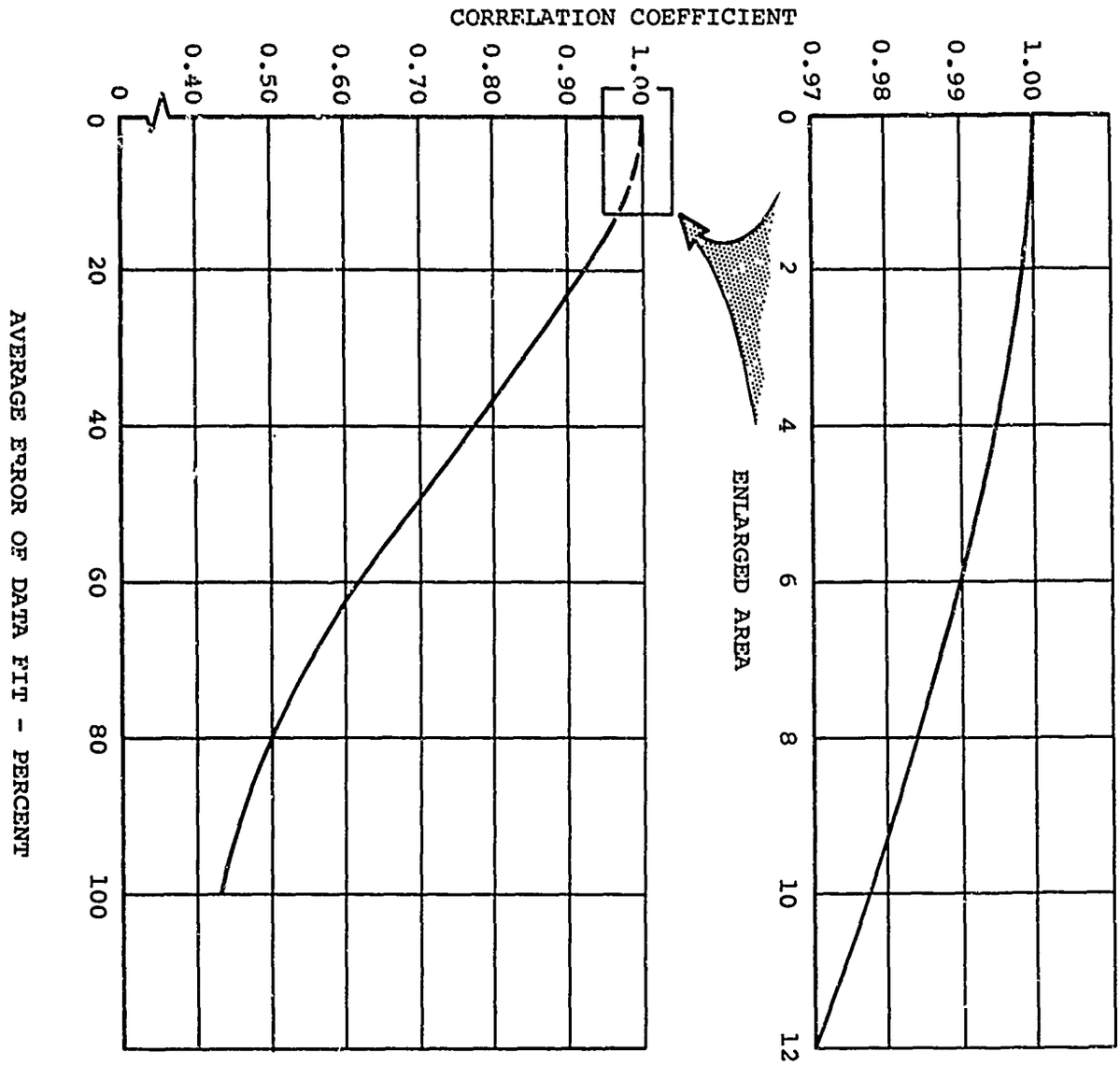

Figure 22. Relation Between Correlation Coefficient and Average Error of Curve Fitting.

Calculations were performed for each of the loading points, p, and for each of the n gages for each of the k types of load. Due to the voluminous results, these data are difficult to comprehend except for specific loading conditions. Particularly interesting percent contribution values are those of the maximum loads, especially the combined loads, and the zero loads.

The calculation of hysteresis and deviation of a calibration are routine; however, the definitions of these terms are not obvious. In calculating hysteresis, a curve (usually linear) with a constant term was fitted to the calibration values obtained from the ascending load values. A similar curve was fitted to the descending load values. Hysteresis was defined as the load difference between the ascending and the descending curves at the maximum gage output, expressed as a percentage of the average load value. This relationship is illustrated in Figure 23. With this definition, true hysteresis effects are accounted for without confusion with deviation or nonlinearity effects.

Deviation is defined as the excursion of the various data points from the best fit calibration curve, as illustrated in Figure 23. Deviation is usually caused by errors or nonlinearities in an assumed linear calibration. Values of deviation are generally expressed as a percentage of the maximum load applied during the calibration considered.

The correlation coefficients were applied generally only to the interaction calibrations, since the usual definitions of accuracy were of limited value. Hysteresis and maximum deviation, however, were calculated to determine the quality of all calibrations. These measures of accuracy are believed to provide ample substantiation of the validity of the calibration, depending only on the applied load and recording system accuracies for a complete summation of the quality of the calibrations.

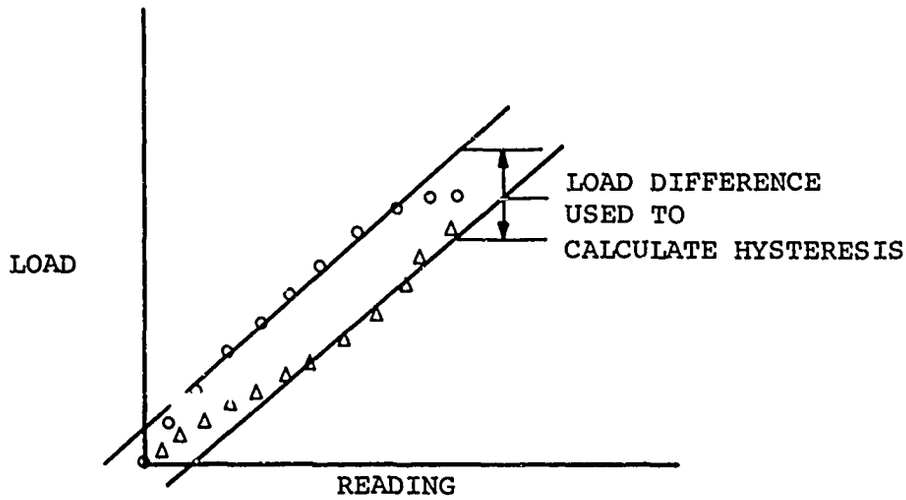

A. HYSTERESIS

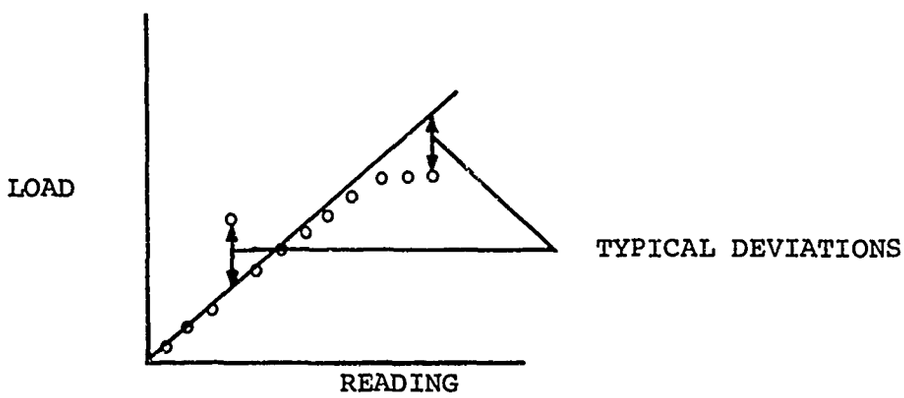

B. DEVIATION

Figure 23. Illustration of Definitions Used to Calculate Hysteresis and Deviation.

EXPERIMENTAL RESULTS

The results that were obtained include calibration data from the transducers and dynamic response data for the rotor blades and airframe accelerometers. Rotor blade tracking data were also obtained and are included. In order that all calibration data can be treated in a similar manner, the interaction load matrices for the shafts and the blades are discussed separately from their primary load coefficients. Comparisons of the results which were obtained during similar tests are presented and discussed.

PRIMARY CALIBRATION COEFFICIENTS

The primary calibration results obtained for all the transducers are presented. Some of these coefficients were measured in different ways, and a comparison of the results is shown. The changes in the primary calibrations from interaction are shown for the shafts and blades in particular.

To differentiate between interaction coefficients and the usual calibration coefficients, the primary calibration coefficients have been defined as the slopes of the gage outputs when a design load is applied in the design direction. These coefficients are conveniently converted to equivalent loads by multiplying by the transducer output due to a shunt calibration resistance (obtained with the same excitation used during the calibration).

Equivalent load values for the rotor shaft strain gages are presented in Table XI. Load values as determined from both single-load and interaction-load calibrations are given. Also shown are the percent differences in the load values obtained from the two calibrations, and the percent contribution of the primary gage reading to the primary calibration load as determined from the interaction data. The amount by which the percent contribution differs from 100 is that amount of gage output which is caused by the interaction effects. The percent difference between the two equivalent loads is also indicative of interaction, since the single-load data analysis considered only the primary load. Note the generally good agreement in percent interaction content between the two independent measures. Where the percent difference is small and the percent contribution is near 100, the interaction effects canceled one another, and the single-load calibrations are accurate. The results of

TABLE XI

EQUIVALENT LOAD VALUES - ROTOR SHAFT STRAIN GAGES

Gage	Standardization Resistance (KΩ)	Single-Load Calibration	Interaction Load Calibration	Percent Diff. in Equiv. Loads	Percent Contribution of Primary Gage
		Forward Shaft			
0-180 Bending	160	97,390 in.-lb	94,445 in.-lb	3.12	102.5
90-270 Bending	160	96,254 in.-lb	101,358 in.-lb	5.30	99.15
Torque	50	439,550 in.-lb	434,868 in.-lb	1.07	100.0
0-180 Shear	300	9,575 lb	13,947 lb	45.70	140.0
90-270 Shear	300	12,208 lb	15,667 lb	28.30	119.1
Lift	750	23,665 lb	22,416 lb	5.60	99.8
		Aft Shaft			
0-180 Bending	160	121,544 in.-lb	122,000 in.-lb	0.37	90.75
90-270 Bending	160	122,460 in.-lb	118,368 in.-lb	3.46	92.35
Torque	50	434,970 in.-lb	429,074 in.-lb	1.37	97.5
0-180 Shear	300	6,376 lb	5,620 lb	13.45	122.9
90-270 Shear	300	7,597 lb	5,552 lb	36.80	101.2
Lift	750	19,308 lb	19,239 lb	0.36	100.5

the interaction calibration data checks promote a high level of confidence in the accuracy of the results of these tests. The data of Table XI point out the need for consideration of interaction effects in calibrations of this type.

Similar equivalent load values for the rotor blade strain gages are presented in Table XII. Except for the blade tension gage, there are surprisingly large differences between the single-load and the combined-loads calibrations. These differences presently cannot be explained since, due to the increased complexity of the blade calibration, the percent differences of the calibrations could not be calculated. However, it can readily be seen in the data that there are sizable interactions in the outputs of the blade gages. This is because of the complexity of the blade cross section and the resultant lack of definition of the elastic axes of the blade. As will be noted later, this blade calibration was accurately performed and should give accurate data when used in flight-test data reduction. The combined-loads calibration coefficients will give considerably different results from those obtained with the single-load calibration.

Equivalent load values for the rotor blade radial tension gages as determined by whirl tests and the static calibration are shown in Figure 24. A comparison of the data obtained by these different methods shows a maximum difference in equivalent load values of 5 percent for both blades. As shown, the static calibration data are obtained for relatively small tension values as compared to that which can be achieved by whirl testing. Since flat-pitch whirl testing causes only small interaction loads in torsion and essentially no flap bending, the whirl test equivalent loads are believed to be the best calibration available, and these values were used in the data analysis. It is unfortunate, but not at all limiting, that the available whirl test data for the two blades are not exactly comparable. The forward blade data were obtained during ground runs of the aircraft, whereas the aft blade data were obtained on the whirl tower. In each case, the comparable data for the other blade were lost because of recording system difficulties. The difference in environment and instrumentation between the aircraft and the whirl tower is negligible.

Except for the above comparisons, the primary calibrations are of little interest. This is especially true for the routine calibrations of the control components presented in Table XIII.

TABLE XII
INTERACTION AND SINGLE-LOAD CALIBRATION VALUES FOR
FORWARD AND AFT BLADES

Gage	Blade Station (inches)	Forward Blade			Aft Blade		
		Standardization Resistance (KΩ)	Interaction Load Calibration *	Single-Load Calibration *	Standardization Resistance (KΩ)	Interaction Load Calibration *	Single-Load Calibration *
Torsion	46	353.9	5,200	16,045	350.1	7,284	16,956
Tension	46	75.18	67,700	61,748	75.01	60,792	54,663
Flap bending	89	39.98	890	59,708	40.14	598	59,876
Chord bending	89	500.4	347	57,414	500.8	20	56,935
Flap bending	124	75.01	12,400	31,137	75.01	28,156	31,174
Torsion	140	200.15	12,300	12,490	200.1	7,796	10,068
Flap bending	159	60.1	21,650	31,512	60.08	4,354	30,216
Chord bending	159	400.1	52,500	78,153	399.7	4,829	77,853
Flap bending	195	59.88	18,600	22,989	60.17	9,506	24,302
Flap bending	231	75.15	17,580	19,565	75.12	21,033	19,474
Chord bending	231	500.9	768	55,878	500.3	80	57,708
Flap bending	267	60.125	24,000	25,018	60.13	22,784	24,246
Flap bending	300	74.505	1,960	19,016	74.9	670	18,635
Chord bending	300	752.0	245	32,993	750.2	115	32,107
Flap bending	339	200.0	73	8,262	200.0	14	7,780

*Units for tension gage are pounds; all others are inch-pounds.

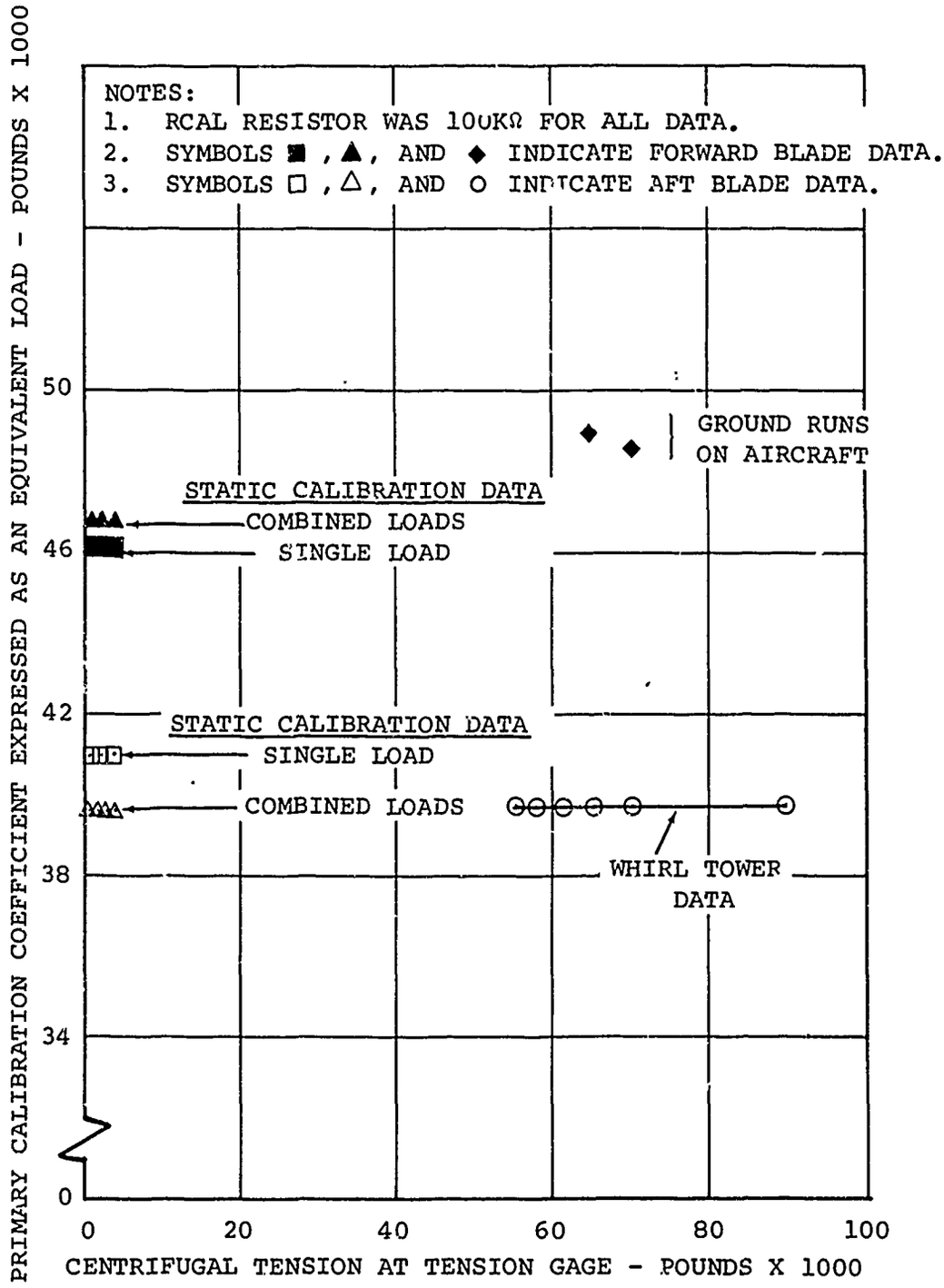

Figure 24. Comparison of Static and Whirl Test Calibrations of Blade Tension Gages.

The presentation of these data at this time is mainly to provide unified reference documentation for the data reduction input values. The equivalent load values given were inserted in the Primary Load Calibration Program (M-40) of the data system as described in Volume III of this report. Since pressure transducer sensitivity could be regulated by means of adjustable resistors on the aircraft, no equivalent load values are presented for these gages.

TABLE XIII
PRIMARY CALIBRATION COEFFICIENTS - CONTROL COMPONENTS

Gage Identification	Standardization Resistance (KΩ)	Primary Coefficient (lb)
Forward longitudinal cyclic trim actuator	160	4550
Aft longitudinal cyclic trim actuator	160	4817
Forward swivelling actuator load	160	2123
Aft swivelling actuator load	160	2078
Forward pivoting actuator load	160	2183
Aft pivoting actuator load	160	2051
Forward pitch link load	100	1529
Aft pitch link load	100	1504

INTERACTION MATRICES FOR ROTOR SHAFTS

Interaction matrices obtained for the two rotor shafts are presented in Table XIV. The effect of various load combinations on the magnitudes of the coefficients is also discussed. There is essentially only one instrumented section on each rotor shaft, so there is only one interaction matrix per shaft.

The rotor shaft interaction effects were shown during calibration to be rather sizable. For example, Figures 25 and 26 show, for the forward shaft 0-180 shear gage, the variations in gage output which were possible due to various types of loads and load combinations. Note that, with no applied shear load, the uncorrected gage output indicates a shear of about 2000 pounds, dependent on the type of applied load. An interaction due to bending moment is also shown. By changing the

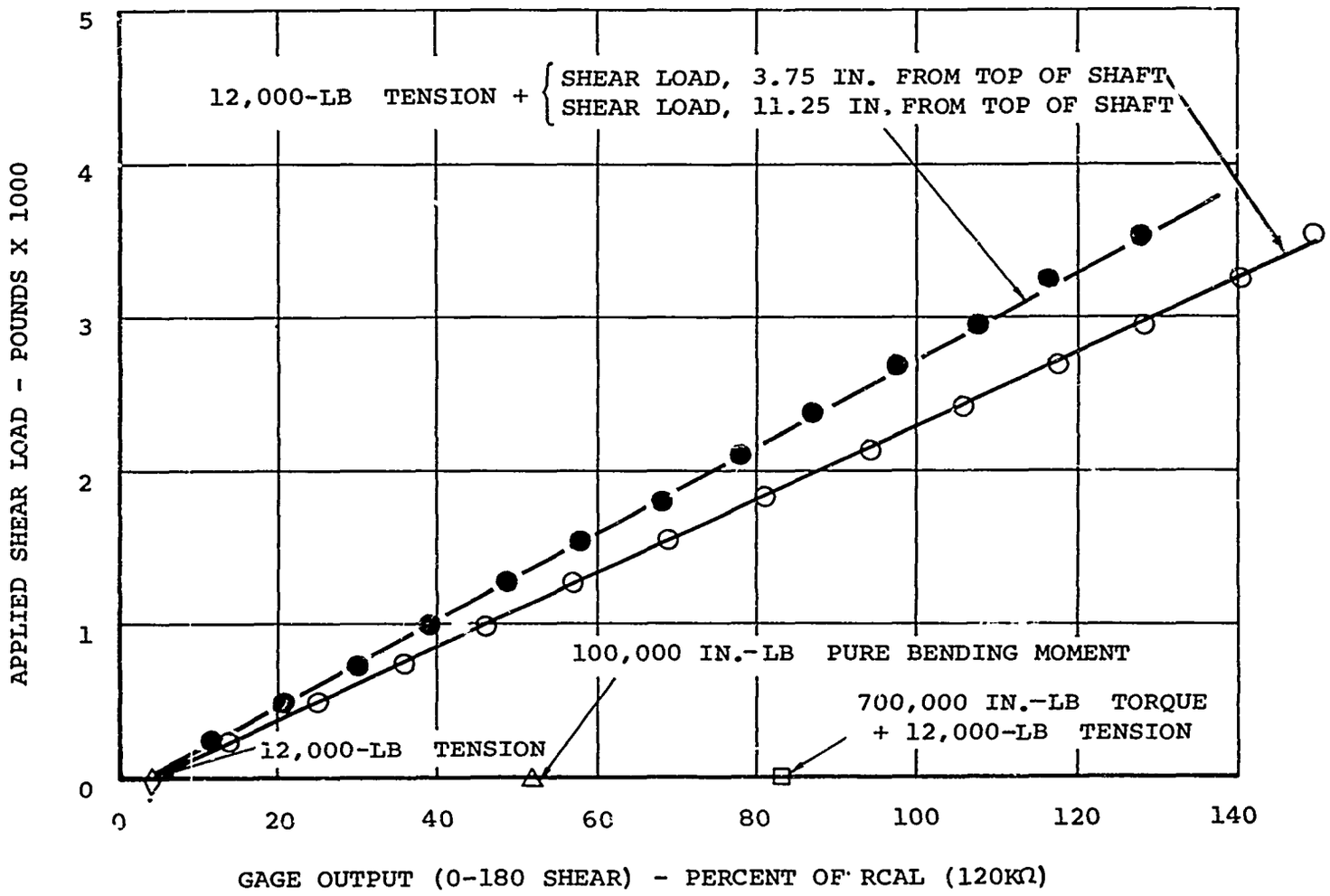

Figure 25. Rotor Shaft Calibration Data Showing Interactions in Forward Shaft Shear Readings.

TABLE XIV
ROTOR SHAFT INTERACTION COEFFICIENTS

Primary Load	Shear 0-180	Shear 90-270	Lift	Moment 0-180	Moment 90-270	Torque
			Interaction Loads			
			Forward Rotor Shaft			
Shear 0-180	1.0	0.1412	-0.0001234	-0.002584	0.001345	0.004502
Shear 90-270	-0.1491	1.0	0.002241	0.003526	0.03590	0.002007
Lift	0.01196	0.1579	1.0	-0.0009585	0.008622	0.02478
Moment 0-180	0.1660	0.7245	0.00384	1.0	0.05955	-0.01646
Moment 90-270	0.3682	-0.6155	-0.001698	0.003736	1.0	0.006718
Torque	0.06492	0.1751	-0.09456	-0.02784	-0.01287	1.0

TABLE XIV - Continued

Primary Load	Shear 0-180	Shear 90-270	Lift	Moment 0-180	Moment 90-270	Torque
			Aft Rotor Shaft			
Shear 0-180	1.0	0.06544	-0.002198	-0.01528	-0.001306	-0.0000692
Shear 90-270	-0.05093	1.0	-0.001648	-0.002667	0.01216	0.0002008
Lift	0.01770	0.05859	1.0	-0.001963	-0.0008981	-0.004008
Moment 0-180	1.667	0.1707	0.02015	1.0	0.01577	0.009180
Moment 90-270	-0.1605	-1.4963	0.03981	0.008722	1.0	0.005984
Torque	-0.06687	-0.1444	0.02430	-0.01778	-0.03108	1.0

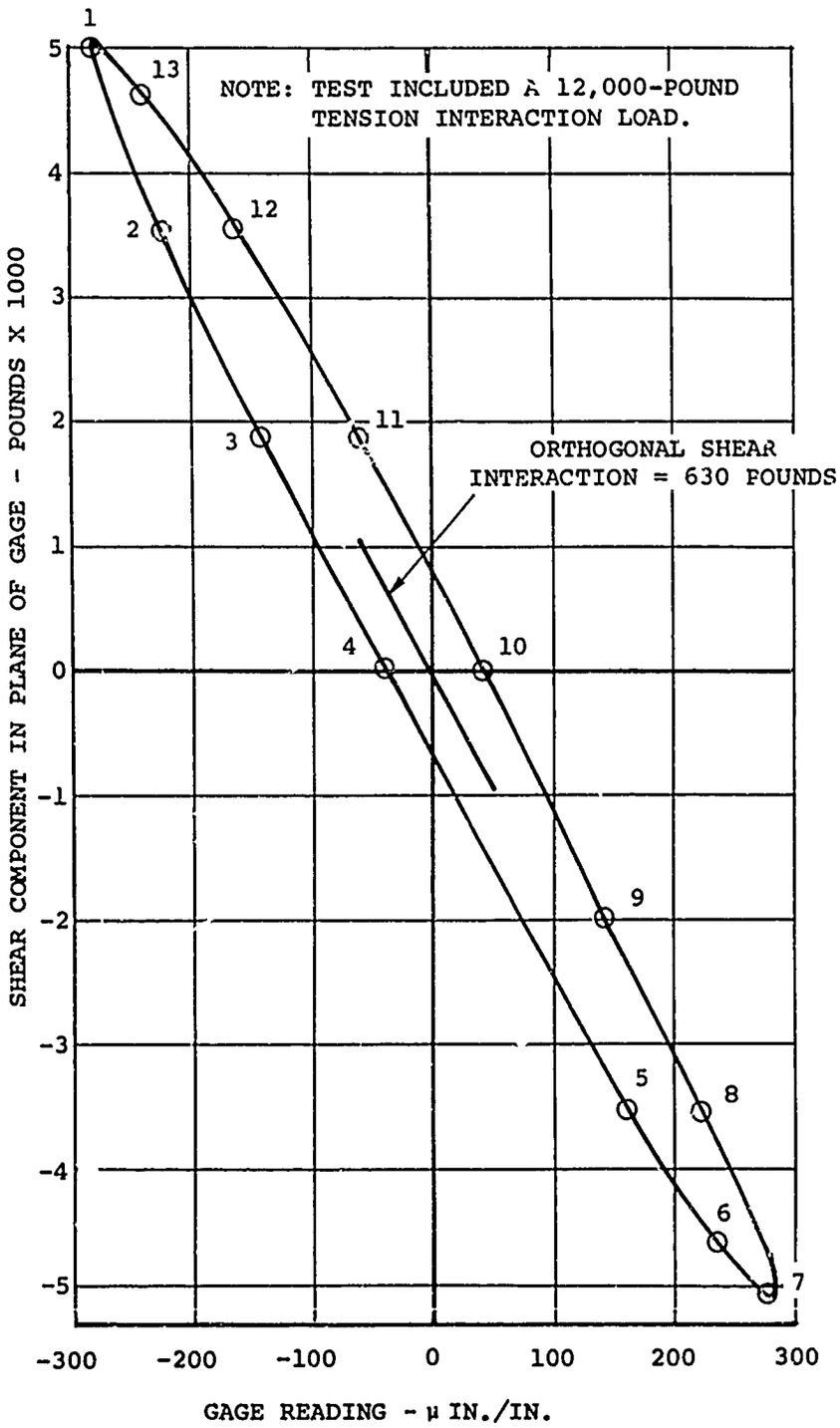

Figure 26. Interactions of 0-180 Shear Gage Readings Due to an Orthogonal Shear on the Forward Shaft.

point of application of the shear load or the magnitude of the bending moment at the gage location, a change in shear gage output of 1.1 percent of Rcal, or 400 pounds indicated shear, is experienced. Interaction effects are also shown in Figure 26, demonstrating the change in the indicated shear as a result of rotating the shaft in the fixture while holding the direction and magnitude of the shear load fixed. The gage reading for point 4 of Figure 26 illustrates the interaction effects (an indicated shear of 630 pounds) caused by the 500-pound shear load applied perpendicular to the plane of the gages. These data are presented as an indication of the interactions possible in the gage outputs. The method of data analysis corrected for these variations and ensured that the coefficients of each gage were suitable for converting strain-gage data to measurements of isolated desired loads for any arbitrary load condition.

It should be noted that the matrix given here for the forward rotor shaft differs from that presented in reference 4. The previously published matrix was in error, in that it did not utilize the gage deflections from a no-load condition when variable shear was applied in combination with a 12,000-pound tension; it considered only the deflection which occurred due to the variable shear load. The primary coefficients changed very little (approximately 1 percent), whereas the off diagonal elements were changed significantly. The magnitudes of the interaction coefficients of lift with the 0-degree and 90-degree shears were reduced by factors of 100 and 10, respectively.

ROTOR BLADE INTERACTION MATRICES

Since the rotor blades were instrumented at 10 stations, there are 10 interaction matrices for each rotor blade. These matrices are presented in Table XV for the forward and aft instrumented blades. The coefficients of the matrices shown apply to the gages available at the instrumented stations of interest. All other coefficients are zero or unity. It is noted that the correction for interactions due to loads for which no gage is available requires an estimated value of the interaction load. This procedure is followed in the data system using extrapolations of the data from adjacent blade stations to estimate the interaction loads. See Volume III of this report for a discussion of the Interaction Load Equivalents Program.

TABLE XV
ROTOR BLADE INTERACTION COEFFICIENTS

	Flap Bending	Chord Bending	Torsion	Flap Shear	Chord Shear	Tension
Forward Rotor Blade						
Station 46						
Flap Bending	1.0	0	0	0	0	0
Chord Bending	0	1.0	0	0	0	0
Torsion	68.2	3.53	1.0	2640	63.4	0.717
Flap Shear	0	0	0	1.0	0	0
Chord Shear	0	0	0	0	1.0	0
Tension	1.48	0.742	-0.211	56.7	12.2	1.0
Station 89						
Flap Bending	1.0	0.0346	0.0284	-74.1	-0.626	-0.285
Chord Bending	-0.812	1.0	0.00153	0.542	-59.1	-0.0047
Torsion	0	0	1.0	0	0	0
Flap Shear	0	0	0	1.0	0	0
Chord Shear	0	0	0	0	1.0	0
Tension	0	0	0	0	0	1.0
Station 124						
Flap Bending	1.0	0.128	0.0290	45.0	-0.860	-0.192
Chord Bending	0	1.0	0	0	0	0
Torsion	0	0	1.0	0	0	0
Flap Shear	0	0	0	1.0	0	0
Chord Shear	0	0	0	0	1.0	0
Tension	0	0	0	0	0	1.0
Station 141						
Flap Bending	1.0	0	0	0	0	0
Chord Bending	0	1.0	0	0	0	0
Torsion	0.0468	0.0203	1.0	6.35	-0.00394	-0.241
Flap Shear	0	0	0	1.0	0	0
Chord Shear	0	0	0	0	1.0	0
Tension	0	0	0	0	0	1.0

TABLE XV - Continued

	Flap Bending	Chord Bending	Torsion	Flap Shear	Chord Shear	Tension
Forward Rotor Blade						
Station 159						
Flap Bending	1.0	0.172	0.0689	11.5	-1.96	0.133
Chord Bending	-0.874	1.0	0.592	-14.4	-17.5	-1.45
Torsion	0	0	1.0	0	0	0
Flap Shear	0	0	0	1.0	0	0
Chord Shear	0	0	0	0	1.0	0
Tension	0	0	0	0	0	1.0
Station 195						
Flap Bending	1.0	0.309	0.0194	8.22	-24.6	0.234
Chord Bending	0	1.0	0	0	0	0
Torsion	0	0	1.0	0	0	0
Flap Shear	0	0	0	1.0	0	0
Chord Shear	0	0	0	0	1.0	0
Tension	0	0	0	0	0	1.0
Station 231						
Flap Bending	1.0	1.41	0.0158	-3.79	15.5	0.331
Chord Bending	0.0727	1.0	-0.0644	-4.60	119.0	0.124
Torsion	0	0	1.0	0	0	0
Flap Shear	0	0	0	1.0	0	0
Chord Shear	0	0	0	0	1.0	0
Tension	0	0	0	0	0	1.0
Station 267						
Flap Bending	1.0	-0.919	-0.0203	-5.99	91.8	0.435
Chord Bending	0	1.0	0	0	0	0
Torsion	0	0	1.0	0	0	0
Flap Shear	0	0	0	1.0	0	0
Chord Shear	0	0	0	0	1.0	0
Tension	0	0	0	0	0	1.0

TABLE XV - Continued

	Flap Bending	Chord Bending	Torsion	Flap Shear	Chord Shear	Tension
Forward Rotor Blade						
Station 300						
Flap Bending	1.0	-1.69	0.216	45.7	2.35	-0.133
Chord Bending	-0.369	1.0	-0.155	2.29	54.1	-0.0131
Torsion	0	0	1.0	0	0	0
Flap Shear	0	0	0	1.0	0	0
Chord Shear	0	0	0	0	1.0	0
Tension	0	0	0	0	0	1.0
Station 339						
Flap Bending	1.0	-1.05	0.046	15.8	16.8	-0.00603
Chord Bending	0	1.0	0	0	0	0
Torsion	0	0	1.0	0	0	0
Flap Shear	0	0	0	1.0	0	0
Chord Shear	0	0	0	0	1.0	0
Tension	0	0	0	0	0	1.0
Aft Rotor Blade						
Station 46						
Flap Bending	1.0	0	0	0	0	0
Chord Bending	0	1.0	0	0	0	0
Torsion	54.2	89.1	1.0	2090.	1560	0.6974
Flap Shear	0	0	0	1.0	0	0
Chord Shear	0	0	0	0	1.0	0
Tension	2.51	4.11	0.008941	97.2	71.7	1.0
Station 89						
Flap Bending	1.0	-2.20	0.0312	-72.4	-0.924	-0.266
Chord Bending	-2.28	1.0	0.00249	-1.59	-59.1	-0.0268
Torsion	0	0	1.0	0	0	0
Flap Shear	0	0	0	1.0	0	0
Chord Shear	0	0	0	0	1.0	0
Tension	0	0	0	0	0	1.0

TABLE XV - Continued

	Flap Bending	Chord Bending	Torsion	Flap Shear	Chord Shear	Tension
Aft Rotor Blade						
Station 124						
Flap Bending	1.0	0.202	0.00113	22.7	-0.0454	0.0695
Chord Bending	0	1.0	0	0	0	0
Torsion	0	0	1.0	0	0	0
Flap Shear	0	0	0	1.0	0	0
Chord Shear	0	0	0	0	1.0	0
Tension	0	0	0	0	0	1.0
Station 141						
Flap Bending	1.0	0	0	0	0	0
Chord Bending	0	1.0	0	0	0	0
Torsion	0.0330	0.00883	1.0	1.13	0.03770	-0.0812
Flap Shear	0	0	0	1.0	0	0
Chord Shear	0	0	0	0	1.0	0
Tension	0	0	0	0	0	1.0
Station 159						
Flap Bending	1.0	0.1057	-0.109	74.9	-5.67	-0.452
Chord Bending	38.1	1.0	-0.476	231.0	-17.6	-3.26
Torsion	0	0	1.0	0	0	0
Flap Shear	0	0	0	1.0	0	0
Chord Shear	0	0	0	0	1.0	0
Tension	0	0	0	0	0	1.0
Station 195						
Flap Bending	1.0	1.58	-0.356	31.4	-226.0	-0.485
Chord Bending	0	1.0	0	0	0	0
Torsion	0	0	1.0	0	0	0
Flap Shear	0	0	0	1.0	0	0
Chord Shear	0	0	0	0	1.0	0
Tension	0	0	0	0	0	1.0

TABLE XV - Continued

	Flap Bending	Chord Bending	Torsion	Flap Shear	Chord Shear	Tension
Aft Rotor Blade						
Station 231						
Flap Bending	1.0	-2.470	0.125	11.3	21.8	0.400
Chord Bending	0.05778	1.0	-0.0809	-2.65	121.0	0.161
Torsion	0	0	1.0	0	0	0
Flap Shear	0	0	0	1.0	0	0
Chord Shear	0	0	0	0	1.0	0
Tension	0	0	0	0	0	1.0
Station 267						
Flap Bending	1.0	1.30	0.149	2.86	-100.0	0.106
Chord Bending	0	1.0	0	0	0	0
Torsion	0	0	1.0	0	0	0
Flap Shear	0	0	0	1.0	0	0
Chord Shear	0	0	0	0	1.0	0
Tension	0	0	0	0	0	1.0
Station 300						
Flap Bending	1.0	-2.13	0.252	49.6	1.80	-0.200
Chord Bending	-0.5837	1.0	-0.168	1.29	54.4	0.00991
Torsion	0	0	1.0	0	0	0
Flap Shear	0	0	0	1.0	0	0
Chord Shear	0	0	0	0	1.0	0
Tension	0	0	0	0	0	1.0
Station 339						
Flap Bending	1.0	-1.09	0.0776	15.7	17.4	-0.00582
Chord Bending	0	1.0	0	0	0	0
Torsion	0	0	1.0	0	0	0
Flap Shear	0	0	0	1.0	0	0
Chord Shear	0	0	0	0	1.0	0
Tension	0	0	0	0	0	1.0

When considering the blade interaction data, it should be noted that, due to the elasticity of the blade and the freedoms of motion of the blade in the test rig whenever any load is applied to the blade, all forces and moments are likely to change. For example, there is a very large change in flapwise bending of the blade from tension since the blade is initially deflected by gravity. This effect is not an interaction, since it is the actual bending moment which is changing. Interactions cause a change in gage output without a change in the primary load.

The flap bending moment calibration data for blade station 231 are shown in Figure 27 to illustrate the interactions which were evaluated. It can be seen in these data that a chordwise loading causes a significant interaction in flap bending at this station. Tension and torsion are shown to cause almost no interaction. Similarly, as shown in Figure 28, there is a significant interaction of flapwise loads in the chordwise bending gage output. These interactions are understandable since the locations of the elastic axes of the blades are not well-defined. The gage installations were based on the elastic axes which were calculated, neglecting the fairing box structural contributions.

TEMPERATURE AND ACCELERATION INTERACTIONS ON PRESSURE TRANSDUCERS

Coefficients to correct for temperature-induced zero shifts and sensitivity changes in the differential-pressure transducers are given in Table XVI. Considering the maximum values of correction coefficients (as noted by an asterisk in the table) for each type of transducer, the temperature corrections required range from 4.3 to 5.5 percent for zero shift, and from 2.2 to 2.5 percent for sensitivity changes, if the temperature change is as large as 50°F. Note that in each case the maximum values are considered and that the majority of the coefficients are much less than the maximum. An evaluation of the effect of this error on the final data results is included in Volume I of this report. Similar data were also obtained for the absolute-pressure transducers. The data were used to select pairs of transducers for measuring differential pressures over the spar area of the blades. The temperature sensitivity of the pair of transducers is not the simple algebraic difference in the sensitivity of each transducer but must be determined by test. Results of these tests are described in Volume IV of this

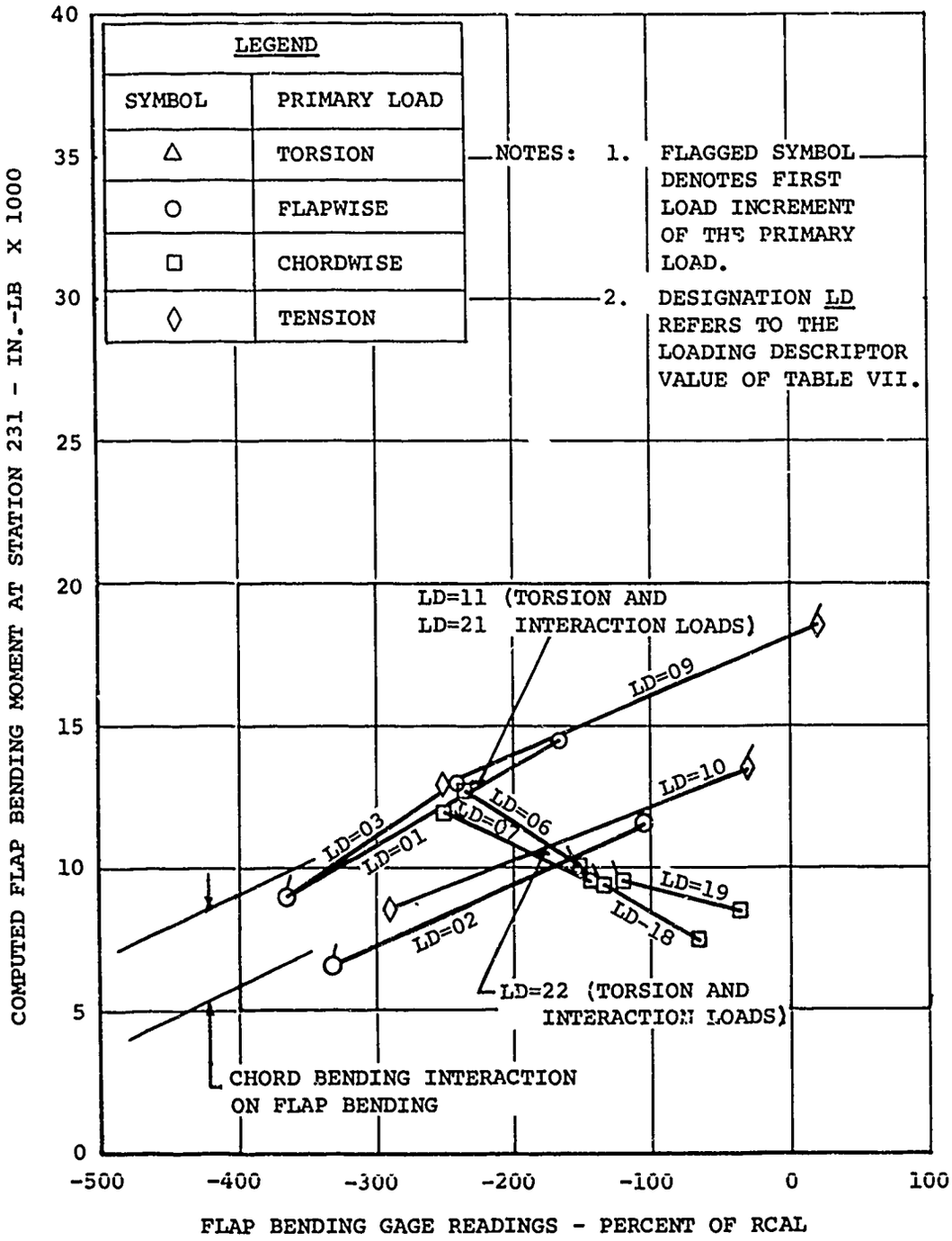

Figure 27. Interactions in Readings of Flap Bending Gage at Station 231 of the Forward Blade.

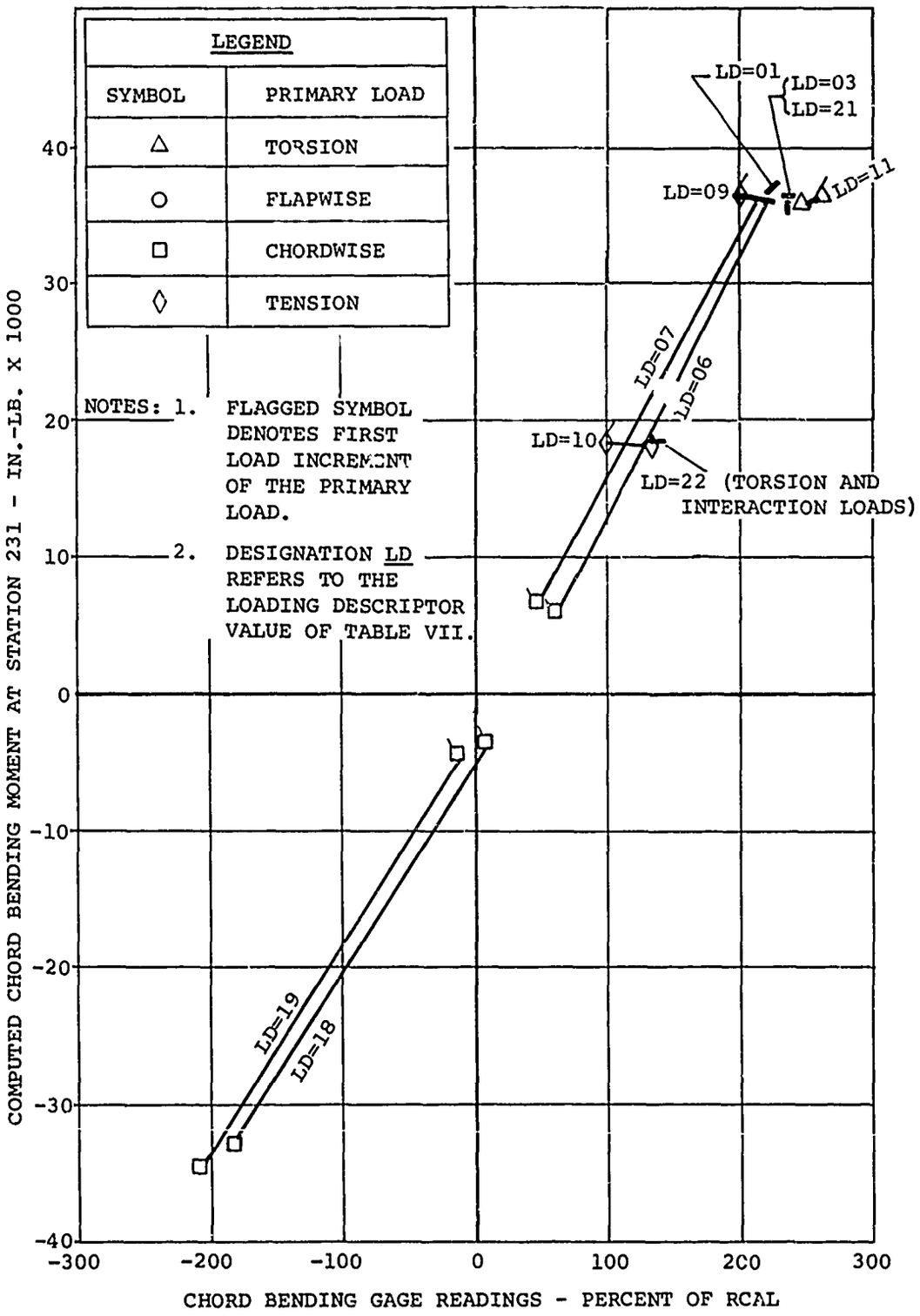

Figure 28. Interactions in Readings of Chord Bending Gage at Station 231 of the Forward Blade.

report. Since the temperature sensitivity data on the absolute pressure transducers were not used in the data analysis, they are not included here.

TABLE XVI
TEMPERATURE CORRECTION COEFFICIENTS - ROTOR BLADE DIFFERENTIAL-PRESSURE TRANSDUCERS

Transducer Serial No.	Correction Coefficients: Zero Shift (% Full Scale/°F)	Correction Coefficients: Sensitivity Changes (% Full Scale/°F)
E-3	0.027	0.051*
E-4	0.022	0.017
E-5	0.019	0.041
E-6	0.034	0.019
E-7	0.104	0.036
E-8	0.073	0.028
E-9	0.049	0.015
E-11	0.047	0.021
E-12	0.044	0.036
E-13	0.023	0.027
E-14	0.067	0.022
E-15	0.055	0.033
E-16	0.104	0.049
E-19	0.105	0.025
E-21	0.075	0.029
E-22	0.043	0.027
E-23	0.093	0.017
E-24	0.057	0.021
E-26	0.109	0.030
E-27	0.020	0.017
E-28	0.052	0.011
E-29	0.112*	0.037
E-32	0.029	0.037
E-34	0.068	0.034
E-36	0.031	0.024
E-37	0.049	0.003
E-39	0.016	0.047
E-40	0.030	0.048
E-41	0.033	0.014
E-42	0.066	0.015
E-43	0.019	0.023
E-44	0.031	0.042
E-45	0.084	0.046
F-1	0.065	0.052*

TABLE XVI- Continued

Transducer Serial No.	Correction Coefficients Zero Shift (% Full Scale/°F)	Sensitivity Changes (% Full Scale/°F
F-2	0.038	0.036
F-5	0.086	0.034
F-7	0.066	0.030
F-8	0.088*	0.023
F-9	0.077	0.049
F-10	0.046	0.032
F-11	0.038	0.020
F-12	0.050	0.039
F-13	0.063	0.020
F-14	0.007	0.029
F-15	0.017	0.031
F-17	0.041	0.014
F-18	0.057	0.012
F-19	0.027	0.028
F-21	0.048	0.026
F-23	0.030	0.017
G-1	0.064	0.040
G-2	0.022	0.044*
G-3	0.050	0.024
G-4	0.039	0.025
G-5	0.065	0.021
G-6	0.018	0.019
G-7	0.050	0.025
G-8	0.011	0.019
G-9	0.082	0.022
G-10	0.032	0.026
G-11	0.056	0.025
G-12	0.010	0.026
G-13	0.086*	0.029
G-14	0.016	0.022
G-15	0.083	0.026

*Noted values are maxima obtained for each transducer sensitivity range.

Sensitivity to acceleration for a typical pressure transducer is shown in Figure 29. Note that for frequencies to 100 cycles per second and acceleration to 70 g the maximum measured transducer output was less than one-half of 1 percent of the transducer full-scale range. For the transducer tested, a

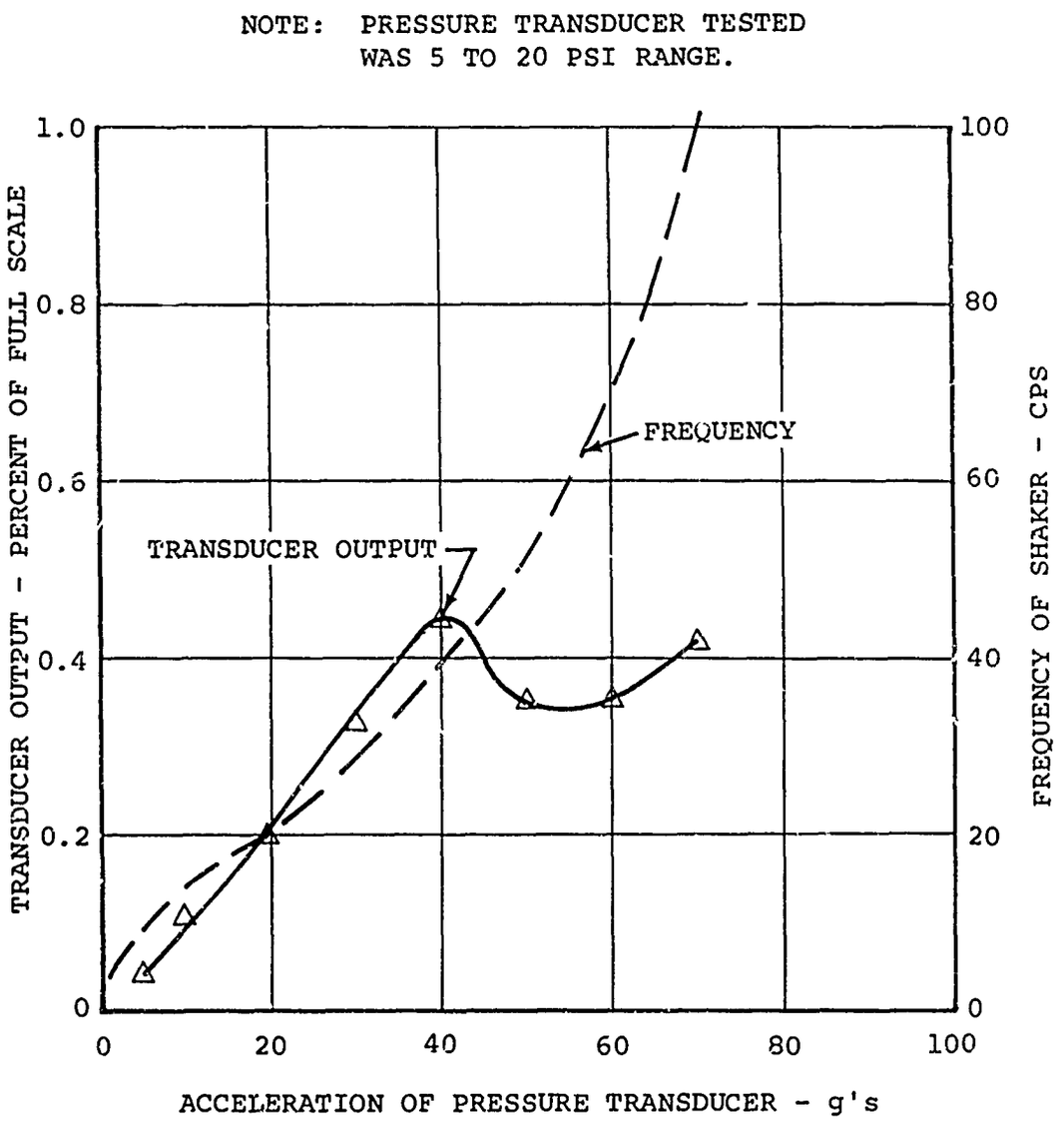

Figure 29. Typical Test Data Obtained from Normal Acceleration Test of a Pressure Transducer.

5 to 20 psi type, the measured output would be equivalent to 0.06 psi. This effect is negligible.

DYNAMIC RESPONSE OF ACCELEROMETERS

Figures 30 and 31 summarize the frequency response and output signal phase lag of the fuselage accelerometers. The standard response is the midpoint of the range of measurements obtained for all accelerometers and was used in data analysis. The results for all accelerometers fell within the maximum and minimum allowable deviations shown in the figures. The allowable deviation was approximately 5 percent in each case for the range of frequencies of interest.

ROTOR BLADE DYNAMIC RESPONSE

The most pertinent blade shake test data are summarized in Figure 32. This figure shows the relationship between the shaker motion and the resultant amplitude of the response as a function of shaker frequency. Tests at various input force levels showed that the resonant frequency was essentially independent of the force level within the expected accuracy of the test. Also shown in the figure are calculated frequencies of the tested blade and the noninstrumented blade as balanced to the airloads-instrumented blade.

Figure 33 shows the calculated mode shapes of the instrumented blade together with experimentally determined node points. The mode shapes were calculated using a coupled flap-torsion analysis and the physical properties of the airloads-instrumented blade from Tables II and III. The test data show generally good agreement with the calculated values.

ROTOR BLADE TRACKING DATA

Tracking data for the forward and aft sets of blades are given in Figures 34 and 35. The difference in blade tip height was measured optically for each set of blades using the instrumented blade tip height as the zero reference. The data are all within the tolerance which is considered acceptable for instrumented blades. These data are presented for reference purposes to support future analyses of rotor vibratory loads.

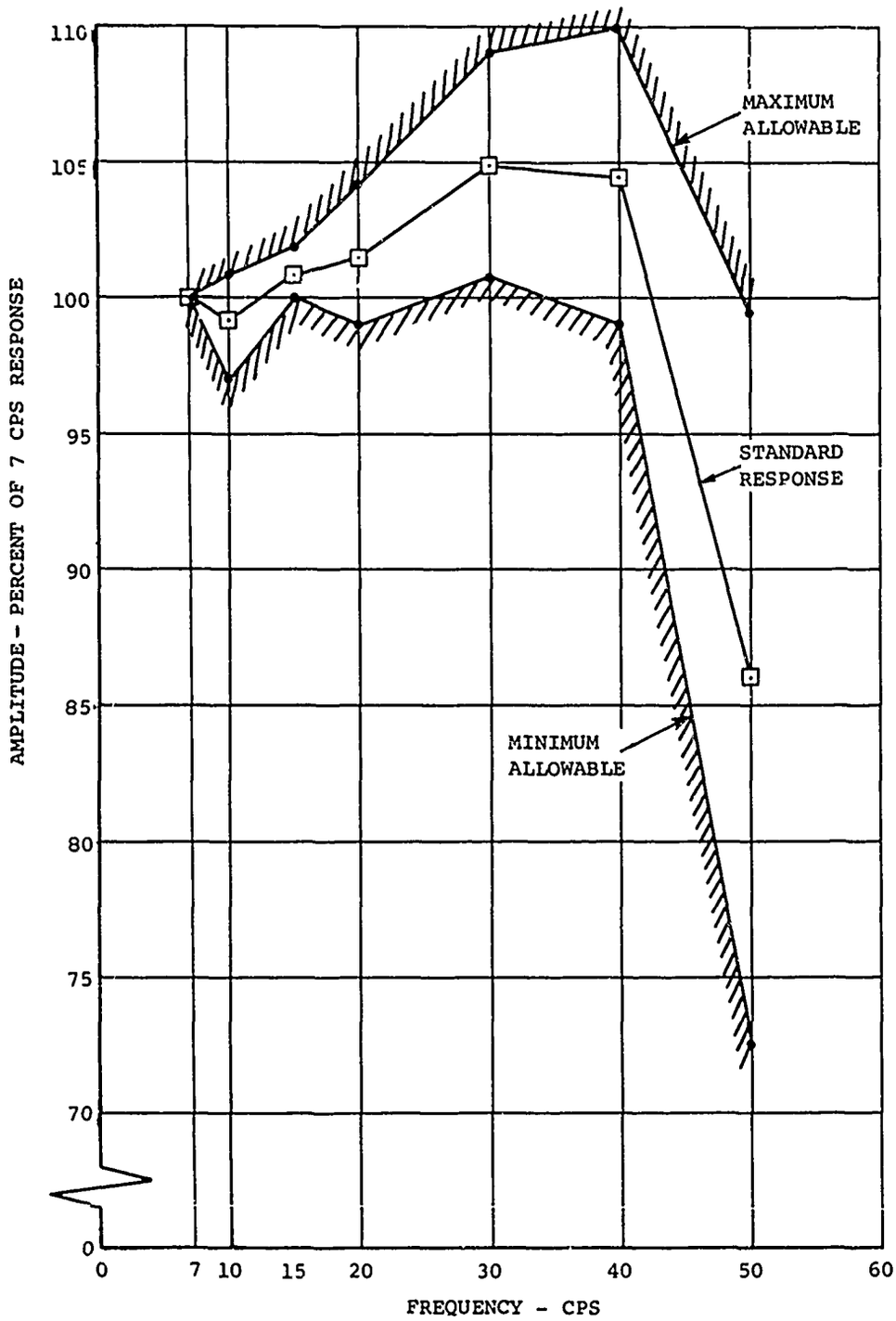

Figure 30. Frequency Response of Airframe Accelerometers.

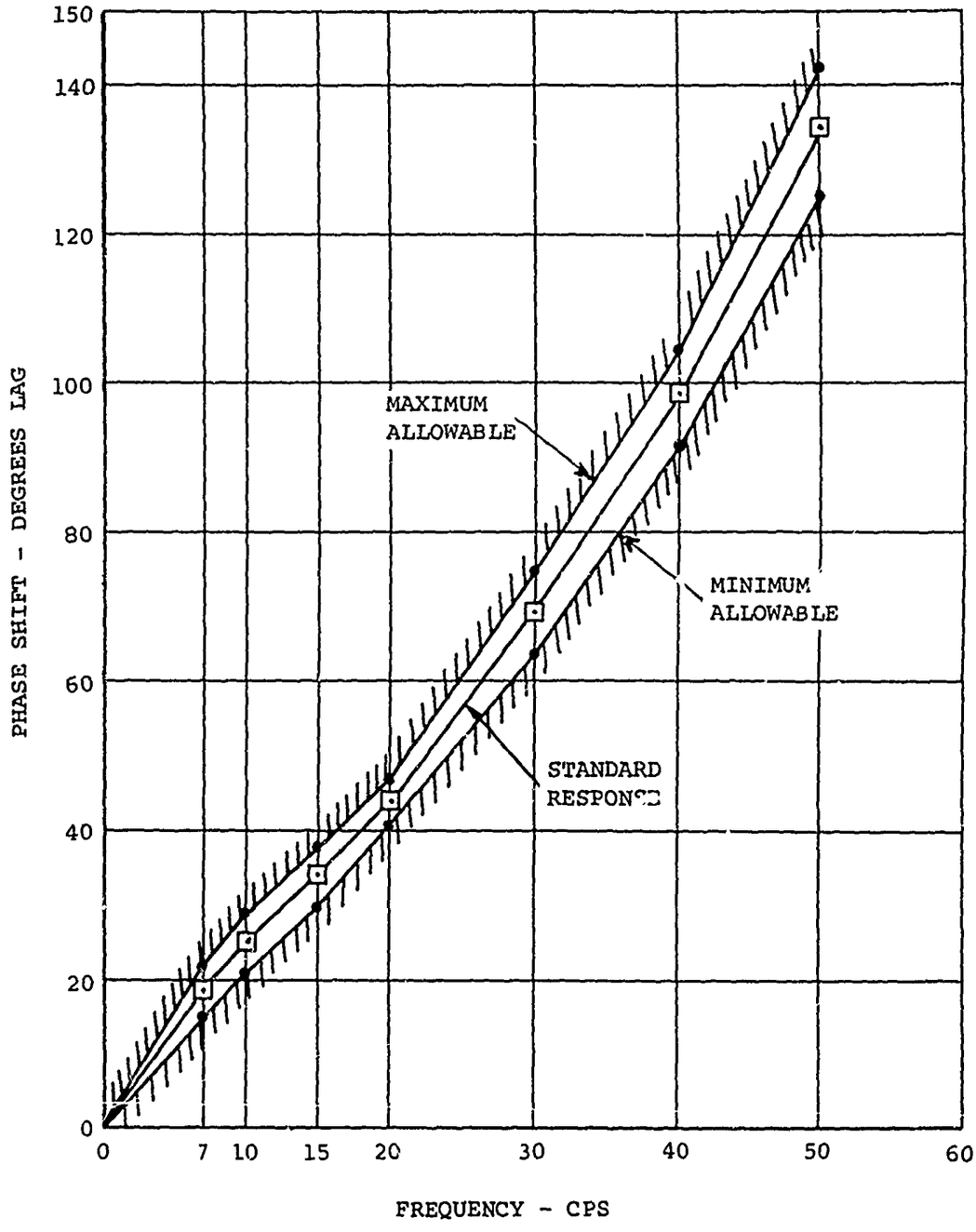

Figure 31. Phase Lag of Airframe Accelerometer Output Signals.

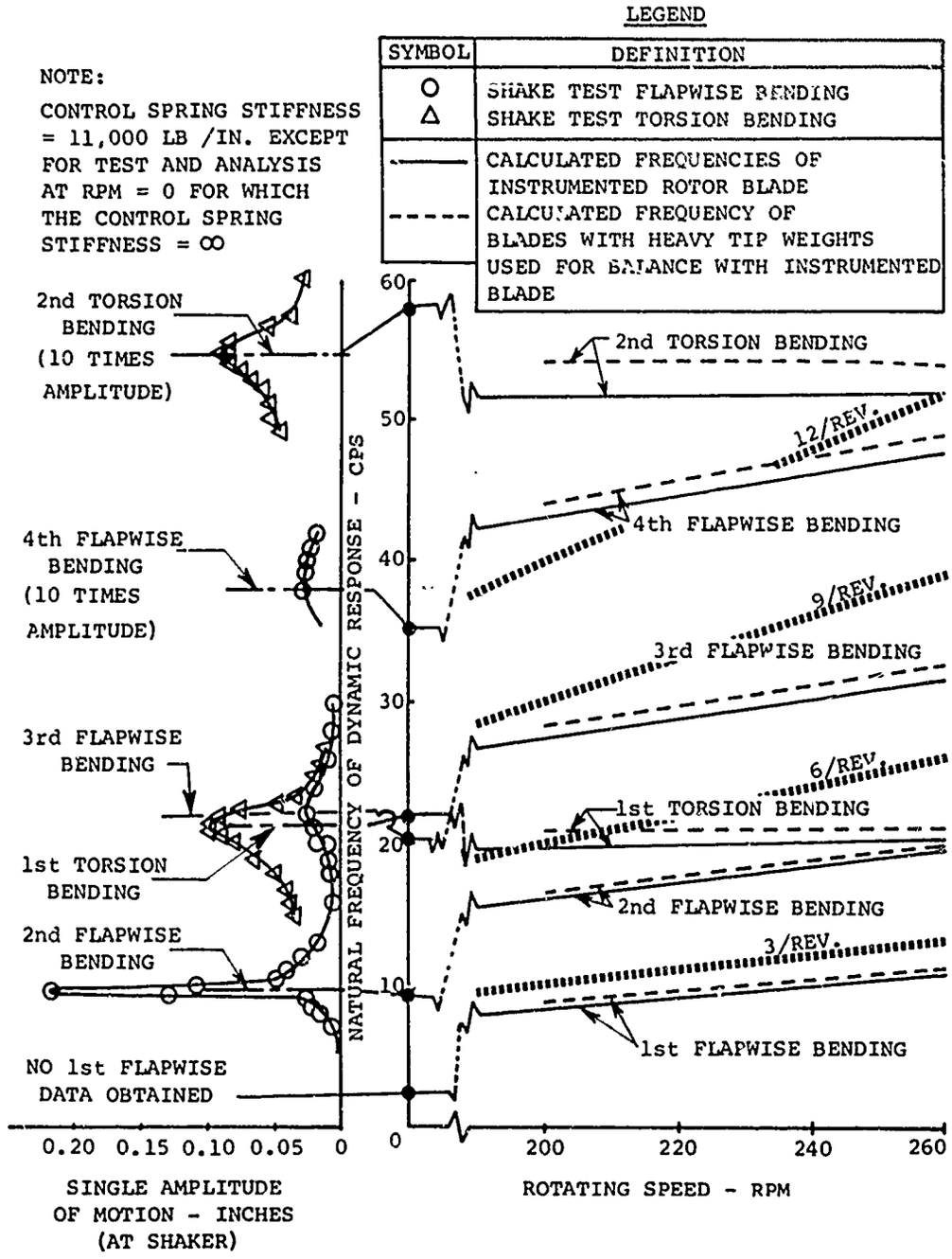

Figure 32. Calculated Rotor Blade Dynamic Characteristics and Comparative Nonrotating Test Data.

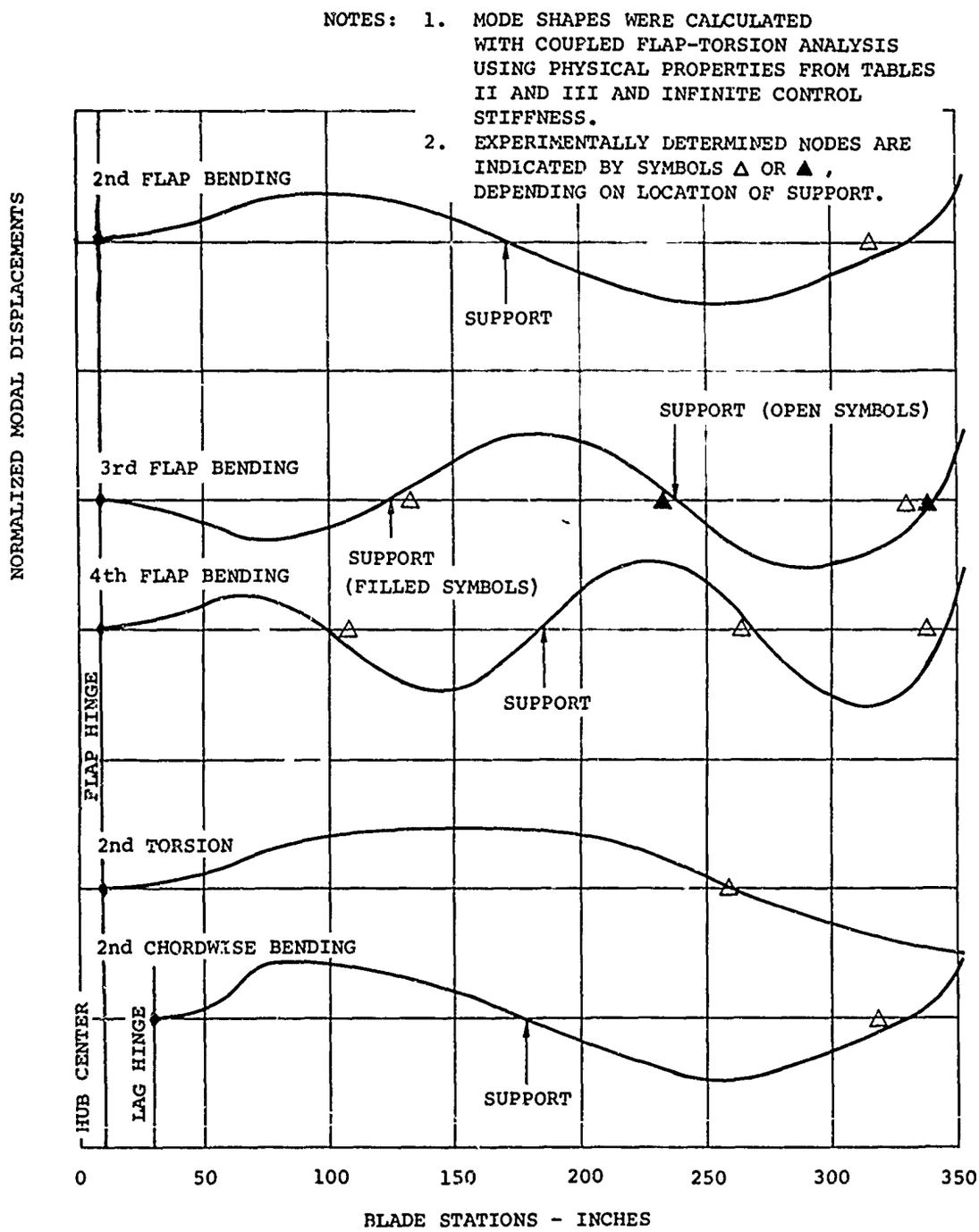

Figure 33. Nodal Points Obtained in Nonrotating Blade Response Tests.

NOTES: 1. ALL TRACKING DATA OBTAINED WITH BLADES IN FLAT PITCH (2° AT r/R = 0.75).
2. DOTTED LINES INDICATE DATA OBTAINED AFTER PITCH LINK ADJUSTMENTS.

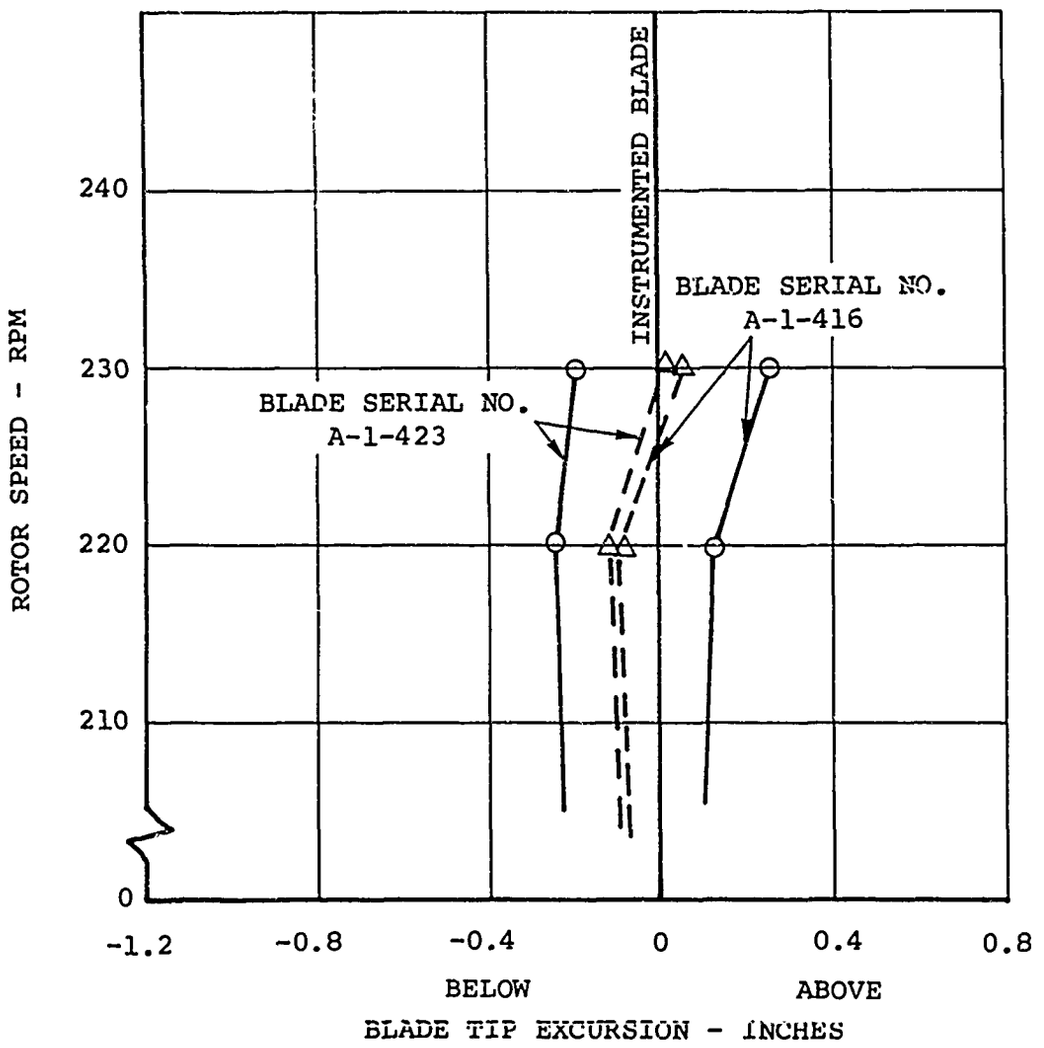

Figure 34. Forward Rotor Tracking Data.

NOTES: 1. ALL TRACKING DATA OBTAINED WITH BLADES IN FLAT PITCH (2° AT r/R = 0.75).
2. NO PITCH LINK ADJUSTMENTS WERE REQUIRED.

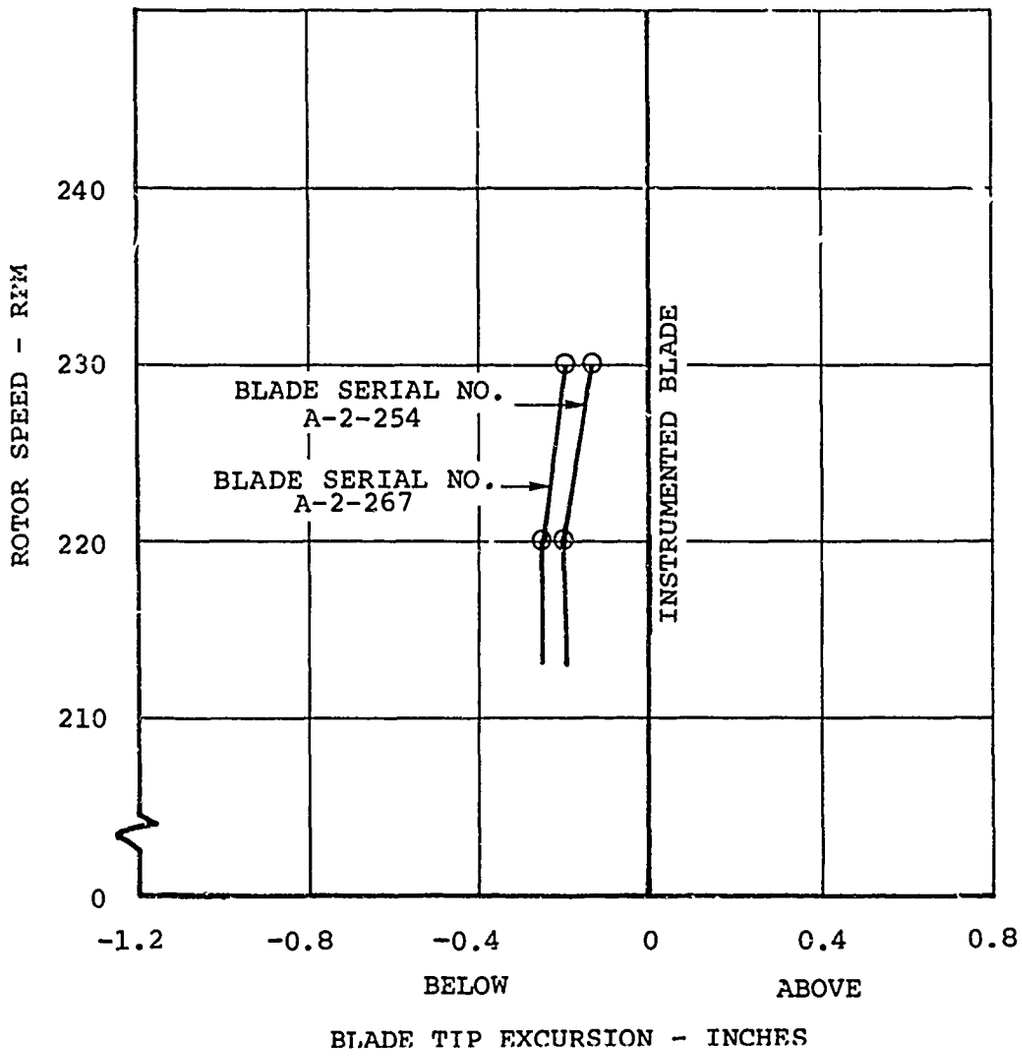

Figure 35. Aft Rotor Tracking Data.

EVALUATION

The results which require an evaluation in this report are the calibration data. Such an evaluation generally consists of the determination of the uncertainties due to hysteresis and deviation. For this program, which emphasized the blade pressure measurements, the pressure transducers were calibrated three times. A comparison of the results shows poor repeatability and indicates that in situ calibrations of these units are necessary to achieve accurate results. The other data presented in this report require no further evaluation as the following conclusions were obtained:

1. Accelerometer and rotor blade dynamic response data are within a reasonable tolerance of the expected results.

2. Pressure transducer interactions due to acceleration are shown to be negligibly small.

3. Temperature corrections for the pressure transducers are within the specifications and were substantiated in ground testing of the instrumented helicopter.

4. Rotor blade tracking data are within the tolerance known to give satisfactory performance.

QUALITY OF CALIBRATION

The uncertainty of single-load calibrations is shown by the maximum deviation of the test data from calibration relation, and by one-half of the maximum hysteresis (as defined in this report) with consideration of the load application and the recording system accuracies. Combined-loads calibrations are generally combinations of several calibrations including the single-load, and therefore a statistical averaging of errors is provided by the correlation coefficient calculation. These measures of calibration quality are discussed in subsequent sections. The errors in the load applications and recording experienced in this program caused significantly less than 1-percent uncertainty in the calibrations, and therefore these errors will not be considered further.

Hysteresis and Deviation of Single-Load Calibrations

A summary of the hysteresis and deviation data which were obtained is shown in Figure 36. In the majority of cases, these data show that the calibrations had approximately 1-percent uncertainty (root sum of squares). The largest values of hysteresis and deviation are shown by the blade chordwise gages and are believed to be from hysteresis of the adhesive and fiber glass structure of the blade. Initial test apparatus problems due to joint friction are considered to be a source of some uncertainty. Note in the data of Figure 36 that the forward blade (which was calibrated second) generally showed less error than the aft blade. Figure 37 was prepared, illustrating these relatively poor data, to show the consistency which was obtained. This graph is also a good illustration of the fact that the uncertainty is one-half the value of the hysteresis as presently defined.

It should be noted that, of the data shown in Figure 36, only the data for the control components are directly applicable to the estimation of data accuracy. The blade and shaft data uncertainty is better evaluated by means of the correlation determination. Pressure transducer errors were eliminated by means of an in situ calibration.

Repeatability of Pressure Transducer Calibration

An increase in accuracy of pressure transducer measurements was obtained through the in situ calibration of the transducers, which is described in Volume I of this report. Figure 38 shows the differences obtained between the manufacturer's quoted sensitivities as determined in a laboratory calibration of each transducer, as well as the differences in the laboratory calibration and the in situ calibrations. The data show these transducers to be highly sensitive to the recording equipment with which they are used; the necessity of an in situ calibration is thus indicated. Had the transducers been used either with the manufacturer's data or with the laboratory calibration data, errors of the magnitude indicated in Figure 38 would have occurred in the final data results.

Correlation of Rotor Shaft Calibration

Further evidence of the quality of the shaft calibration data is the value of the interaction loading correlation coefficients summarized in Table XVII. This coefficient, which was

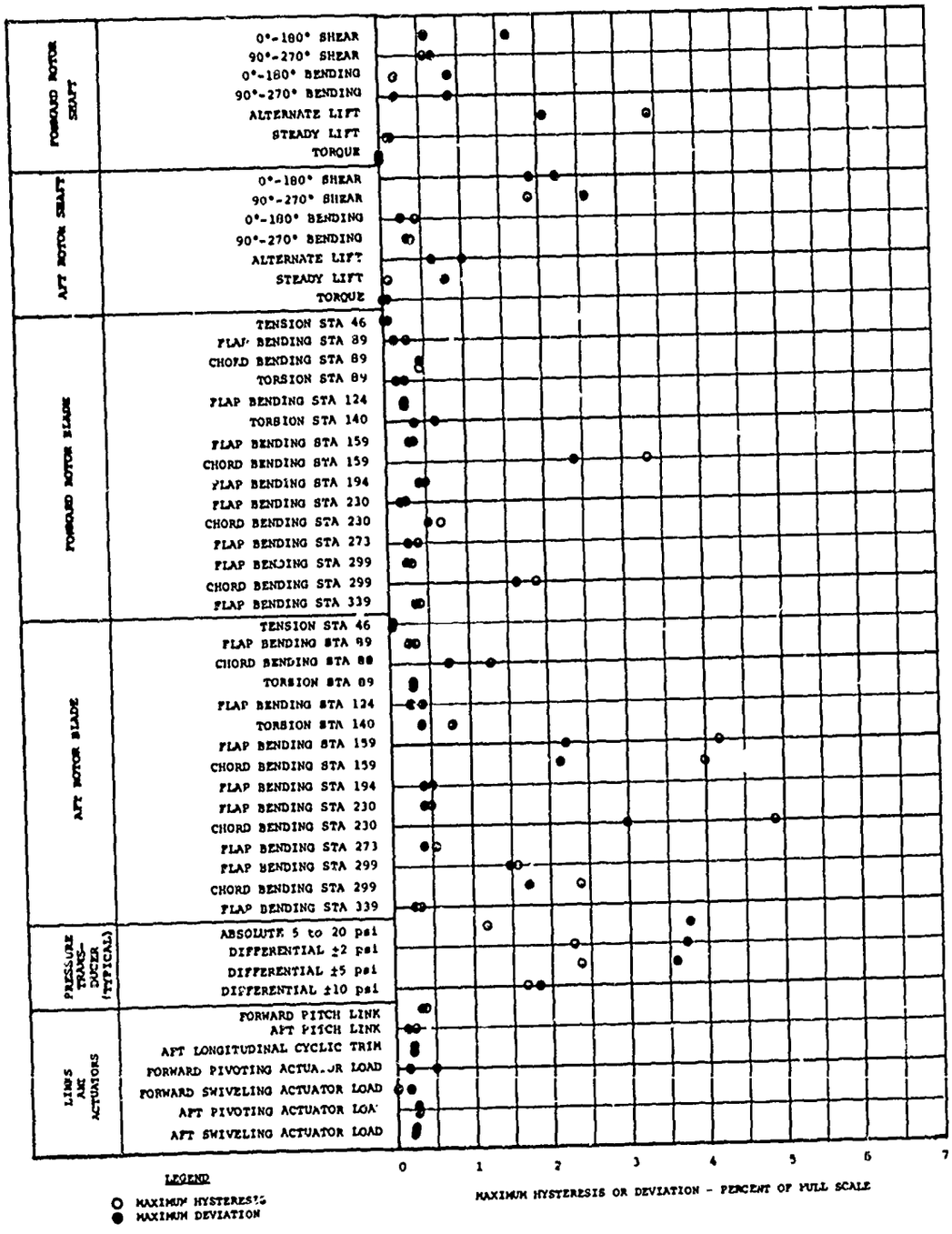

Figure 36. Summary of Data on the Quality of Single-Load Calibrations.

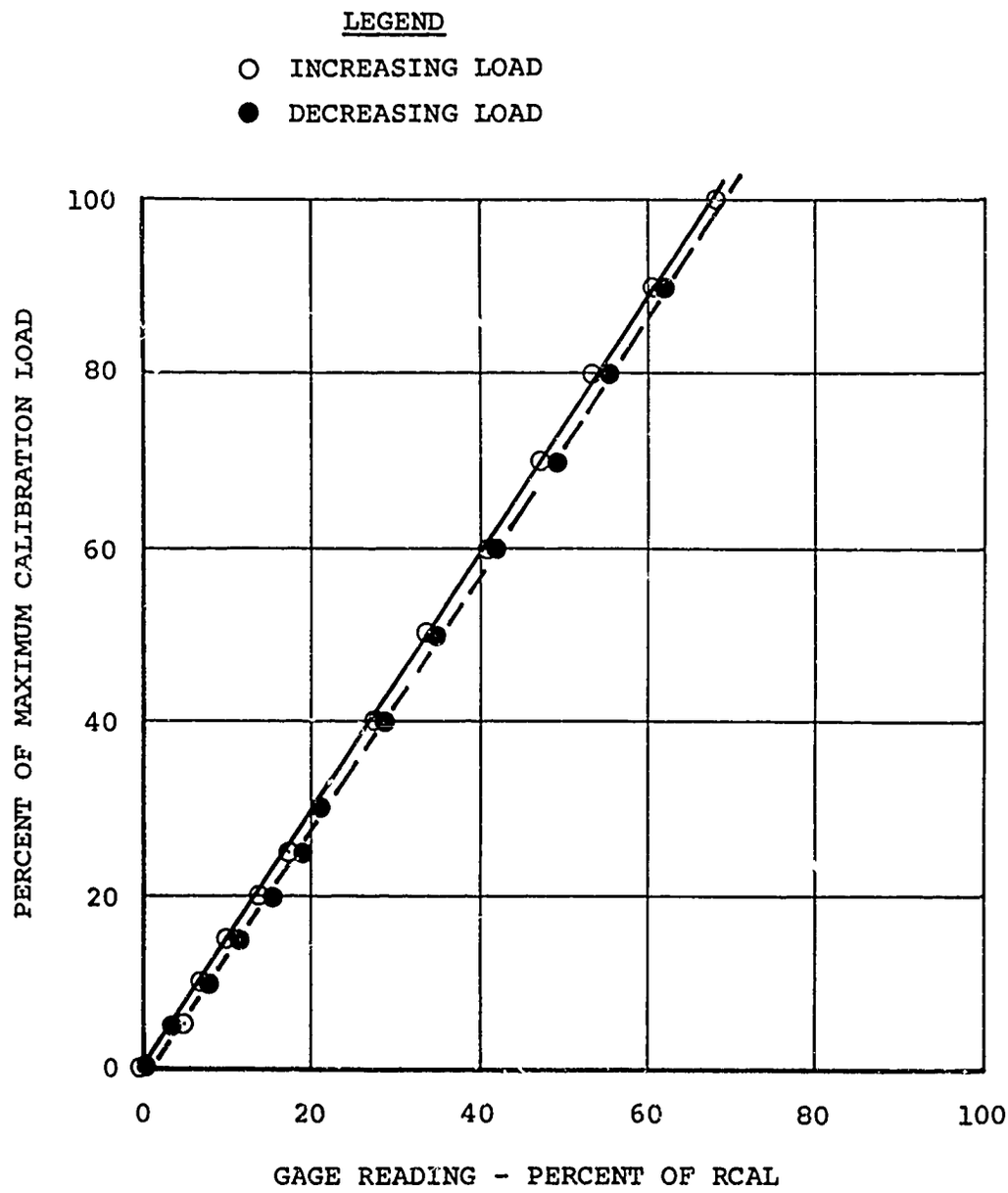

Figure 37. Single-Load Calibration of the Chordwise Bending Gage at Station 230, Illustrating a Case of High Hysteresis.

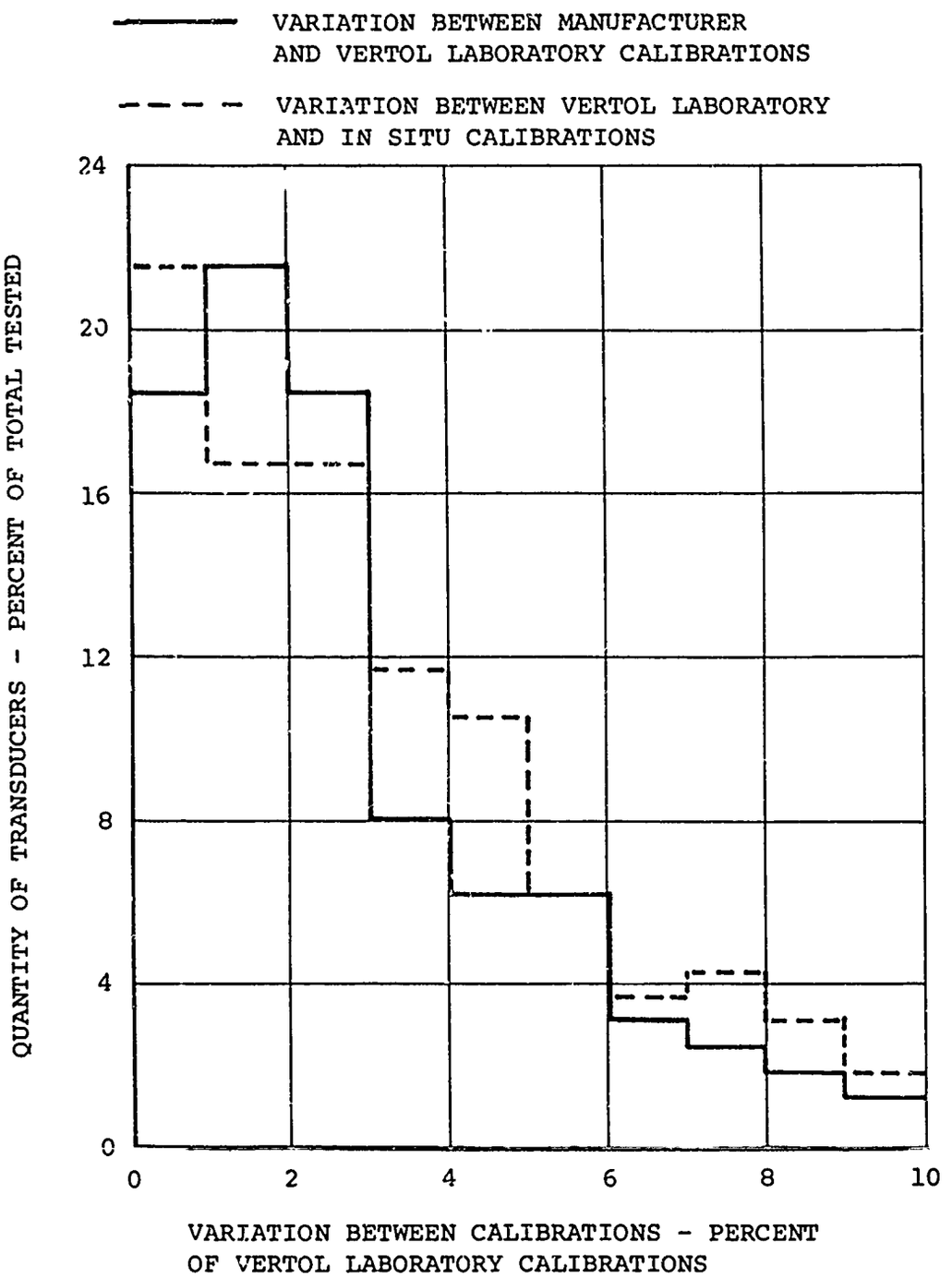

Figure 38. Repeatability of Airloads Pressure Transducer Calibrations.

defined in the calibration data analysis section, is a measure of the overall error of the data fit. The correlation coefficient varies inversely with the error; a correlation coefficient of 1.00 indicates zero error.

As shown in Table XVII, the smallest correlation coefficient obtained in the rotor shaft calibrations was 0.99947 which, as shown in Figure 22, is equivalent to a statistically averaged error of 1.5 percent. The correlation coefficients that were generally obtained were greater than 0.9999, indicating an error of less than 0.5 percent.

TABLE XVII
CORRELATION COEFFICIENTS OF ROTOR SHAFT COMBINED-LOADS CALIBRATION

Primary Load	Correlation Coefficient
Forward Shaft	
0 - 180 Shear	0.99952
90 - 270 Shear	0.99943
Lift	0.99616
9 - 180 Moment	0.99980
90 - 270 Moment	0.99991
Torque	1.00000
Aft Shaft	
0 - 180 Shear	0.99924
90 - 270 Shear	0.99978
Lift	0.99947
0 - 180 Moment	0.99986
90 - 270 Moment	0.99996
Torque	1.00000

A relatively poor correlation was obtained on the data for the forward shaft lift gage. These data were studied to determine the source of the error with the expectation that a mistake could be uncovered. It was found that the error is due to a nonlinear interaction of shear with lift. This type of interaction could result from a small misalignment in positioning the strain gages which measure lift.

Since a nonlinear interaction coefficient would have caused considerable data reduction complexity, and since the contribution of this interaction was small, no further effort was made to correct for this effect. There was no evidence of this interaction in the aft shaft data.

A further check of the interaction coefficients was provided by using the calibration matrix and the strain-gage readings obtained during each calibration and by calculating the load values which were apparently present to produce the gage readings. This exercise was performed for all loading conditions tested, and the calculated loads were compared to the loads measured during the calibration. Results of the comparison were within the error appropriate for the correlation shown in Table XVII.

Correlation of Rotor Blade Calibration

The accurate isolation of the interaction effects in the rotor blade strain-gage instrumentation was considerably more difficult than for the rotor shafts. In particular, the consistency of the zero reference for the calibration was not as good and is much more difficult to check. This effect is illustrated in Figure 27 by the apparently arbitrary starting points of each of the separate loading conditions. Relatively small shifts of these starting points cause a significant statistical error, since a considerable number of data points result from each loading condition. However, the correlation coefficients for the rotor blades shown in Table XVIII indicate acceptable accuracy of the calibration and also show that an improvement in the results will be obtained by using the interaction coefficients.

TABLE XVIII
CORRELATION COEFFICIENTS OF ROTOR BLADE COMBINED-LOADS CALIBRATION

Blade Station	Primary Load	Correlation Coefficient
	Forward Blade	
46	Torsion	0.93599
46	Tension	0.99838
89	Flap bending	0.99998

TABLE XVIII - Continued

Blade Station	Primary Load	Correlation Coefficient
89	Chord bending	1.00000
124	Flap bending	0.99447
141	Torsion	0.91215
159	Flap bending	0.98535
159	Chord bending	0.98695
195	Flap bending	0.98805
231	Flap bending	0.99354
231	Chord bending	0.99997
267	Flap bending	0.99526
300	Flap bending	0.99976
300	Chord bending	1.00000
339	Flap bending	1.00000
	Aft Blade	
46	Torsion	0.96009
46	Tension	0.99878
89	Flap bending	0.99997
89	Chord bending	1.00000
124	Flap bending	0.99690
141	Torsion	0.95226
159	Flap bending	0.95317
159	Chord bending	0.97721
195	Flap bending	0.96941
231	Flap bending	0.99267
231	Chord bending	0.99996
267	Flap bending	0.99747
300	Flap bending	0.99987
300	Chord bending	1.00000
339	Flap bending	0.99999

BIBLIOGRAPHY

1. Childs, R.C., and Grant, W.J., Tabular Test Data Summary of Measurements of Dynamic Airloads on a CH-47A Tandem Rotor Helicopter, Boeing Document D8-0387, to be issued.

2. Pruyn, R., and Alexander, W.T.,Jr., The USAAVLABS Tandem Rotor Airloads Measurement Program, paper to be presented at the Aerodynamic Testing Conference of the American Institute of Aeronautics and Astronautics, Boeing Document D8-0381, September 1966.

3. Pruyn, R.R., Lamb, H., and Grant, W.J., Results of Whirl Testing of Partially Instrumented Forward Rotor Blade, Boeing Document R-433, 20 May 1965.

4. Pruyn, R.R., Obbard, J., and Shakespeare, C., The Measurement and Analysis of Rotor Blade Airloads and the Resulting Dynamic Response of a Large Tandem Rotor Helicopter, paper presented at the Fourth International Aerospace Instrumentation Symposium, Boeing Document D8-0296, March 1966.

5. Pruyn, R.R., Preliminary Data Report of Dynamic Airloads Flight Test Results as Prepared for Cornell Aeronautical Laboratories Correlation Studies, Boeing Document D8-0408, June 1966.

APPENDIX I

ANALYSIS OF AN ELASTIC STRUCTURE UNDER PREDOMINANTLY AXIAL LOAD FOR COMBINED-LOADS CALIBRATION OF INSTRUMENTATION FOR MEASURING BENDING AND TORSION

The purpose of this computer program is to correlate readings of strain gages, mounted on a rotor blade, with applied static loads.

To accomplish this task, a static deflection test was performed on both the forward and aft blades. The computer program was written specifically for this test to determine the theoretical bending moments, shears, tension, and torsion at each of the instrumented blade stations. The theory and static tests considered combined-loads effects so that their interactions could be evaluated. This was necessary since deflections of the blade caused changes in applied loads. Several interaction equations were required to include this effect of interactions. The interaction equations relating these loads and deflections are given in equations (13) through (39).

To compute the deflections of the blade, three differential equations are required (equations (40), (41), and (42)). These are solved by an iteration procedure which is continued until the desired degree of accuracy is obtained.

This program ultimately yields the blade deflections, shears, bending moments, and resultant loads acting on the blade at several stations along the length of the blade. The assumptions made in this program are:

(1) small deflections
(2) small initial twist.

The test setup is shown in schematic form in Figures 39 and 40. The coordinates used in the derivation of the equations are shown in Figure 41. Figures 42 and 43 show the details of the load applications and the geometry involved.

SYMBOLS AND DEFINITIONS

The symbols and definitions that were used in this analysis are defined as follows:

AE_j Axial stiffness

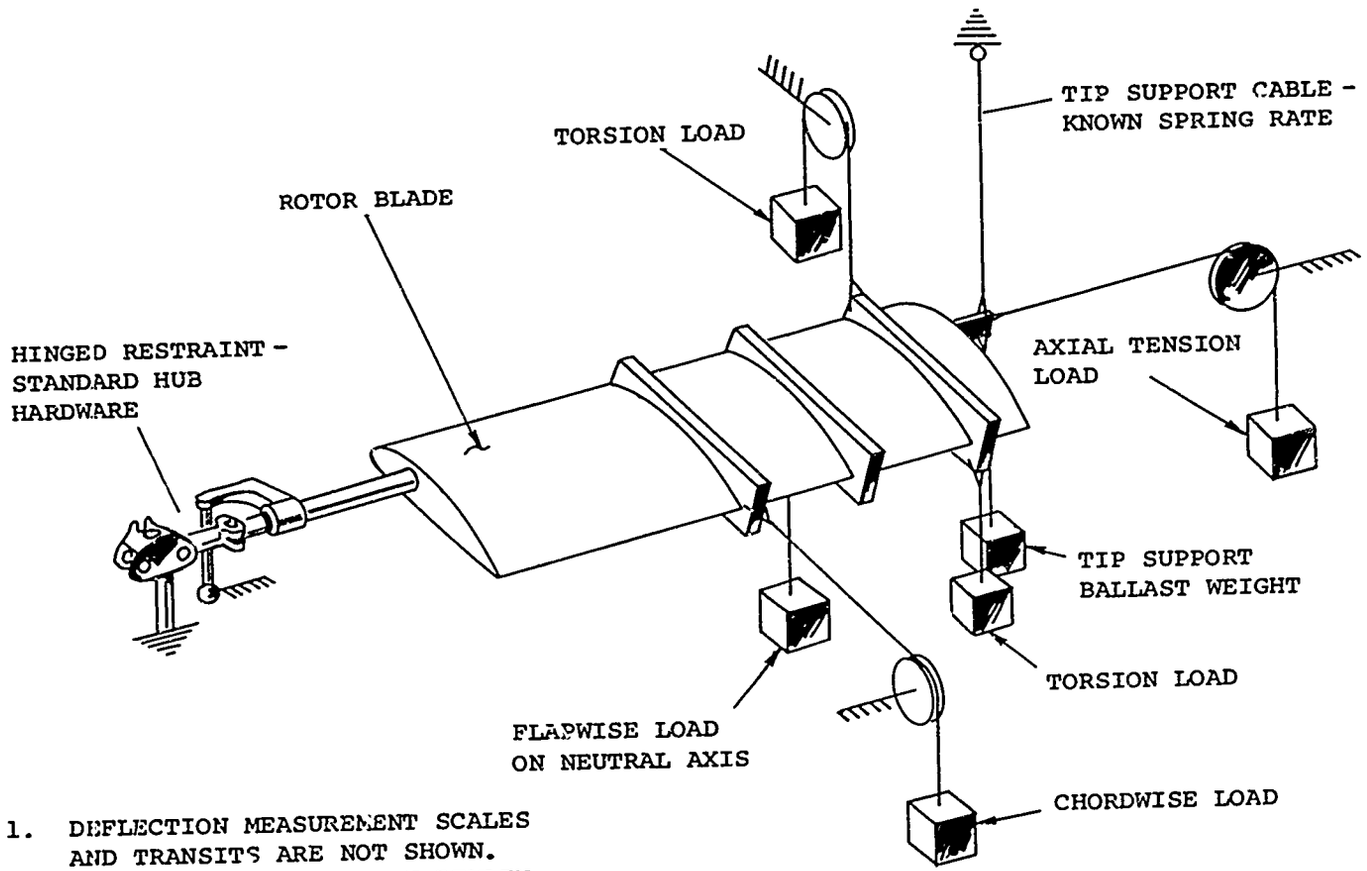

NOTES: 1. DEFLECTION MEASUREMENT SCALES AND TRANSITS ARE NOT SHOWN.
2. ALL FIXED POINTS SHOWN REMAIN FIXED FOR ALL LOAD VALUES. LOAD POINTS ARE NOT ADJUSTABLE BUT CAN BE DISCONNECTED.

Figure 39. Schematic Diagram of Blade Calibration with Combined Loads.

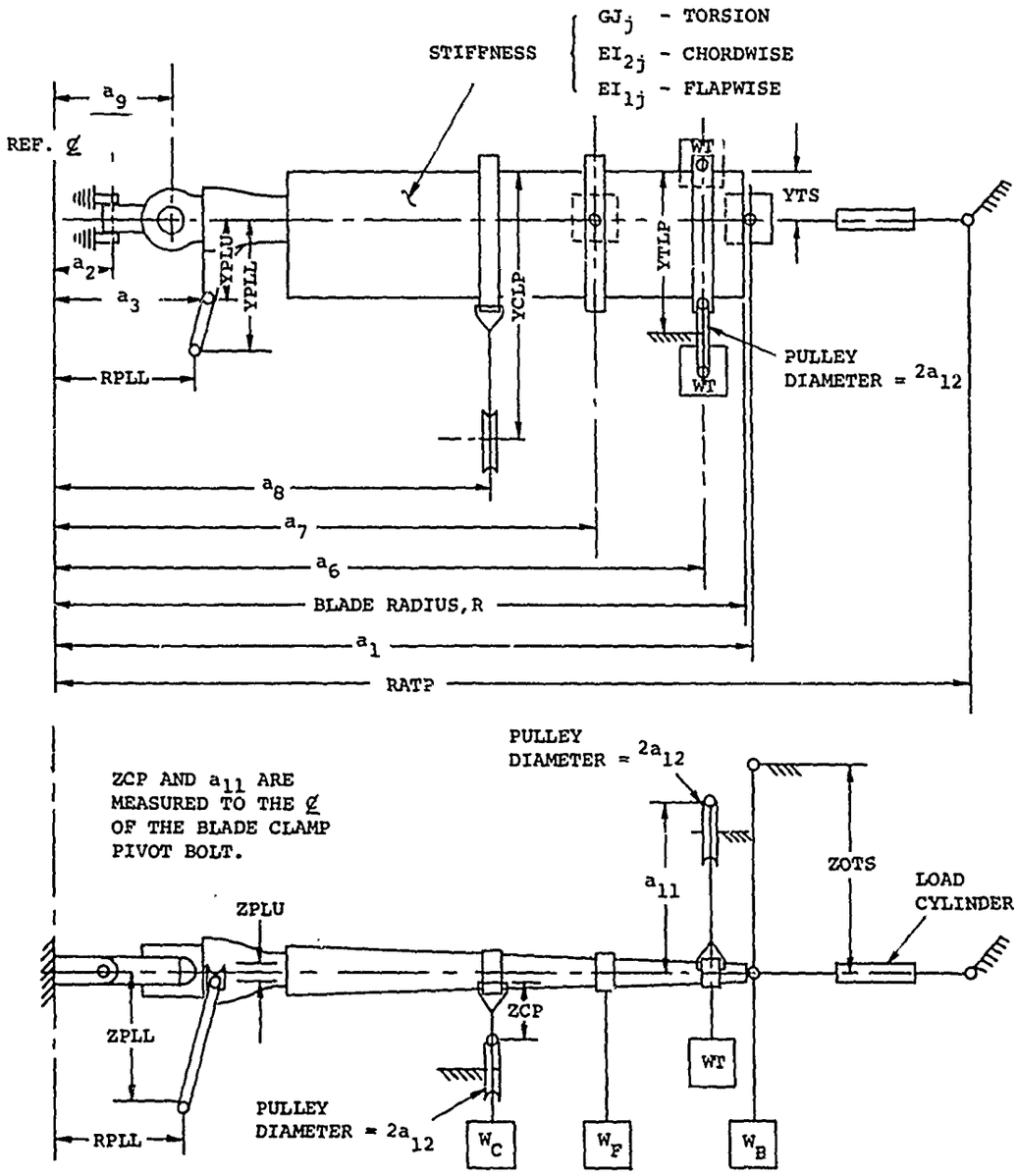

Figure 40. Illustration of Geometry and Notation of Blade Calibration Problem.

a_1	Distance from hub centerline to tip support along x axis
a_2	Distance from hub centerline to flap hinge pin along x axis
a_3	Distance from hub centerline to pitch link along x axis
a_4	Weight of torque load applied at leading edge
a_5	Weight of torque load applied at trailing edge
a_6	Distance from hub centerline to torque load along x axis
a_7	Distance from hub centerline to flap load along x axis
a_8	Distance from hub centerline to chord load along x axis
a_9	Distance from hub centerline to lag hinge pin along x axis
a_{11}	Distance from centerline of blade clamp pivot to top of torque load pulley
a_{12}	Torque load pulley diameter divided by 2
$a(x), b(x), c(x), d(x), F(x), g(x),$	Coefficients in system of differential equations at station x
$B_2(x_j)$	Section coefficient at x_j
E	Young's Modulus
$EI_{1,j}$	Bending stiffness at x_j about major principle axis
$EI_{2,j}$	Bending stiffness at x_j about minor principle axis
e.a.	Elastic axis
GJ_j	Torsional stiffness at x_j
i	Index denoting i^{th} iteration
j,j+1	Indices denoting j^{th}, $j+1^{st}$ radial station (with coordinates x_j and x_{j+1} respectively)

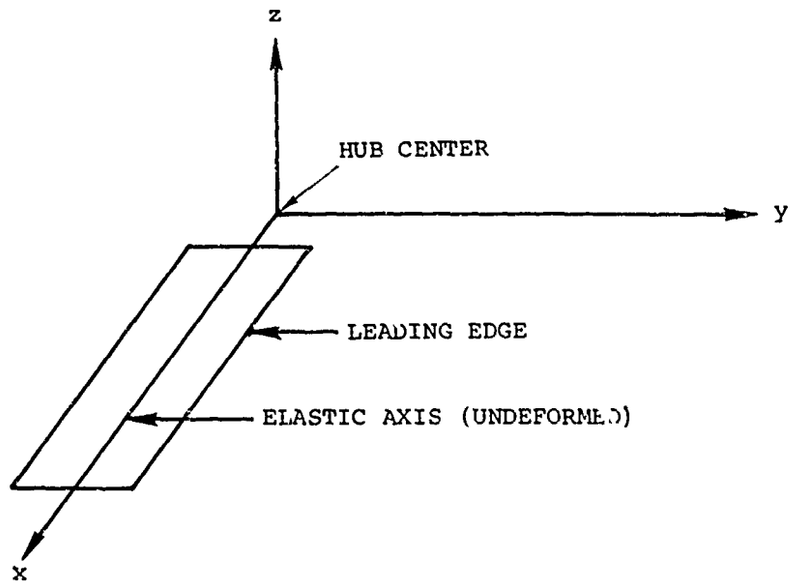

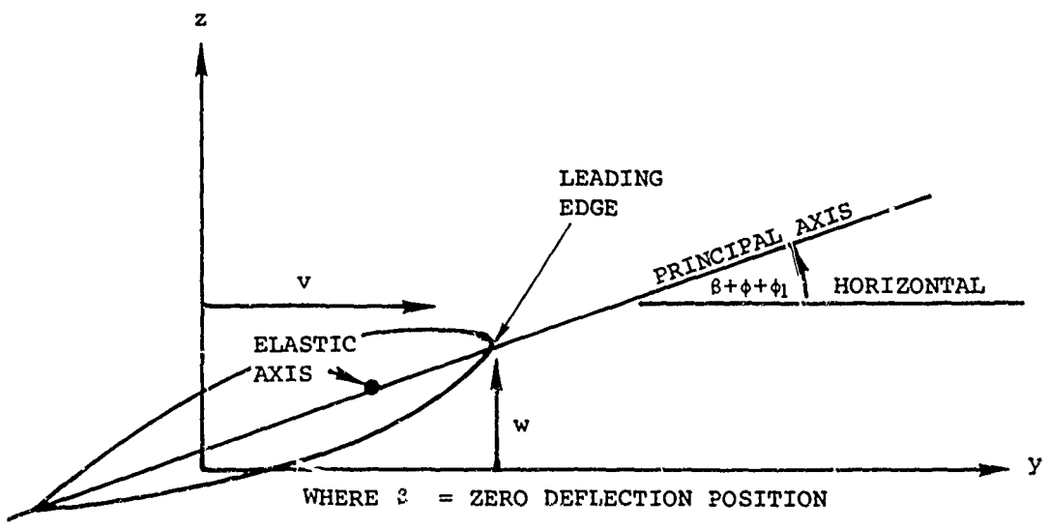

WHERE β = ZERO DEFLECTION POSITION

ϕ = TWIST DISTORTION

ϕ_1 = DEFLECTION DUE TO TWIST OF MOUNTING

NOTE: THE UNDEFORMED (ZERO DEFLECTION, NEUTRAL) POSITION IS DEFINED AS THE POSITION OF THE BLADE SUBJECT ONLY TO:

1. HUB RESTRAINT
2. TIP SUPPORT AND TIP BALLAST LOAD.

Figure 41. Rotor Blade Coordinates.

K	Spring constant of tip support cable
k	Index denoting k^{th} chordwise station, having a range of values $-m, -m+1, \ldots 0, \ldots p-1, p$
k_j	Polar radius of gyration at x_j
ℓ	Number of last iteration
$M_{ix}(x)$	Pseudo torque at station x in i^{th} iteration
$M_{iy}(x)$	Pseudo bending moment about y-axis at station x in i^{th} iteration
$M_{iz}(x)$	Pseudo bending moment about z axis at station x in i^{th} iteration
Prime	Derivative, with respect to x
Q	Torque tending to twist blade mounting
R	Rotor radius
T	Tension weight (W_A)
$\bar{T}$	Tension in tip support cable
$t(\eta), t(\eta_k)$	Thickness of blade at η, ηx
u_1	Distance from elastic axis to leading edge cable attachment for torque load measured horizontally with no deflection
u_2	Distance from elastic axis to trailing edge cable attachment for torque load measured horizontally with no deflection
u_3	Vertical distance from elastic axis to flap load cable attachment
u_4	Distance from center of chord load pulley to cable attachment
u_5	Horizontal distance from elastic axis to chord load cable attachment with no deflection
u_6	Horizontal distance from tension pulley center to tip cable attachment
v	Deflection of load attachment points in y direction
W_A	Tension weight

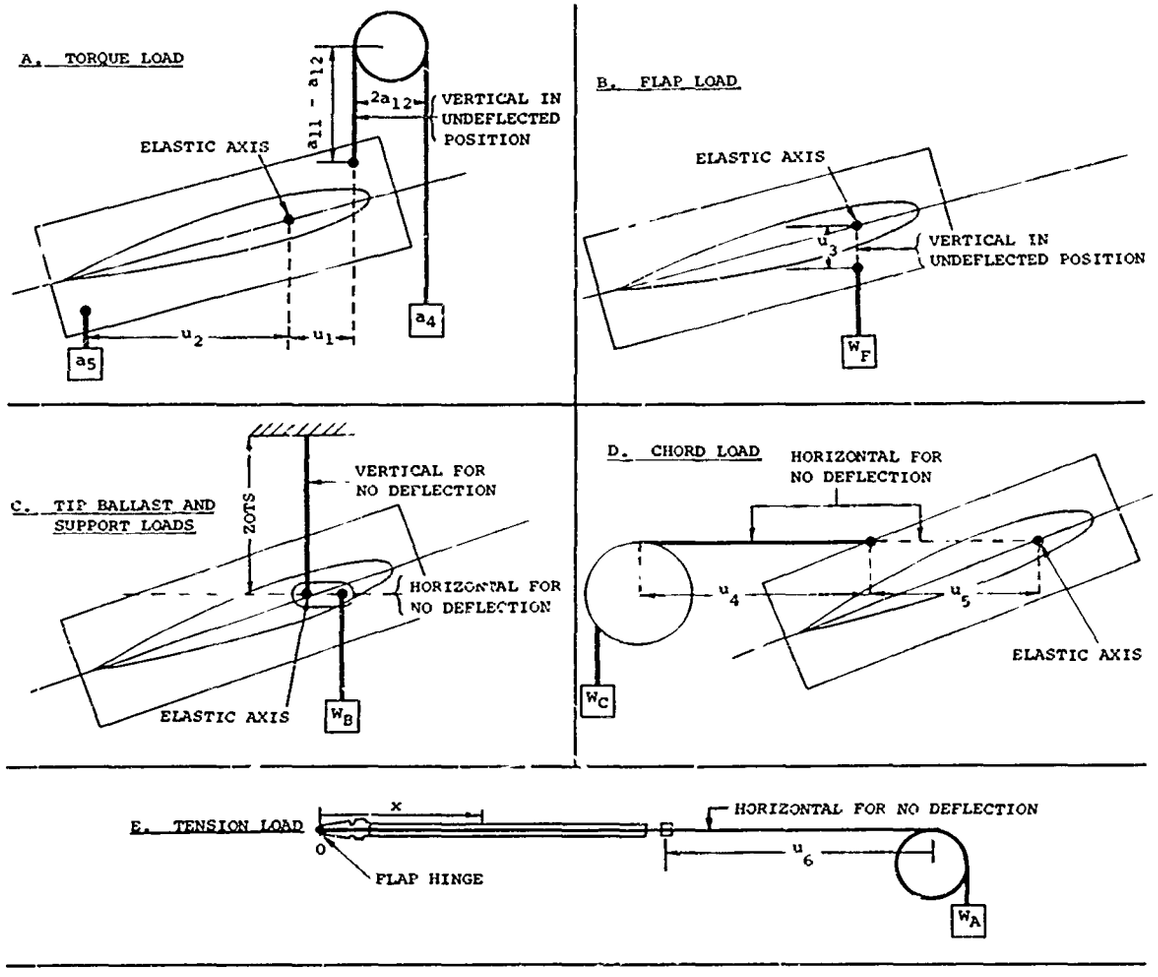

Figure 42. Details of Blade Load Application Geometry.

W_B	Tip ballast weight
W_C	Chord load
W_F	Flap load
w	Deflection of load attachment points in z direction
x	Axis fixed in inertial space, in direction of undeflected blade elastic axis
$x_o, x_1 \ldots x_n$	Distances from rotor hub such that $x_o=0$, $x_n=a_1$ points at which output desired, defining intervals of iteration for differential equation
y	Axis fixed in inertial space perpendicular to x axis in chord direction, positive toward leading edge
z	Axis fixed in inertial space perpendicular to x and y axes
ZOTS	Vertical distance from elastic axis to tip support cable fixture
β	Zero deflection twist angle, positive for leading edge up
β'	Derivative of twist angle = constant
β_j	Blade undeflected twist at x_j, positive for leading edge up; measured between principal axis and horizontal
100ε	Approximate percentage of unaccounted-for deflection
η	Coordinate along principal axis from elastic axis, positive toward leading edge and negative toward trailing edge; also, dummy variable of integration
η_m	Coordinate of trailing edge
η_p	Coordinate of leading edge
ϕ	Twist deflection due to torsion and torsion interaction loads
ϕ_1	Twist deflection due to rigid body motions

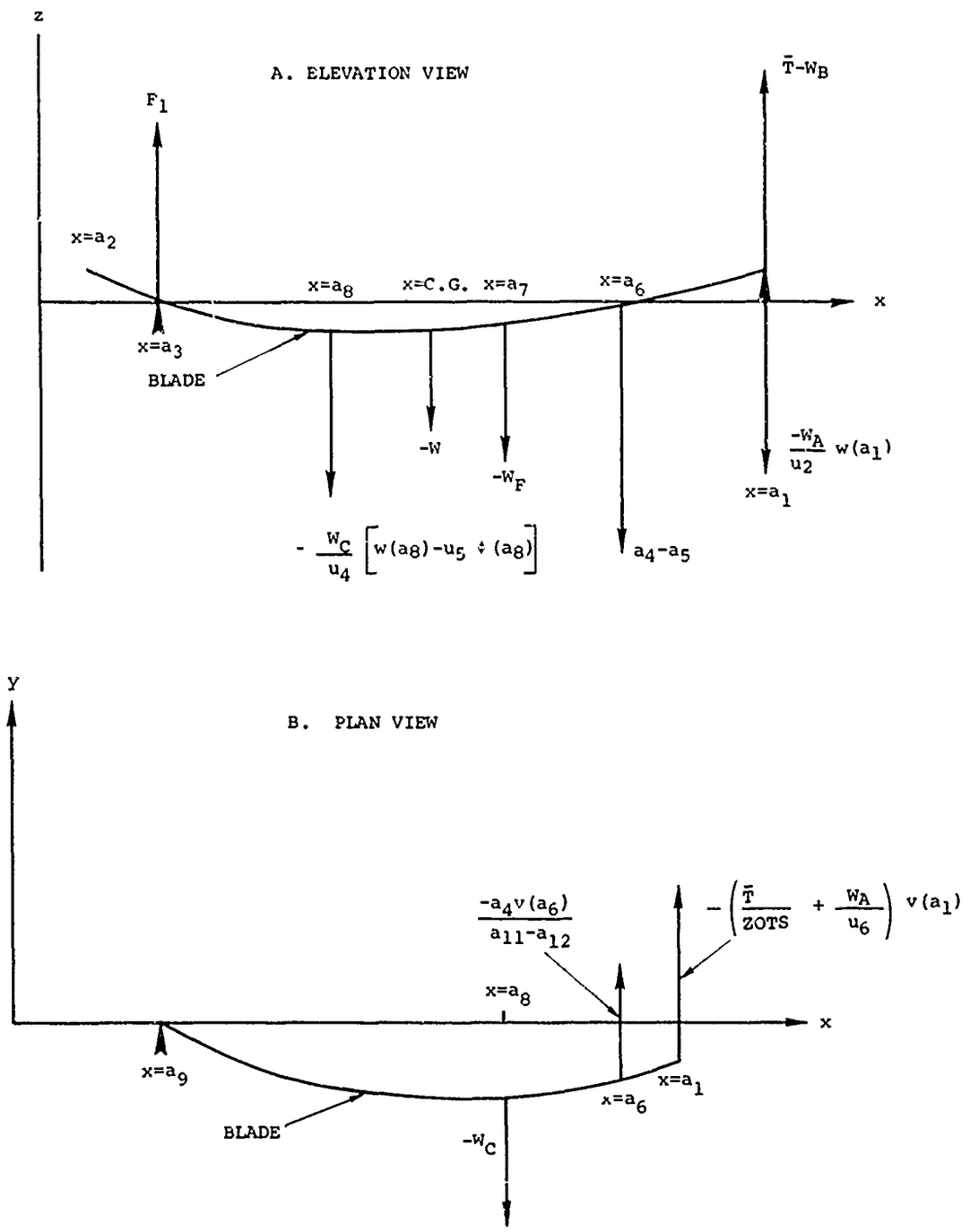

Figure 43. Blade Loads and Geometry of Application.

The input data requirements for this computer program were as follows:

$AE, \ldots\ldots AE_n$	a_{12}	u_5
a_1	E	u_6
a_2	$EI_{1,1}, EI_{1,2}, \ldots EI_{1,n}$	W_A
a_3	$EI_{2,1}, EI_{2,2}, \ldots EI_{2,n}$	W_C
a_4	$GJ, \ldots GJ_n$	W_F
a_5	K	$x_0, x_1, \ldots x_u$
a_6	$t(\eta_{-m}) \ldots t(\eta_p)$	ZOTS
a_7	u_1	β'
a_8	u_2	$\beta_1, \ldots \beta_n$
a_9	u_3	ε
a_{11}	u_4	$\eta_{-m}, \eta_{-m+1}, \ldots 0, \ldots \eta_p$

The computer output data which resulted from this program were as follows:

ℓ	Number of iterations needed to be within error limit requirement
$\bar{M}_{ox}(x_j)$	Bending about x-axis at x_j without considering blade deflection
$\bar{M}_{\ell x}(x_j)$	Bending about x-axis at x_j considering blade deflection
$\bar{M}_{oy}(x_j)$	Bending moment about y-axis at x_j without considering blade deflection
$\bar{M}_{\ell y}(x_j)$	Bending moment about y-axis at x_j considering blade deflection
$\bar{M}_{oz}(x_j)$	Bending moment about z-axis at x_j without considering blade deflection
$\bar{M}_{\ell z}(x_j)$	Bending moment about z-axis at x_j considering blade deflection

$T_{ox}(x_j), T_{\ell x}(x_j)$	Torque loading at x_j without and with consideration of blade deflections, respectively
$V_{oy}(x_j), V_{\ell y}(x_j)$	Shears in the y-direction without and with consideration of blade deflections, respectively
$V_{oz}(x_j), V_{\ell z}(x_j)$	Shears in the z-direction without and with consideration of blade deflections, respectively

INTERACTION EQUATIONS

1. Torque loads and their interaction effects (excluding bending moments)

   In a deflected position the blade loads due to torsion are:

$$\text{Torque} = a_4 u_1 + a_5 u_2 \ , \tag{13}$$

$$\text{Flap shear} = a_4 - a_5 \ , \tag{14}$$

$$\text{Chord shear} = \frac{-a_4 v(a_6)}{a_{11} - a_{12}} \ . \tag{15}$$

2. Flap shear loads and their interaction effects (excluding bending moments)

   In a deflected position the blade loads due to flap shear loading are:

$$\text{Flap shear} = -W_F \ , \tag{16}$$

$$\text{Blade torque} = -W_F u_3 \phi(a_7) \ , \tag{17}$$

Torque reaction at blade mounting =

$$-W_F[u_3\phi(a_7) + v(a_7)] \ . \tag{18}$$

3. Tip ballast and tip support loads and their interaction effects (excluding bending moments)

In a deflected position the blade loads due to these blade tip forces are:

$$\text{Flap shear} = \bar{T} - W_B \ , \tag{19}$$

$$\text{Chord shear} = \frac{-\bar{T}v(a_1)}{ZOTS} \ . \tag{20}$$

4. Chord loads and their interaction effects (excluding bending moments)

In a deflected position the blade loads due to chord loading are:

$$\text{Flap shear} = \frac{W_C}{u_4}\left[w(a_8) - u_5\phi(a_8)\right] \ , \tag{21}$$

$$\text{Chord shear} = -W_C \ , \tag{22}$$

$$\text{Torque} = \frac{u_5}{u_4} W_C\left[w(a_8) - u_5\phi(a_8)\right] \ . \tag{23}$$

5. Tension loads and their interaction effects (excluding bending moments)

In a deflected position the blade loads due to tension are:

$$\text{Flap shear} = -\frac{W_A}{u_6} w(a_1) \ , \tag{24}$$

$$\text{Chord shear} = -\frac{W_A}{u_6} v(a_1) \ , \tag{25}$$

Torsion acting on blade =

$$Tw'\left[v - (-x + a_1 + u_6)\frac{v(a_1)}{u_6}\right] \ . \tag{26}$$

Bending moments caused by these various loads will now be determined. Consider first the bending moments about the y axis (see Figure 43A). The deflection at the blade tip, with y direction, is first required. It is

$$w(a_1) = -\frac{1}{(a_1-a_3)\left(K+\frac{W_A}{u_6}\right)}\Big\{(a_5-a_4)(a_6-a_3) + W_F(a_7-a_3)$$

$$+ \frac{W_C}{u_4}\left[w(a_8) - u_5\phi(a_8)\right](a_8 - a_3)\Big\}. \qquad (27)$$

The bending moment about the y axis is

$$M_y(x) = \left(-K + \frac{W_A}{u_6}\right)w(a_1)(a_1 - x)$$

$$+ W_A\left[w - (-x + a_1 + u_6)\frac{w(a_1)}{u_6}\right],$$

$$a_6 \le x \le a_1 . \qquad (28)$$

$$M_y(x) = \left(-K + \frac{W_A}{u_6}\right)w(a_1)(a_1 - x) + (a_5 - a_4)(a_6 - x)$$

$$+ W_A\left[w - (-x + a_1 + u_6)\frac{w(a_1)}{u_6}\right], \qquad a_7 \le x \le a_6 . \qquad (29)$$

$$M_y(x) = \left(-K + \frac{W_A}{u_6}\right)w(a_1)(a_1 - x) + (a_5 - a_4)(a_6 - x)$$

$$-W_F(a_7 - x) + W_A\left[w - (-x + a_1 + u_6)\frac{w(a_1)}{u_6}\right],$$

$$a_8 \le x \le a_7 . \qquad (30)$$

$$M_y(x) = \left(-K + \frac{W_A}{u_6}\right)w(a_1)(a_1 - x) + (a_5 - a_4)(a_6 - x)$$

$$- W_F(a_7 - x) - \frac{W_C}{u_4}\left[w(a_8) - u_5\phi(a_5)\right](a_8 - x)$$

$$+ W_A\left[w - (-x + a_1 + u_6)\frac{w(a_1)}{u_6}\right], \qquad a_3 \le x \le a_8 . \qquad (31)$$

The bending moment distribution along the blade about the z axis is as follows:

$$M_z(x) = -\left(\frac{\overline{T}}{ZOTS} + \frac{W_A}{u_6}\right)v(a_1)(a_1 - x)$$

$$+ W_A\left[v - (-x + a_1 + v_6)\frac{v(a_1)}{u_6}\right], \quad a_6 \leq x \leq a_1 . \quad (32)$$

$$M_z(x) = -\left(\frac{\overline{T}}{ZOTS} + \frac{W_A}{u_6}\right)v(a_1)(a_1 - x) - \frac{a_4 v(a_6)}{a_{11} - a_{12}}(a_6 - x)$$

$$+ W_A\left[v - (-x + a_1 + v_6)\frac{v(a_1)}{u_6}\right], \quad a_8 \leq x \leq a_6 . \quad (33)$$

$$M_z(x) = -\left(\frac{\overline{T}}{ZOTS} + \frac{W_A}{u_6}\right)v(a_1)(a_1 - x) - \frac{a_4 v(a_6)}{a_{11} - a_{12}}(a_6 - x)$$

$$- W_C(a_8 - x) + W_A\left[v - (-x + a_1 + v_6)\frac{v(a_1)}{u_6}\right],$$

$$a_{10} \leq x \leq a_8 . \quad (34)$$

The torsion loads acting on the blade along its length are

$$M_x(x) = Tw'\left[v + (x - a_1 - u_6)\frac{v(a_1)}{u_6}\right], \quad a_6 \leq x \leq a_1 . \quad (35)$$

$$M_x(x) = Tw'\left[v + (x - a_1 - u_6)\frac{v(a_1)}{u_6}\right] + a_4 u_1 + a_5 u_2,$$

$$a_7 \leq x \leq a_6 . \quad (36)$$

$$M_x(x) = Tw'\left[v + (x - a_1 - u_6)\frac{v(a_1)}{u_6}\right] + a_4 u_1 + a_5 u_2$$

$$- W_F u_3 \phi(a_7), \quad a_8 \leq x \leq a_7 . \quad (37)$$

$$M_x(x) = Tw'\left[v + (x - a_1 - u_6)\frac{v(a_1)}{u_6}\right] + a_4u_1 + a_5u_2$$

$$- W_F u_3\phi(a_7) + \frac{u_5}{u_9} W_C[w(a_8) - u_5\phi(a_8)],$$

$$\frac{a_9 + a_3}{2} \leq x \leq a_8 . \quad (38)$$

The torque reaction at the blade mounting is

$$Q = \frac{u_5}{u_4} W_C[w(a_8) - u_5\phi(a_8)] - W_F[u_3\phi(a_7) + v(a_2)]$$

$$+ a_4u_1 + a_5u_2 - \int_{\frac{a_9+a_3}{2}}^{R} v(x)M(x)dx. \quad (39)$$

The coupled differential equations which must be solved to determine the deflection of the blade elastic axis are

$$a(x)w_i'' + b(x)v_i'' - c(x)\phi_i' - W_A w_i$$

$$= - \frac{W_A}{u_6}(-x + a_1 + u_6)w_{i-1}(a_1) + M_{iy}(x), \quad (40)$$

$$b(x)w_i'' + d(x)v_i'' + f(x)\phi_i' - W_A v_i$$

$$= - \frac{W_A}{u_6}(-x + a_1 + u_6)v_{i-1}(a_1) + M_{iz}(x), \quad (41)$$

$$c(x)w_i'' + f(x)v_i'' + g(x)\phi_i' -$$

$$W_A w_i'\left[v_i + (x - a_1 - u_6)\frac{v_{i-1}(a_1)}{u_6}\right] = -M_{ix}(x), \quad (42)$$

where $x_o = 0 \le x \le x_n$; the boundary conditions are

$$w_i(a_2) = 0, \tag{43}$$

$$w_i(a_1) = -\frac{1}{(a_1 - a_3)\left(K + \frac{W_A}{u_6}\right)}\Big\{(a_5 - a_4)(a_1 - a_3) + W_F(a_7 - a_3) + \frac{W_C}{u_4}\Big[w_{i-1}(a_3) - u_5\phi_{i-1}(a_8)\Big](a_8 - a_3)\Big\}, \tag{44}$$

$$v_i(a_9) = 0, \tag{45}$$

$$v_i(a_{10}) = 0, \tag{46}$$

$$\phi_i(a_3) = 0, \tag{47}$$

for which the initial values are

$$w_i(0) = w_i'(0) = v_i(0) = v_i'(0) = \phi_i(0) = 0. \tag{48}$$

The coefficients occurring above in equations (40) through (42) are defined as follows:

$$a(x) = \frac{a(x_{j+1}) - a(x_j)}{x_{j+1} - x_j}(x - x_j) + a(x_j)$$

$$\text{for } x_j \le x < x_{j+1},\ j = 1, \ldots, n - 1, \tag{49}$$

$$\text{where } a(x_j) = EI_{1,j} + \beta_j^2 EI_{2,j},\ j = 1, \ldots, n - 1; \tag{50}$$

$$\text{and } a(x_o) = a(x_1), \tag{51}$$

$$a(x_n) = a(x_{n-1}), \tag{52}$$

$$b(x) = \frac{b(x_{j+1}) - b(x_j)}{x_{j+1} - x_j}(x - x_j) + b(x_j)$$

for $x_j \leq x \leq x_{j+1}$, $j = 1, \ldots, n - 1$, (53)

where $b(x_j) = \beta_j EI_{2,j}$, $j = 1, \ldots, n - 1$; (54)

and $b(x_o) = b(x_1)$, (55)

$$b(x_n) = b(x_{n-1}), \tag{56}$$

$$c(x) = \frac{c(x_{j+1}) - c(x_j)}{x_{j+1} - x_j}(x - x_j) + c(x_j)$$

for $x_j \leq x \leq x_{j+1}$, $j = 1, \ldots, n - 1$, (57)

where $c(x_j) = E\beta_2(x_j)\beta_j\beta'$, (58)

where $\beta_2(x_j) = \int_{\eta_{-m}}^{\eta_p} t(\eta)\eta\left[\eta^2 + \frac{[t(\eta)]^2}{12} - k^2 j\right]d\eta$,

$x_j > a_{10}$, (59)

where $\beta_2(x_j) = 0$, $x_j \leq a_{10}$, (60)

where $k_j^2 = \frac{EI_{1,j} + EI_{2,j}}{AE_j}$, (61)

$$t(\eta) = \frac{t(\eta_{k+1}) - t(\eta_k)}{\eta_{k+1} - \eta_k}(\eta - \eta_k) + t(\eta_k) \tag{62}$$

for $\eta_k \leq \eta \leq \eta_{k+1}$,

$k = -m, \ldots, p - 1.$

The integral equation (59) is to be approximated using Simpson's Rule and the points $\eta_{-m}, \ldots \eta_p$.

$$d(x) = \frac{d(x_{j+1}) - d(x_j)}{x_{j+1} - x_j} (x - x_j) + d(x_j)$$

for $x_j \leq x \leq x_{j+1}$, $j = 1, \ldots, n - 1$, (63)

where $d(x_j) = EI_{2,j}$, $j = 1, \ldots n - 1$; (64)

and $d(x_o) = d(x_1)$, (65)

$d(x_n) = d(x_{n-1})$, (66)

$$f(x) = \frac{f(x_{j+1}) - f(x_j)}{x_{j+1} - x_j} (x - x_j) + f(x_j)$$

for $x_j \leq x \leq x_{j+1}$, $j = 1, \ldots, n - 1$, (67)

where $f(x_j) = E_{\beta_2}(x_j)\beta'$, $j = 1, \ldots, n - 1$; (68)

and $f(x_o) = f(x_1)$, (69)

$f(x_n) = f(x_{n-1})$, (70)

$$g(x) = \frac{g(x_{j+1}) - g(x_j)}{x_{j+1} - x_j} (x - x_j) + g(x_j)$$

for $x_j \leq x \leq x_{j+1}$, $j = 1, \ldots, n - 1$, (71)

where $g(x_j) = GJ_j, \quad j = 1, \ldots, n-1;$ (72)

and $g(x_o) = g(x_1)$, (73)

$$g(x_{n-1}) = g(x_n), \tag{74}$$

$$M_{iy}(x) = \left[\left(-K + \frac{W_A}{u_6}\right) w_{i-1}(a_1)(a_1 - x) + (a_5 - a_4)(a_6 - x) - W_F(a_7 - x) - \frac{W_C}{u_4}\left(w_{i-1}(a_8) - u_5\phi_{i-1}(a_8)\right)(a_8 - x)\right],$$

$$a_3 \leq x \leq a_1, \tag{75}$$

$$M_{iy}(x) = 0, \qquad 0 \leq x \leq a_3, \tag{76}$$

where $(a_6 - x)$, $(a_7 - x)$, and $(a_8 - x)$ are to be set equal to zero if they are negative.

$$M_{ix}(x) = (a_4)(u_1) + (a_5)(u_2), \qquad a_7 \leq x \leq a_6, \tag{77}$$

$$M_{ix}(x) = (a_4)(u_1) + (a_5)(u_2) - W_F u_3 \phi_{i-1}(a_7),$$

$$a_8 \leq x \leq a_7, \tag{78}$$

$$M_{ix}(x) = (a_4)(u_1) + (a_5)(u_2) - W_F u_3 \phi_{i-1}(a_7) + \frac{u_5}{u_4} W_C[w_{i-1}(a_8) - u_5\phi_{i-1}(a_8)],$$

$$\frac{a_5 + a_3}{2} \leq x \leq a_8, \tag{79}$$

$$M_{ix}(x) = 0, \qquad 0 \leq x \leq \frac{a_9 + a_3}{2}, \tag{80}$$

$$M_{iz}(x) = -\left(\frac{\overline{T}_{i-1}}{ZOTS} + \frac{W_A}{u_6}\right)v_{i-1}(a_1)(a_1 - x) -$$

$$\frac{a_4 v_{i-1}(a_6)}{(a_{11} - a_{12})}(a_6 - x) - W_C(a_8 - x),$$

$$a_9 \leq x \leq a_1, \tag{81}$$

$$M_{iz}(x) = 0, \qquad 0 \leq x \leq a_9, \tag{82}$$

where $(a_6 - x)$, $(a_8 - x)$, $(a_{10} - x)$ are to be set equal to zero if they are negative.

Where $\overline{T}_{i-1} = \frac{W_A}{u_6} w_{i-1}(a_1) + (a_5 - a_4)\left(\frac{a_6 - a_3}{a_1 - a_3}\right) +$

$$W_F\left(\frac{a_7 - a_3}{a_1 - a_3}\right) + \frac{W_C}{u_4}\left(w_{i-1}(a_8) - u_5\phi_{i-1}(a_8)\right)\left(\frac{a_8 - a_3}{a_1 - a_3}\right), \tag{83}$$

where $W_o(a_8) = \phi_o(a_8) = W_o(a_1) = v_o(a_1)$

$$= \phi_o(a_7) = v_o(a_6) = 0, \tag{84}$$

repeat for i = 2, 3 .....

until

$$\frac{\sum_{j=1}^{n}\left\{|\phi_i(x_j)-\phi_{i-1}(x_j)|+|w_i(x_j)-w_{i-1}(x_j)|+|v_i(x_j)-v_{i-1}(x_j)|\right\}}{\sum_{j=1}^{n}\left\{|\phi_i(x_j)-\phi_1(x_j)|+|w_i(x_j)-w_1(x_j)|+|v_i(x_j)-v_1(x_j)|\right\}} < \varepsilon \tag{85}$$

This procedure will repeat itself until the quotient of equation (85) is less than ε. The value of i will generally be less than 10 for a reasonable value of ε.

When this condition is satisfied, the following computations are performed:

$$\overline{M}_{iy}(x_j) = M_{i+1,y}(x_j) + W_A\left[w_i(x_j) - (-x_j + a_1 + u_6)\frac{w_i(a_1)}{u_6}\right], \tag{86}$$

$$\overline{M}_{iz}(x_j) = M_{i+1,z}(x_j) + W_A\left[v_i(x_j) - (-x_j + a_1 - u_6)\frac{v_i(a_1)}{u_6}\right], \tag{87}$$

$$\overline{M}_{ix}(x_j) = M_{i+1,x}(x_j) + W_A w_i'(x_j)\left[v_i(x_j) + (x_j - a_1 - u_6)\frac{v_i(a_1)}{u_6}\right] \tag{88}$$

for $i = 0$, $i = \ell$; $j = 1, \ldots, n$.

Finally, using the results of equations (86), (87), and (88), an n-1 order polynomial approximation (least squares) will be fitted to $\overline{M}_{iy}$, $\overline{M}_{iz}$, $\overline{M}_{ix}$ at the points $x_1 \ldots x_n$. They are of the form

$$\overline{M}_{iy}(x) = \sum_{m=0}^{n-1} a_{myi} x^m , \qquad i = 0, \ell , \tag{89}$$

$$\overline{M}_{iz}(x) = \sum_{m=0}^{n-1} a_{mzi} x^m , \qquad i = 0, \ell , \tag{90}$$

$$\overline{M}_{ix}(x) = \sum_{m=0}^{n-1} a_{mxi} x^m , \qquad i = 0, \ell . \tag{91}$$

Using these equations, we can now take their first derivatives with respect to x to determine the following:

$$T_{xi}(x_j) = -\sum_{m=1}^{n-1} m a_{mxi} x_j^{m-1} \qquad j = 1, \ldots n, \quad i = 0, \ell, \tag{92}$$

$$v_{yi}(x_j) = -\sum_{m=1}^{n-1} m a_{mzi} x_j^{m-1} \qquad j = 1, \ldots n, \quad i = 0, \ell, \tag{93}$$

$$v_{zi}(x_j) = -\sum_{m=1}^{n-1} m a_{myi} x_j^{m-1} \qquad j = 1, \ldots n, \quad i = 0, \ell . \tag{94}$$

The results of equations (89) through (94) are printed out by the computer.

APPENDIX II
MULTIPARAMETER LEAST-SQUARES-CURVE FITTING ANALYSIS

The analysis used for preparing the calibration data presented in this report is a least-squares routine which can treat problems which are defined by numerous parameters. Characteristically in structural calibrations the problem is defined by consideration of three orthogonal forces (two shears, one tension) and three orthogonal moments (torsion or torque and two bending moments). This analysis was prepared so that these six parameters, the six squares of these parameters, and a constant term could be included. The limitation on the number of parameters used is the capacity of the available computer to perform the matrix arithmetic.

A general relationship of k times p variables in terms of others can be written in matrix form as

$$[Z_{kp}] = [a_{kn}] \quad [g_{np}] \tag{95}$$

A particular element of the $[Z_{kp}]$ matrix is determined by the sum

$$Z_{kp} = \sum_n a_{kn} \, g_{np}. \tag{96}$$

If the coefficients, a_{kn}, which determine this relationship are unknown, but enough data (values of Z_{kp} and the corresponding g_{np}) are available, the method of least squares can be applied to determine these coefficients. This method determines a_{kn} such that the squares of the differences between the left and right sides of equation (96) are at the minimum value. The square of their difference is formed, and the partial derivative is determined with respect to each coefficient a_{kn}. Hence, we have

$$\frac{\partial}{\partial a_{\ell m}} \left(Z_{kp} - \sum_n a_{kn} \, g_{np}\right)^2 = 0, \tag{97}$$

where ℓ and m represent a particular a_{kn} (i.e., $k=\ell$, $n=m$).

Reverting back to matrix form, we have

$$\frac{\partial}{\partial a_{\ell m}} \left[\left(Z_{kp} - \sum_n a_{kn} \, g_{np}\right)^2\right] = 0. \tag{98}$$

Therefore, taking the derivative yields

$$[2(Z_{\ell p} - \sum_n a_{\ell n}\, g_{np})\ (-g_{mp})] = 0,$$

or

$$[(Z_{\ell p} - \sum_n a_{\ell n}\, g_{np})\ (g_{mp})] = 0. \qquad (99)$$

Expanding equation (99) for clarity, and to illustrate the form of the matrices, let $k = \ell = 1$ and $n = m = 2$. Thus, for $\frac{\partial}{\partial a_{1m}} = \frac{\partial}{\partial a_{12}}$, we have

$$\begin{bmatrix} (Z_{11}-(a_{11}g_{11}+a_{12}g_{21}+..+a_{1n}g_{n1}))g_{21}+..+ & (Z_{1p}-(a_{11}g_{1p}+a_{12}g_{2p}+..+a_{1n}g_{n1}))g_{2p} \\ 0 \quad +..+ & 0 \\ \vdots & \vdots \\ 0 \quad +..+ & 0 \end{bmatrix} = 0,$$

or

$$[(Z_{11}-(\Sigma a_{1n}g_{n1}))g_{21}\cdots(Z_{1p}-(\Sigma a_{1n}g_{np}))g_{2p}] = 0\ ,$$

or

$$[Z_{11}-\Sigma a_{1n}g_{n1}\cdots Z_{1p}-\Sigma a_{1n}g_{np}] \begin{Bmatrix} g_{21} \\ \vdots \\ g_{2p} \end{Bmatrix} = 0\ . \qquad (100)$$

If all the values of m, 1...n, are introduced, we have

$$[Z_{11}-\sum_n a_{1n}g_{n1}\cdots Z_{1p}-\sum_n a_{1n}g_{np}]\ [g_{pn}] = 0\ , \qquad (101)$$

where g_{pn} is the transposition of g_{np}. The summation in equation (101) can also be written in matrix form as

$$\sum_n a_{ln} g_{np} = [a_{ln}] \; [g_{np}] \; . \tag{102}$$

All the matrix elements also involve differences between Z_{lp} values and this summation; they can therefore be written as the difference of two matrices, using equation (102):

$$\left[[Z_{lp}] - [a_{ln}] \; [g_{np}] \right] \; [g_{pn}] = 0 \; . \tag{103}$$

If all the values of ℓ, 1..k, are now included we have

$$\left[[Z_{kp}] - [a_{kn}] \; [g_{np}] \right] \; [g_{pn}] = 0. \tag{104}$$

This can now be solved for $[a_{kn}]$ as

$$[a_{kn}] = [Z_{kp}] \; [g_{np}]^T \left[[g_{np}] \; [g_{np}]^T \right]^{-1} , \tag{105}$$

where

T = transpose, -1 = inverse.

In using this analysis for calibrations, the Z_{kp} are the applied loads and the g_{np} are the gage readings. Each subscript k represents one of six type loads (two bending moments, torsion, two shears, and tension), whereas each of the subscripts n represents one of six type gages corresponding to each of the six type loads. The remaining subscript p represents a particular test loading for which six values of Z_{kp} (which may include zero values) are applied, and six values of g_{np} are thereby determined. The number of tests performed, p, must be equal to or greater than n for a solution to exist. In general p is much larger than n. A larger number of tests performed will result in a more accurate determination of the calibration coefficients a_{kn}, since errors will tend to cancel.

UNCLASSIFIED

Security Classification

DOCUMENT CONTROL DATA - R&D

(Security classification of title, body of abstract and indexing annotation must be entered when the overall report is classified)

1. ORIGINATING ACTIVITY (Corporate author) The Boeing Company Vertol Division Morton, Pennsylvania 19070	2a. REPORT SECURITY CLASSIFICATION UNCLASSIFIED 2b. GROUP None

3. REPORT TITLE IN-FLIGHT MEASUREMENT OF ROTOR BLADE AIRLOADS, BENDING MOMENTS, AND MOTIONS, TOGETHER WITH ROTOR SHAFT LOADS AND FUSELAGE VIBRATION, ON A TANDEM ROTOR HELICOPTER
VOLUME II CALIBRATIONS AND INSTRUMENTED COMPONENT TESTING

4. DESCRIPTIVE NOTES (Type of report and inclusive dates)
Final Report - Part 2 of 5 parts

5. AUTHOR(S) (Last name, first name, initial)
Grant, William J., and
Pruyn, Richard R.

6. REPORT DATE May 1967	7a. TOTAL NO. OF PAGES 134	7b. NO. OF REFS 5
8a. CONTRACT OR GRANT NO. DA44-177-AMC-124(T) b. PROJECT NO. Task No. 1F125901A14604 d.	9a. ORIGINATOR'S REPORT NUMBER(S) USAAVLABS Technical Report 67-9B 9b. OTHER REPORT NO(S) (Any other numbers that may be assigned this report) D8-0382-2	

10. AVAILABILITY/LIMITATION NOTICES

Distribution of this document is unlimited.

11. SUPPLEMENTARY NOTES None	12. SPONSORING MILITARY ACTIVITY U.S. Army Aviation Materiel Laboratories (USAAVLABS) Fort Eustis, Virginia

13. ABSTRACT

Calibration and instrumented component testing were performed to provide reliable instrumentation for the measurement of dynamic airloads on a large tandem rotor helicopter. All equipment underwent single-load calibration and much of it was calibrated for combined loads. Blade tension instrumentation was calibrated by whirl testing.

The combined-loads calibrations represent an extension of the state of the art, especially for elastic structures such as rotor blades. All calibrations were evaluated qualitatively and a summary of the quality of all calibrations is presented. The general error in all calibrations is less than 3 percent.

Component testing consisted of whirl tests and dynamic response tests of the rotor blades, and functional testing of the airloads pressure transducers. These tests determined the structural integrity of the blade instrumentation and provided references for isolating the effects of such factors as blade bending, acceleration, and temperature.

DD FORM 1 JAN 64 1473

UNCLASSIFIED

Security Classification

UNCLASSIFIED

Security Classification

14. KEY WORDS	LINK A ROLE	LINK A WT	LINK B ROLE	LINK B WT	LINK C ROLE	LINK C WT
CALIBRATION						
INSTRUMENTED COMPONENT TESTING						
SINGLE-LOAD TESTS						
COMBINED-LOADS TESTS						
INTERACTION EFFECTS						
3-PERCENT ERROR						
WHIRL TESTS						
FUNCTIONAL TESTS						
ISOLATION OF TRANSIENT EFFECTS						
REPEATABILITY						

INSTRUCTIONS

1. ORIGINATING ACTIVITY. Enter the name and address of the contractor, subcontractor, grantee, Department of Defense activity or other organization *(corporate author)* issuing the report.

2a. REPORT SECURITY CLASSIFICATION: Enter the overall security classification of the report. Indicate whether "Restricted Data" is included. Marking is to be in accordance with appropriate security regulations.

2b. GROUP: Automatic downgrading is specified in DoD Directive 5200.10 and Armed Forces Industrial Manual. Enter the group number. Also, when applicable, show that optional markings have been used for Group 3 and Group 4 as authorized.

3. REPORT TITLE: Enter the complete report title in all capital letters. Titles in all cases should be unclassified. If a meaningful title cannot be selected without classification, show title classification in all capitals in parenthesis immediately following the title.

4. DESCRIPTIVE NOTES: If appropriate, enter the type of report, e.g., interim, progress, summary, annual, or final. Give the inclusive dates when a specific reporting period is covered.

5. AUTHOR(S): Enter the name(s) of author(s) as shown on or in the report. Enter last name, first name, middle initial. If military, show rank and branch of service. The name of the principal author is an absolute minimum requirement.

6. REPORT DATE: Enter the date of the report as day, month, year; or month, year. If more than one date appears on the report, use date of publication.

7a. TOTAL NUMBER OF PAGES: The total page count should follow normal pagination procedures, i.e., enter the number of pages containing information.

7b. NUMBER OF REFERENCES: Enter the total number of references cited in the report.

8a. CONTRACT OR GRANT NUMBER. If appropriate, enter the applicable number of the contract or grant under which the report was written.

8b, 8c, & 8d. PROJECT NUMBER: Enter the appropriate military department identification, such as project number, subproject number, system numbers, task number, etc.

9a. ORIGINATOR'S REPORT NUMBER(S): Enter the official report number by which the document will be identified and controlled by the originating activity. This number must be unique to this report.

9b. OTHER REPORT NUMBER(S): If the report has been assigned any other report numbers *(either by the originator or by the sponsor)*, also enter this number(s).

10. AVAILABILITY/LIMITATION NOTICES: Enter any limitations on further dissemination of the report, other than those imposed by security classification, using standard statements such as:

(1) "Qualified requesters may obtain copies of this report from DDC."

(2) "Foreign announcement and dissemination of this report by DDC is not authorized."

(3) "U. S. Government agencies may obtain copies of this report directly from DDC. Other qualified DDC users shall request through _____."

(4) "U. S. military agencies may obtain copies of this report directly from DDC. Other qualified users shall request through _____."

(5) "All distribution of this report is controlled. Qualified DDC users shall request through _____."

If the report has been furnished to the Office of Technical Services, Department of Commerce, for sale to the public, indicate this fact and enter the price, if known.

11. SUPPLEMENTARY NOTES: Use for additional explanatory notes.

12. SPONSORING MILITARY ACTIVITY: Enter the name of the departmental project office or laboratory sponsoring *(paying for)* the research and development. Include address.

13. ABSTRACT: Enter an abstract giving a brief and factual summary of the document indicative of the report, even though it may also appear elsewhere in the body of the technical report. If additional space is required, a continuation sheet shall be attached.

It is highly desirable that the abstract of classified reports be unclassified. Each paragraph of the abstract shall end with an indication of the military security classification of the information in the paragraph, represented as *(TS)*, *(S)*, *(C)*, or *(U)*.

There is no limitation on the length of the abstract. However, the suggested length is from 150 to 225 words.

14. KEY WORDS: Key words are technically meaningful terms or short phrases that characterize a report and may be used as index entries for cataloging the report. Key words must be selected so that no security classification is required. Identifiers, such as equipment model designation, trade name, military project code name, geographic location, may be used as key words but will be followed by an indication of technical context. The assignment of links, rules, and weights is optional.

UNCLASSIFIED

Security Classification

35 5-67